

EFFECTS OF EARTHQUAKE RECORD SCALING ON NONLINEAR STRUCTURAL RESPONSE

Report on PEER-LL Program Task 1G00 Addendum (Sub-Task 1 of 3)

Nicolas Luco & Paolo Bazzurro
AIR Worldwide Corporation (San Francisco, CA)

Abstract

Limitations in the existing ground motion database force the scaling of real records to obtain accelerograms that are consistent with the ground motion target for structural design and evaluation. In the seismology and engineering communities the acceptance of the limits for “legitimacy” of scaling varies from one (no scaling allowed) to ten. The concerns expressed by detractors are mostly based on the knowledge of systematic and unquestionable differences in ground motion characteristics for different magnitude-distance (M_w - R_{close}) scenarios and much less on their effects on structures. At the other end of the spectrum Cornell and his co-workers at Stanford University have claimed that scaling is not only legitimate but also useful for assessing post-elastic response statistics of structures. Such studies, however, did not draw conclusions valid over the entire spectrum of structural vibration periods and did not state the conditions under which scaling may fail.

This study investigates whether scaling of a record randomly selected from a M_w - R_{close} bin introduces bias in nonlinear structural response. Can one scale up a $M_w=6.5$, $R_{close}=20$ km record to obtain a ground motion level expected for a $M_w=7.25$ event at 5km from the fault? Is scaling legitimate for assessing the response of structures of all periods? Are the effects of scaling constant for all periods and for different levels of nonlinear response? We consider the legitimacy of scaling within a M_w - R_{close} bin and across M_w - R_{close} bins. In both cases, the records are scaled up and down by large factors to determine whether the response to scaled records departs from the response of un-scaled ones that are “naturally” at that level. The answers to these questions are sought by investigating the nonlinear response of a suite of single-degree-of-freedom (SDOF) systems with multiple “strengths” to achieve increasing levels of nonlinear responses. Also considered are elastic and ductile models of a multi-degree-of-freedom (MDOF) building.

The results of this study demonstrate that scaling earthquake records can, in fact, introduce a bias in the nonlinear structural drift response to such records. The extent of bias depends on the period of vibration and overall strength of the structure of interest, and whether its drift response is dominated by excitation input at a single or multiple periods (i.e., SDOF versus MDOF structures). The severity of the bias also depends on the characteristics (e.g., M_w - R_{close}) of the records that are scaled, as well as those of the target ground motion scenario. For the most part, the bias can be explained by systematic differences between the elastic response spectra for records that are scaled up (or down) and those that are naturally (without scaling) at a target spectral acceleration level.

1 Motivation

With the advent of Performance-Based Earthquake Engineering, and the availability of sophisticated structural analysis software and faster computers, nonlinear dynamic time-history analysis (NDTHA) has recently become more widely used for both design and evaluation of structures. Perhaps one of the biggest obstacles preventing more widespread use of NDTHA is the selection of appropriate ground motion records. Engineers often seek to obtain from seismologists real ground motion records that closely match the spectral acceleration at a specified hazard level (e.g., 10% in 50 years) as well as the magnitude-distance (M_w - R_{close}) pair(s) of the events controlling the seismic hazard at the building site. The spectral acceleration of interest at many sites in seismically active regions of the world such as California is often relatively large, and the earthquake scenarios that control the hazard are often large magnitude events generated by nearby faults. Despite the recent increase in the number of records provided by large earthquakes occurred recently around the world (e.g., the 1999 $M_w=7.6$ Chi-Chi Earthquake, the 1999 $M_w=7.5$ Kocaeli Earthquake, the 2002 $M_w=7.9$ Denali Earthquake, and the 2003 $M_w=8.0$ Hokkaido Earthquake), the existing database for such spectral acceleration and M_w - R_{close} conditions is still very limited. Furthermore, the hazard at a site may be characterized by specific rupture-directivity conditions and site classifications (e.g., NEHRP D), further limiting the number of earthquake records available. Given the preference of the vast majority of engineers to use synthetic ground motions, scaling real records to obtain accelerograms that are consistent with a design target ground motion level is often the only remaining option.

In the seismology and engineering communities, the acceptance of ground motion scaling limits varies wildly from one (no scaling allowed) to ten or more (e.g., the earthquake records used for the PEER Testbeds were scaled by factors as large as 11). These limits are based more on a “comfort feeling” than on a sound technical basis. This study attempts to provide the quantitative technical basis for threshold limits beyond which scaling of a record randomly selected from a pool of accelerograms belonging to a magnitude-distance (M_w - R_{close}) scenario introduces bias in the nonlinear response of structures. The bias is computed with respect to an estimate of the “true” structural response that, for these purposes, is taken to be the estimate of the median response to records that are, by nature, already at a particular intensity level without any need for scaling. To avoid any misunderstanding, by “ground motion scaling” here we simply mean multiplying a record by a constant scalar factor in order to reach a target spectral acceleration level. The time scale (and therefore, the frequency content) of the record is left untouched by the scaling operation.

This study was intended to support another PEER Lifelines project (1F01), namely the Design Ground Motion Library (DGML), which will develop a library of recorded ground motions suitable for use by engineers for dynamic analysis of various structures. In addition to the library of earthquake records, the DGML will likely provide guidance for scaling the recommended records, if necessary. The extent to which earthquake records can be scaled before introducing excessive bias in nonlinear structural response, as investigated in this study, is also important for deciding on the recommended records themselves.

2 Background

The issue of whether ground motion scaling produces different structural response statistics has been debated in the engineering community for at least a decade. The concerns expressed by many individuals are mostly based on the knowledge of systematic and unquestionable differences in ground motion characteristics (e.g., spectral shape, duration, etc.) for different M_w - R_{close} scenarios and much less on their effects on structures. The claim that such systematic differences in the input caused systematic differences in the response is often based only on engineering intuition or, at best, on experience gained in evaluating linear elastic rather than nonlinear post-elastic structural responses. Testing the legitimacy of ground motion scaling for assessing nonlinear responses of structures was almost uncharted territory until the studies by Cornell and his students at Stanford University (e.g., Sewell 1989; Inoue and Cornell 1991; Bazzurro and Cornell 1994; Shome *et al.* 1998; Luco 2002). All such studies found that judicious scaling was not only legitimate but, under certain conditions, also useful for the purpose of efficiently assessing post-elastic response statistics of structures.

Perhaps with the exception of the work by Shome *et al.*, however, all the other cited studies have not had a large impact on engineering practice mainly because the main conclusions were obscured by arguments heavily based on statistical concepts and findings. The work by Shome *et al.*, although confined in scope (i.e., only one structure was analyzed, only 20 records for each of four M_w - R_{close} bins were used, and no near-source records were considered) reached out to the practicing engineers by addressing their concerns about ground motion scaling more directly. The study, however, did not reach conclusions over the entire spectrum of structural periods, and did not state the conditions under which scaling may fail. Some of the conclusions that led to the purported legitimacy of scaling were also made somewhat less conclusive by the limited sample size of records adopted. In the study reported on here, in an attempt to avoid obscuring the results we will seek to answer the questions above by keeping statistical arguments to a minimum.

Furthermore, Shome *et al.* addressed the ground motion scaling issue from a slightly different perspective than the one used here. The focus there was on the legitimacy of scaling a pool of records from a source M_w - R_{close} bin to match the median “intensity” level of records belonging to the same bin or a different target M_w - R_{close} bin. The legitimacy was assessed in terms of bias of the median response generated by scaling the entire suite of source records that were scaled, on average, by a certain quantity. Some of the source records were scaled by a large amount and some by a small amount. Here we also tackle a different but very much related issue. Does a record selected at random from a M_w - R_{close} bin and scaled (in practice, almost always up but, perhaps more academically, also down) to a target intensity level produce a nonlinear structural response that is, on average, materially “different” than that generated, on average, by records that are already naturally at the target intensity level? If there is bias, how large is it? Is the bias constant or does it vary with structural period and level of nonlinear response? Does the bias change if the source record scaled to match the target ground motion is characterized by values of M_w and R_{close} that are different from those that control the site hazard? Or, in other words, given the same level of scaling, do the magnitude and distance of the source and target records affect the bias in the nonlinear structural response?

3 Objective

Shortly put, the objective of this study is to investigate whether amplitude scaling of input earthquake records to a target pseudo spectral acceleration (S_a) level introduces a bias in the resulting nonlinear structural drift response. As alluded to above, the bias is defined as

$$\text{Bias} = \frac{\text{median response to scaled records}}{\text{median response to unscaled records (that are naturally at target } S_a)}$$

This definition is used in this study to quantify the bias (if any) and thereby provide a technical basis for limits on scaling.

Also investigated in this study is whether the bias depends on (i) the general characteristics of the target ground motion scenario (e.g., M_w and R_{close}), (ii) the general characteristics of the records that are scaled, (iii) the vibration period(s) of the structure of interest, (iv) the overall strength of the structure, and (v) the contribution of higher (than the first) modes of vibration to the structural response.

4 Organization of Report

In total, 469 earthquake ground motion records grouped into 7 different bins are used in this study, as described in Section 5. As described in Section 6, the nonlinear dynamic response of 48 single-degree-of-freedom (SDOF) and 2 multi-degree-of-freedom (MDOF) structures is analyzed. The procedure developed to quantify the bias induced by scaling is outlined in Section 7, and the results are presented in Section 8. In Section 9 an overall summary of the results is provided, some general conclusions are drawn in Section 10, and Section 11 describes a few potential topics for future work.

5 Description of Earthquake Records

5.1 Bins I to VI

As explained in the introduction, both intra- and inter-bin scaling are investigated in this study. Six different bins based on earthquake magnitude (M_w) and closest source-to-site distance (R_{close}) are defined here, as listed in Table 1.

Besides the M_w and R_{close} differences, the other general characteristics of the six bins are identical. More specifically, they each contain 73 earthquake records that are

- from the PEER Strong Ground Motion Database (processed by Dr. Walt Silva)
- from shallow crustal events,
- from stations that are situated on stiff-soil sites (USGS B-C or Geomatrix B-D classification),

Table 1. Earthquake moment magnitude, M_w , and closest source-to-site distance, R_{close} , ranges for six of the bins of earthquake records considered in this report.

Bin Label	M_w	R_{close}
I	6.4-6.8	0-15km
II	6.4-6.8	15-30km
III	6.4-6.8	30-50km
IV	6.9-7.6	0-15km
V	6.9-7.6	15-30km
VI	6.9-7.6	30-50km

- not from instruments on dams or above the lowest level of buildings, and
- filtered with high- and low-pass corner-frequencies greater than 0.2 hertz and less than 18 hertz, respectively.

The last constraint above is used because, according to Silva, the widest usable bandwidth of such records is $1.25/18=0.07$ to $1/(0.2*1.25)=4$ seconds. As described in a subsequent section, this covers the range of fundamental vibration periods considered in this study.

A complete list of the earthquake records in each bin is provided in the appendix. Note that only a randomly selected subset of the Chi-Chi records that satisfy constraints described above were included in order to minimize the number of records from any one single event.

The "median" (computed as the geometric mean in this paper, unless noted otherwise) of the elastic response spectra for each bin of earthquake records (including the "Near-Source Bin" described in the next subsection) is shown in Figure 1.

5.2 Near-Source Bin

In addition to the six M_w - R_{close} bins of earthquake records described above, a seventh bin of 31 "near-source" earthquake records is also considered. This near-source bin very similar to Bin I (e.g., $M_w=6.5-6.9$ and $R_{close}=0-16$ km), except that all of its earthquake records are (i) from stations in the forward rupture-directivity region, and (ii) strike-normal components of the ground motion. The forward rupture-directivity region is defined using Somerville *et al.*'s (1997) rupture directivity modification factor, by assuming that values greater than unity signify forward directivity. For a detailed description of these near-source earthquake records, the reader is referred to (Luco 2002).

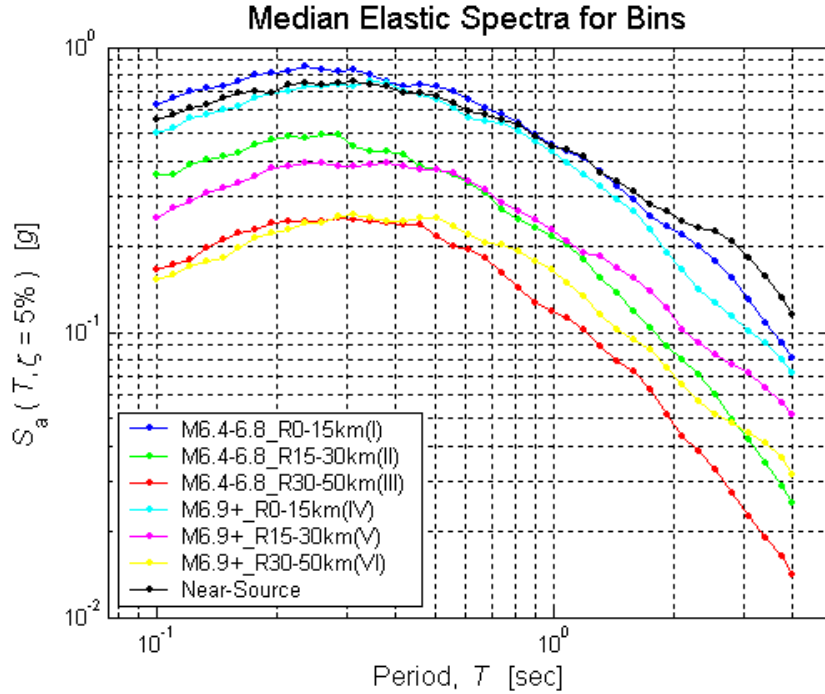


Figure 1. Median (computed as geometric mean) elastic response spectra for the seven bins of earthquake records considered in this report.

6 Description of Structures

As mentioned above, both single-degree-of-freedom (SDOF) and multi-degree-of-freedom (MDOF) structures are considered in this study. In all, 48 SDOF structures of different periods and strength and 2 MDOF structures are considered. The SDOF structures are representative of, for example, first-mode-dominated buildings or bridge bents. Multiple modes contribute significantly to the response of the two MDOF structures, which are elastic and ductile models of a realistic 9-story steel moment-resisting frame (SMRF) building. All of these structures are described in more detail below.

Note that dynamic time-history analysis of the SDOF structures is performed using a MATLAB implementation of Newmark's linear acceleration method (as described in Chopra 1995). For the MDOF structures, DRAIN-2DX (Prakash 1993) is employed, with P-Delta effects included.

6.1 Single-Degree-of-Freedom (SDOF) Oscillators

The SDOF (a.k.a., "lollipop") structures considered have vibration periods of $T = 0.1, 0.2, 0.3, 0.5, 1, 2, 3,$ and 4 seconds. The first six periods are the same as those for which the U.S. Geological Survey has provided seismic hazard curves (Frankel & Leyendecker 2001), whereas the last (and largest) period is based on the filter corners for the earthquake records used (as explained above in Section 5.1). Also like the USGS hazard maps (and typical attenuation relations), the damping ratio for each of the SDOF structures is set to $\zeta=5\%$.

For each vibration period, six different yield forces (F_y 's) of the SDOF structures are considered, each based on the particular target spectral acceleration (S_a) of interest. (Note that, in this paper, S_a always refers to the spectral acceleration at the fundamental period of the structure under consideration). The largest F_y considered is equal to the target S_a multiplied by the mass (m) of the structure (here we use "mass normalized" structures, such that $m=1$), which corresponds to a strength reduction factor of $R=1$ and therefore elastic response. The other five yield forces are fractions of this largest strength, namely (target S_a)* m/R where $R = 2, 4, 6, 8,$ and 10 . In what follows, these strengths of the SDOF structures will be referred to by the corresponding value of R only. Note that $R=10$ corresponds to a highly inelastic structure.

As depicted in Figure 2, the force-displacement hysteretic behavior of the SDOF structures considered is bilinear inelastic with a strain hardening ratio of $\alpha=2\%$.

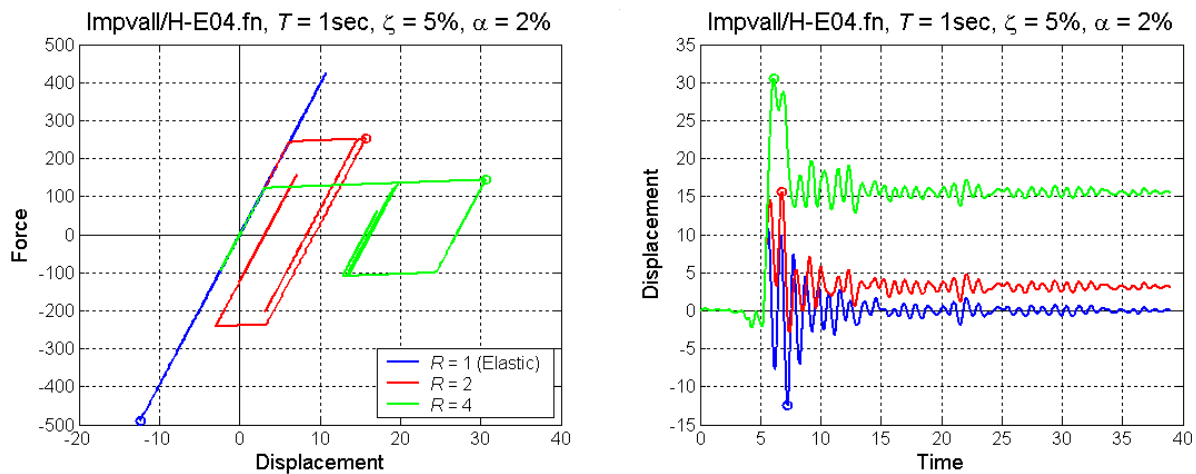


Figure 2. Examples of the force-displacement hysteresis and displacement time histories for the SDOF structures considered in this paper.

6.2 Multi-Degree-of-Freedom (MDOF) Buildings

The two MDOF structures considered are (1) an elastic model and (2) a ductile model of a 9-story (plus basement), 5-bay steel moment-resisting frame (SMRF) building that was designed by consulting engineers for Los Angeles conditions as part of the SAC Steel Project. As illustrated in Figure 3, a two-dimensional model of one of the exterior moment-resisting frames of the building is analyzed. For the ductile model, the beam ends (immediately to the right and left of each column) and column ends (immediately above and below each floor, and at the column splices) are modeled as plastic hinges with 3% strain hardening relative to the elastic stiffness of the beam and column, respectively. The fundamental period of the building model is $T=2.3\text{sec}$, and the first-mode damping ratio is 2%. For additional details, the reader is referred to FEMA 355C (2000) and (Luco 2002).

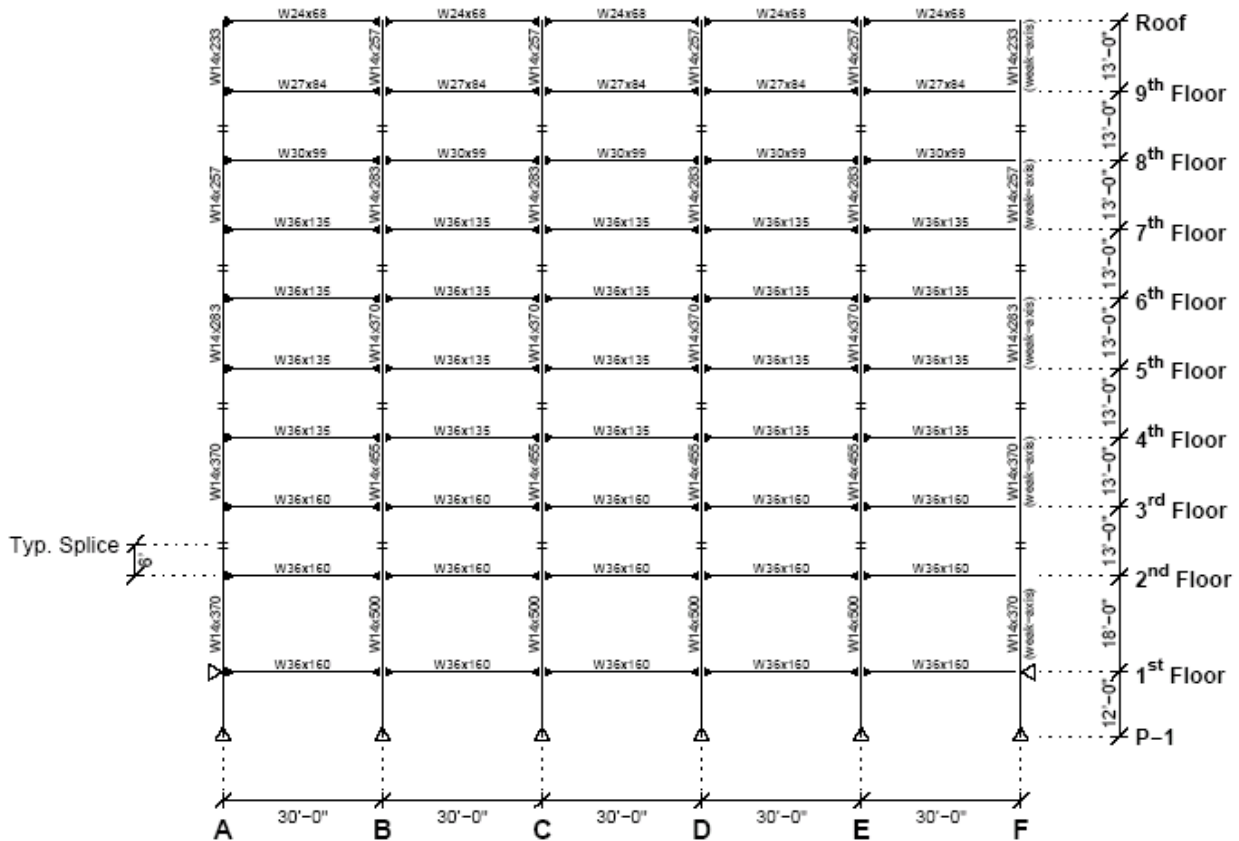


Figure 3. Elevation of a 9-story steel moment-resisting frame designed by practicing engineers for Los Angeles conditions as part of the SAC Steel Project (Phase II). An elastic and a ductile MDOF model of this frame are considered in this report.

Note that the two MDOF building models as considered in order to compare the SDOF results with those for a more realistic structure, as well as to assess how the contribution of higher modes may alter the effects of scaling.

7 Outline of Procedure

The procedure developed for quantifying the bias in nonlinear structural response induced by scaling of the input earthquake record(s) is relatively simple, and the same procedure is applied for both intra- and inter-bin scaling. For a given structure, the following steps are taken:

- (1) Decide on a target spectral acceleration (at the fundamental period of the structure of interest and a damping ratio of 5%) that is associated with an earthquake record in the "target" bin.
- (2) For this earthquake record, un-scaled, compute the nonlinear inelastic structural response (e.g., inelastic spectral displacement for the SDOF structures). This is considered to be the "true" nonlinear structural response that serves as the basis of comparison.

- (3) Scale all of the earthquake records in the "source" bin (same as the target bin for intra-bin scaling, different for inter-bin scaling) to the target spectral acceleration, and record the scale factors.
- (4) Compute the nonlinear inelastic structural response for the scaled earthquake records.
- (5) Plot the ratio of the nonlinear inelastic structure responses for the scaled over un-scaled earthquake records versus the scale factors.
- (6) Repeat Steps 1-5 for another target spectral acceleration associated with another earthquake record in the target bin, until all of them have been considered.

8 Results

The results of the procedure for quantifying the bias induced by intra- and inter-bin scaling are first presented for the suite of simple SDOF oscillators (of a range of different periods and strengths) and then for the two MDOF buildings (one elastic, the other ductile). For one of the SDOF oscillators, namely that of "moderate" period ($T=1\text{sec}$) and strength ($R=4$), the procedure is demonstrated in a step-by-step fashion. For the other structures, only a summary of the final results presented.

Note that in investigating intra-bin scaling for each of the 48 SDOF structures (8 periods and 6 strengths), 73^2 dynamic analyses are carried out for each of Bins I-VI, plus 31^2 for the Near-Source Bin, for a total of 1,580,880 dynamic analyses. Similarly, for 10 different intra-bin scaling combinations considered (as described below), a total of 2,263,584 SDOF dynamic analyses are performed. For each of the 2 MDOF structures, however, just 31^2 and 31×73 dynamic analyses for intra- and inter-bin scaling, respectively, are carried out, for a total of 6448 MDOF dynamic analyses.

8.1 SDOF Structures

For each SDOF oscillator of a given period (T), damping ratio ($\zeta=5\%$), strength reduction factor (R), and strain-hardening ratio ($\alpha=2\%$), note that the nonlinear structural response measure considered is the peak relative (to the ground) displacement, a.k.a., the inelastic spectral displacement S_d^1 .

8.1.1 Intra-Bin Scaling

To reiterate, intra-bin scaling refers to scaling of an earthquake record from a given M_w-R_{close} "source" bin to a target S_a associated with the same M_w-R_{close} bin. The purpose of intra-bin scaling is to obtain a record in the M_w-R_{close} bin that is at the S_a level of interest.

The procedure outlined in Section 7 for quantifying the effects of intra-bin scaling on nonlinear structural response is demonstrated here in a step-by-step fashion for the Near-Source Bin and a moderate period ($T=1\text{sec}$) and strength ($R=4$) oscillator. Subsequently, a summary of the results is provided (i) for Bins I-VI and the same "moderate" oscillator, and (ii) for all 48 oscillators considered and the Near-Source Bin.

8.1.1.1 Near-Source Bin, Moderate Period and Strength Structure

Step 1:

As illustrated in Figure 4a on a plot of the elastic response spectra for all 31 of the earthquake records in the Near-Source Bin, the first target spectral acceleration considered is $S_a=2.0g$. This spectral acceleration value is the largest (at $T=1s$) in the bin, and is associated with the 1994 Northridge Rinaldi Receiving Station (RRS) earthquake record.

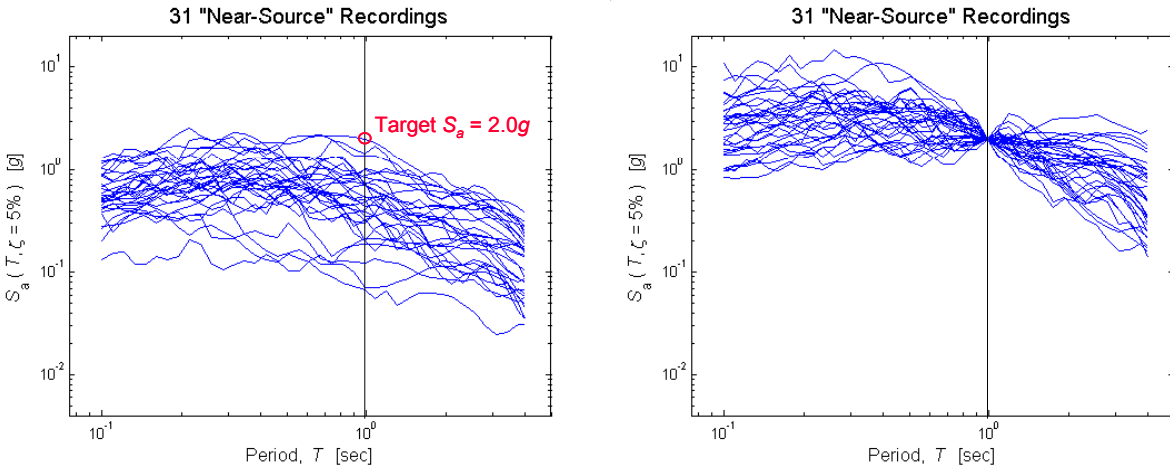


Figure 4. Elastic response spectra (a) before and (b) after scaling (intra-bin) the earthquake records in the Near-Source Bin to a target spectral acceleration of 2.0g (at a period of 1sec).

Step 2:

The inelastic spectral displacement for the un-scaled "target record" specified in Step 1 is shown in Figure 5a. Recall that this value, $S_d^I=49.4cm$, is taken to be the "true" inelastic spectral displacement for this target S_a level. Also shown in the figure, as a basis of comparison, are the S_d^I values for the other records in the bin, before they are scaled in the next step.

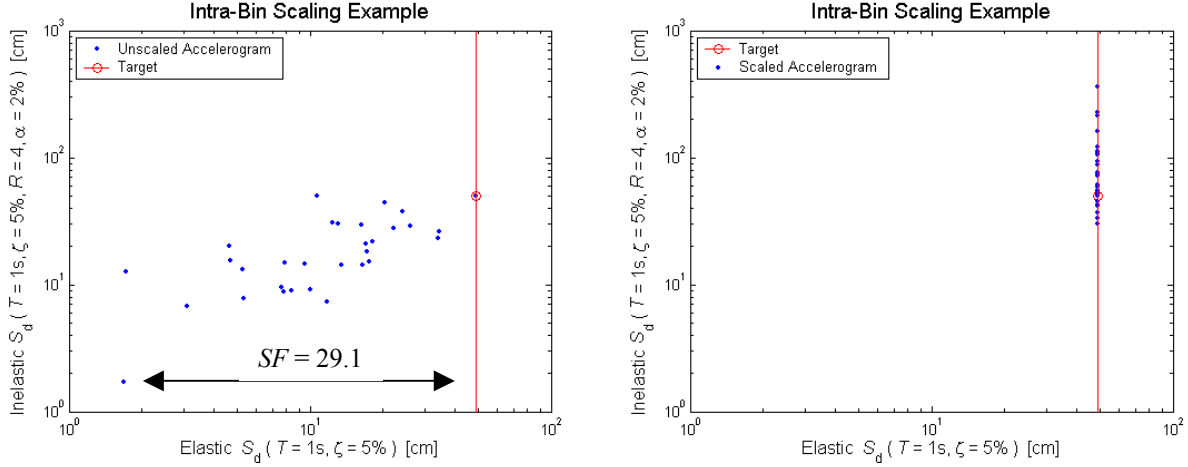


Figure 5. Inelastic spectral displacement responses (versus elastic spectral displacement, which is proportional to spectral acceleration) **(a)** before and **(b)** after scaling (intra-bin) the earthquake records in the Near-Source Bin to a target spectral acceleration of $2.0g$ (or, equivalently, a target elastic spectral displacement of approximately 50cm). Note that the period of the oscillator is $T=1\text{sec}$, and the strength reduction factor is $R=4$.

Step 3:

The elastic response spectra after scaling all of the earthquake records in the Near-Source Bin to the target $S_a=2g$ (specified in Step 1) are shown in Figure 4b. Note how the response spectra (and the underlying records) are scaled in amplitude only, not in shape. As depicted in Figure 5a, the scale factors in this case range from 1 (for the target record) to 29.1, indicative of the substantial intra-bin variability in S_a .

Step 4:

The inelastic spectral displacement responses (S_d^I) to the 30 scaled records from Step 3 are shown in Figure 5b. Note that most of the S_d^I values are larger than the "true" S_d^I from the un-scaled target record.

Step 5:

The ratios of the S_d^I values for the scaled earthquake records (from Step 4) to that for the un-scaled "target" record (from Step 2) are plotted against the corresponding scale factors in Figure 6. Note that there appears to be a trend, albeit noisy, that suggests that the larger the scale factor, the larger the median ratio of the scaled to un-scaled S_d^I (the bias). However, the record-to-record variability of S_d^I for un-scaled records with the same (or similar) values of S_a , as evident in Figure 5a, prevents us from drawing general conclusions before Steps 1-5 are repeated for the other 30 target records and S_a levels in the Near-Source Bin. This is done in Step 6.

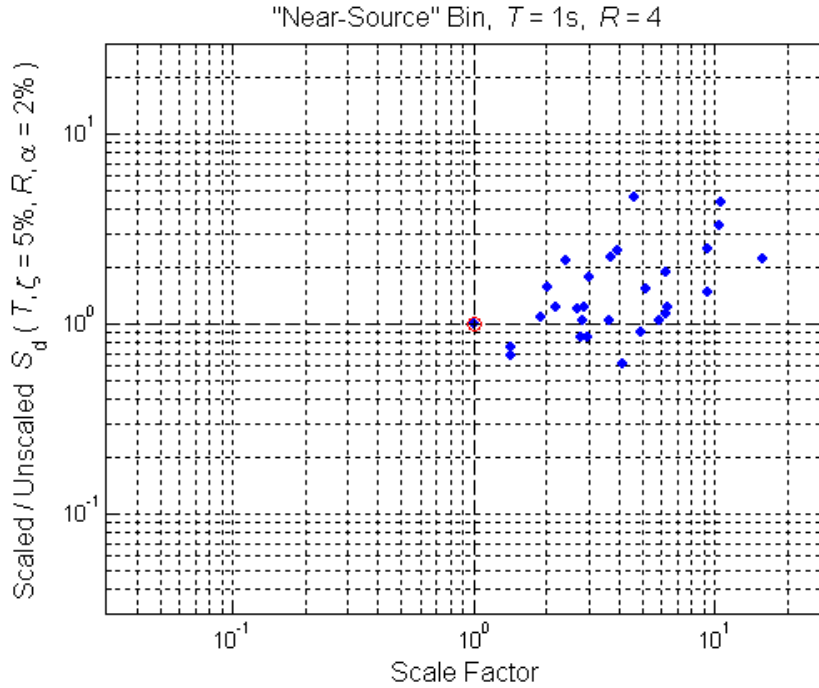


Figure 6. Ratios of the inelastic ($R=4$) spectral displacement responses to (i) the Near-Source records scaled to a target S_a (at $T=1$ sec) of $2.0g$ versus (ii) the un-scaled Near-Source record that is naturally at the target $S_a=2.0g$ (circled in red), all plotted against the corresponding scale factors.

Step 6:

For the second "loop" of the procedure, the next-to-lowest S_a in the Near-Source Bin, namely $0.07g$, is considered as the target. The elastic response spectra before and after scaling are illustrated in Figure 7, and the corresponding ratios of scaled to un-scaled S_d^1 are plotted in Figure 8. Included in this figure are the results that were obtained by scaling to the largest S_a in the Near-Source Bin, i.e., $2.0g$ (first shown in Figure 6). For those results the scale factors were all larger than unity, whereas now the scale factors range from 0.04 to 1.02 .

Like in Figure 6, a trend is apparent in Figure 7 that suggests that the median ratio of the S_d^1 response to scaled versus un-scaled records, i.e., the bias, increases with increasing scale factor (nearly linearly in log-log scale). In one case, however, a small ratio of scaled to un-scaled S_d^1 (in the 0.1 - 0.2 range) is observed at a scale factor near one; as mentioned above in Step 5, this is due to the record-to-record variability in S_d^1 , even for records with similar S_a , and emphasizes the need to consider multiple target records.

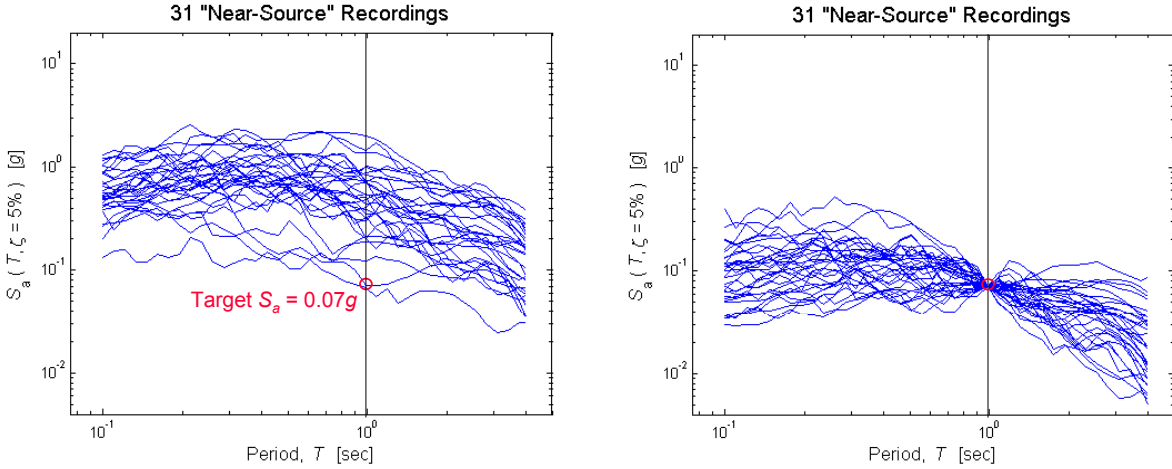


Figure 7. Elastic response spectra (a) before and (b) after scaling (intra-bin) the earthquake records in the Near-Source Bin to a target spectral acceleration of $0.07g$.

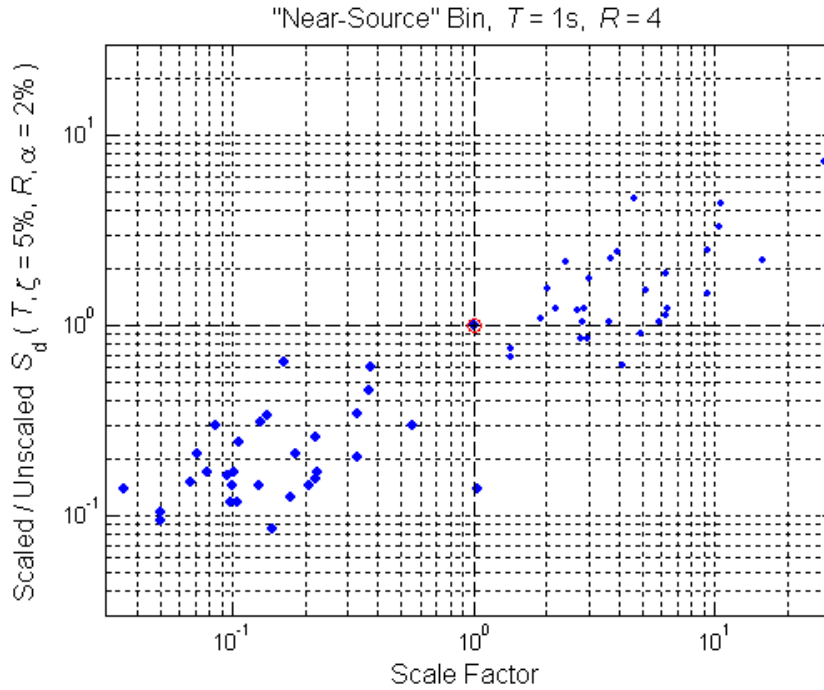


Figure 8. Ratios of the inelastic ($R=4$) spectral displacement responses to (i) the Near-Source records scaled to a target S_a (at $T=1\text{sec}$) of $0.07g$ versus (ii) the un-scaled Near-Source record that is naturally at the target $S_a=0.07g$ (circled in red), all plotted against the corresponding scale factors. The smaller blue data points with scale factors larger than unity are the same as those plotted in Figure 6 above.

As another example, the target S_a level that corresponds to the median (found conventionally in this case, not computed as the geometric mean) of the Near-Source Bin, namely $0.50g$, is considered for the third "loop" of the procedure. The S_d^I responses before and after scaling the earthquake records are shown in Figure 9, and, as obtained from Figure 9b, the ratios of the S_d^I responses for the scaled records to that for the un-scaled target record are plotted in Figure 10. Consistent with the results obtained by scaling to a higher ($2.0g$) and lower ($0.07g$) target S_a (shown in Figure 8), the results in Figure 10 show a positive trend, albeit mild, with scale factor in the scaled to un-scaled S_d^I ratios, abbreviated here as $r(S_d^I)$. Unlike the previous results, however, note that most of the $r(S_d^I)$ values are less than unity, both for scale factors larger and less than unity; again, this is more likely an indication that the S_d^I response to the particular un-scaled target record used in this case is relatively large, not that the S_d^I response to the scaled records is in general biased low. Again, this is why we consider multiple target S_a levels and records.

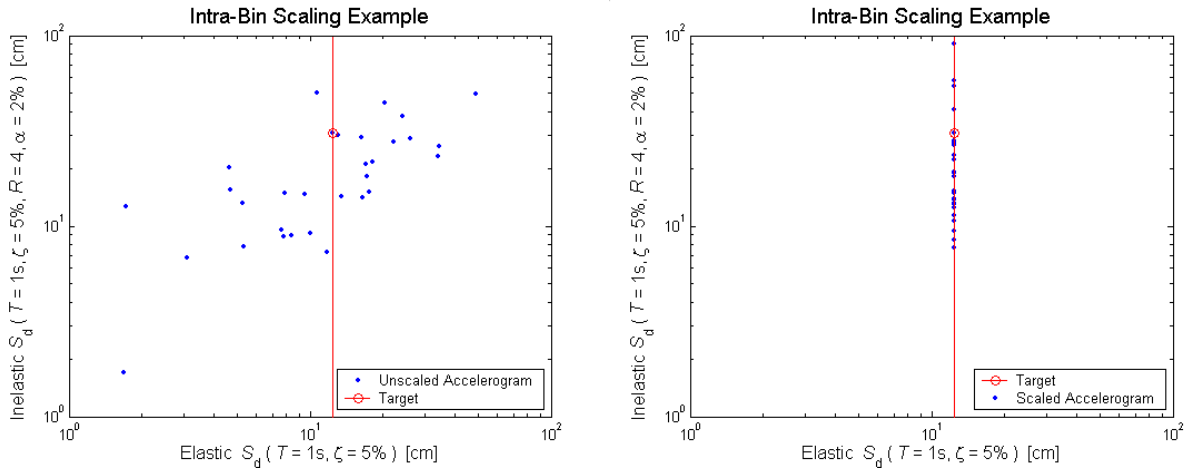


Figure 9. . Inelastic spectral displacement responses (versus elastic spectral displacement, which is proportional to spectral acceleration) (a) before and (b) after scaling (intra-bin) the earthquake records in the Near-Source Bin to a target spectral acceleration of $0.5g$ (or, equivalently, a target elastic spectral displacement of approximately $12cm$).

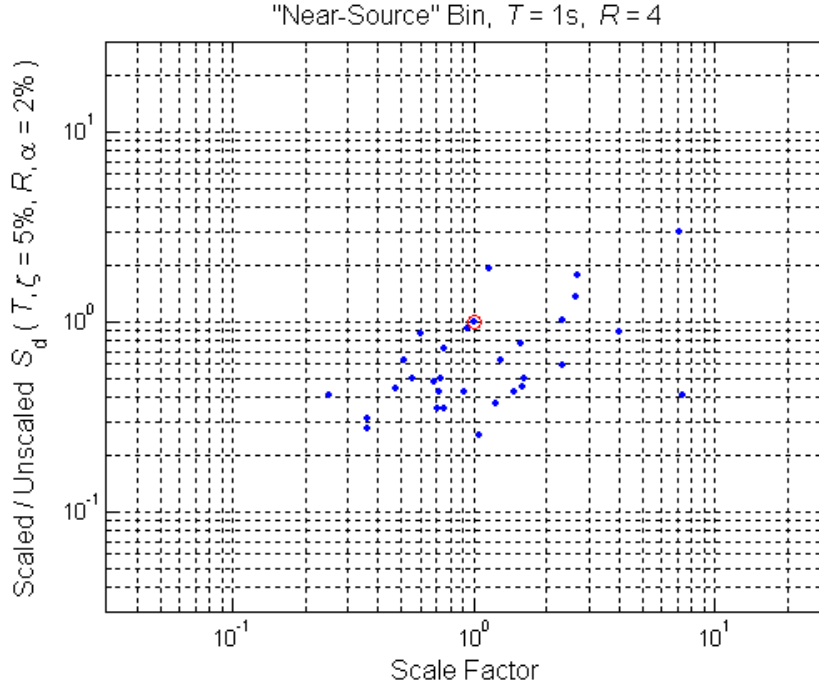


Figure 10. Ratios of the inelastic ($R=4$) spectral displacement responses to (i) the Near-Source records scaled to a target S_a (at $T=1\text{sec}$) of $0.5g$ versus (ii) the un-scaled Near-Source record that is naturally at the target $S_a=0.5g$ (circled in red), all plotted against the corresponding scale factors.

Finally, for all 31 of the target S_a values in the Near-Source Bin (including the highest, next-to-lowest, and median values detailed above), the $r(S_d^I)$ versus scale factor results (analogous to those in Figure 6, Figure 8, and Figure 10) are shown in Figure 11. Recall that each of the 31 records in the bin is scaled to each of the 31 target S_a levels, for a total of 961 data points. Also shown in Figure 11 is a linear (in log-log space) regression fit based on all of the data points. By definition, the regression fit provides the average (expected value) of $\ln[r(S_d^I)]$ for a given value of the scale factor, and therefore the "bias" defined above in Section 3. The parameters of the regression fit, as listed in the figure, indicate that (i) there is no bias when the scale factor is equal to unity (i.e., $a=1$), as expected (but not pre-specified), and (ii) the bias is proportional (in log-log space) to the scale factor, with a slope of $b=0.38$. As examples, at a scale factor of 0.1 and 2 the scaled records result in S_d^I responses that are, on average, 0.4 and 1.3 times higher than un-scaled records, respectively.

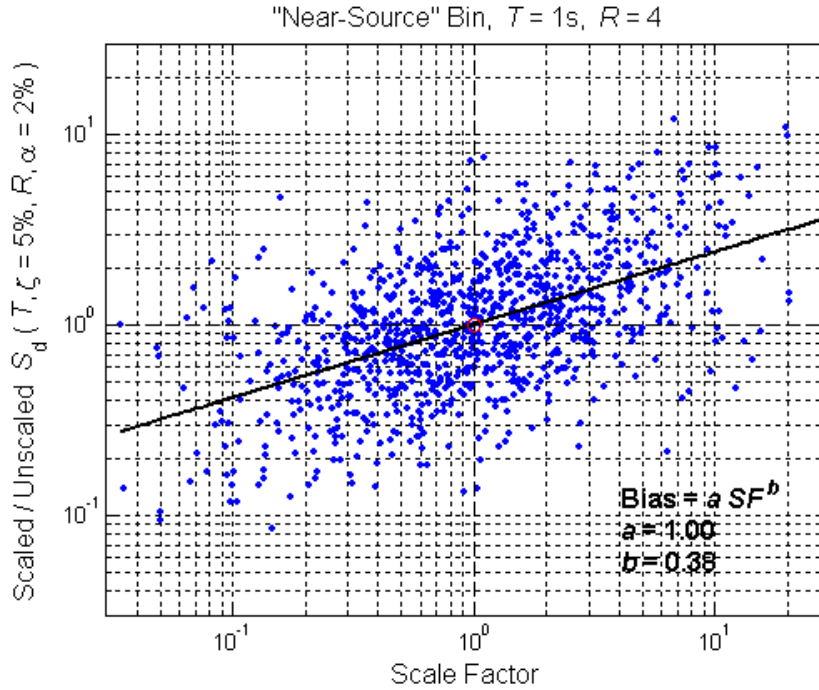


Figure 11. Intra-bin scaling results for the Near-Source earthquake record and the SDOF structure with $T=1$ sec and $R=4$. Note that the blue data points include those shown in Figure 8 and Figure 10 above.

Explanation of Results:

The positive and negative biases observed for scale factors larger and less than one, respectively, can be explained by looking at the shapes of the elastic response spectra for records that are scaled up versus down. In Figure 12a, for example, the response spectra for three of the earthquake records in the Near-Source Bin are highlighted: the "target record" that is naturally (i.e., without scaling) at the target S_d level (in this case $0.5g$), and two records that must be scaled by factors of 6.8 and 0.35 to reach the target S_d . As shown in Figure 12b, after scaling it is apparent that the record scaled by a factor of 6.8 has larger spectral ordinates at periods longer than $T=1$ sec (the period of the oscillator under consideration) than does the target record. As the period of the oscillator, in effect, elongates due to inelasticity, it is therefore expected that the S_d^I response for the scaled record will be larger than that of the un-scaled target record. This is precisely what is observed, on average, in Figure 11 (i.e., positive bias for scale factors greater than one). Conversely, the record scaled by a factor of 0.35 has smaller spectral ordinates than the target record at periods to the right of $T=1$ sec (again, see Figure 12b). It is expected, therefore, to result in smaller S_d^I response than the un-scaled target record, again consistent (on average) with Figure 11.

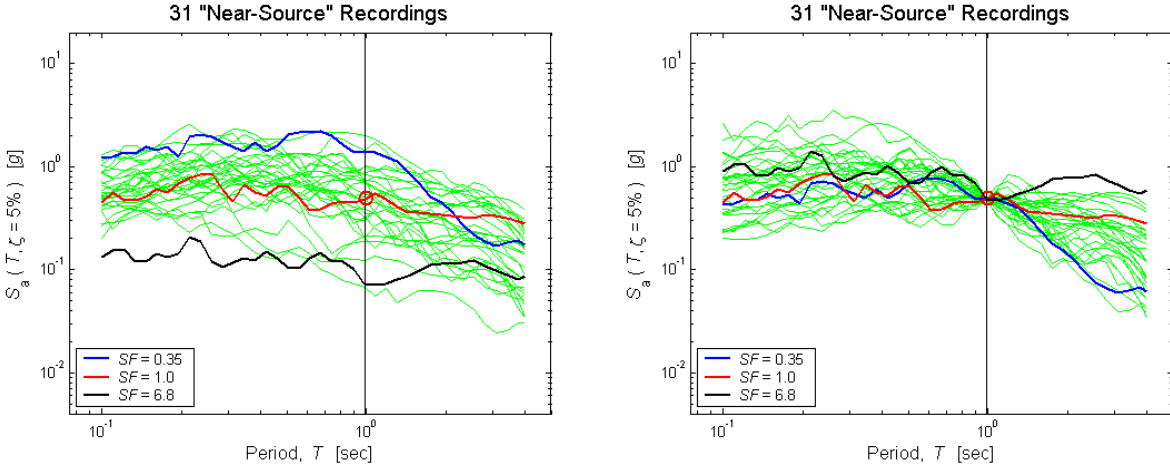


Figure 12. Elastic response spectra for three of the earthquake records in the Near-Source bin **(a)** before and **(b)** after scaling to a target spectral acceleration (0.5g in this case). Note how the spectral ordinates at periods longer than the elastic period of the structure (i.e., $T=1$ sec) are larger for the record that is scaled up, and smaller for the one that is scaled down, relative to the un-scaled response spectrum.

Similar to Figure 12a, Figure 13a shows the median of the elastic response spectra associated with (i) the 10 earthquake records in the Near-Source Bin that have the largest S_a values (at $T=1$ sec), (ii) the 10 that have the smallest, and (iii) the remaining 11 records that have S_a values in between. As noted in the figure, the median of the scale factors needed to reach the target S_a level (0.45g in this case) for each of these three subsets of records is (i) 0.5, (ii) 2.9, and (iii) 1.0. In a more average sense than Figure 12b, Figure 13b also suggests that the spectral shape for records that are scaled up vs. down to the target S_a will result in, respectively, larger vs. smaller S_d^1 responses than records that are naturally at (or near) the target S_a .

Generally speaking, earthquake records that are scaled up to a target S_a are likely scaled up because they exhibit a "pit," or relatively low point in their elastic response spectrum, at the period under consideration. Conversely, records that are scaled down to the target S_a likely exhibit a "peak" in their response spectrum at the period of interest. As demonstrated in Figure 12 and Figure 13, a pit will generally result in biased high S_d^1 response, and a peak in biased low S_d^1 , both relative to un-scaled records.

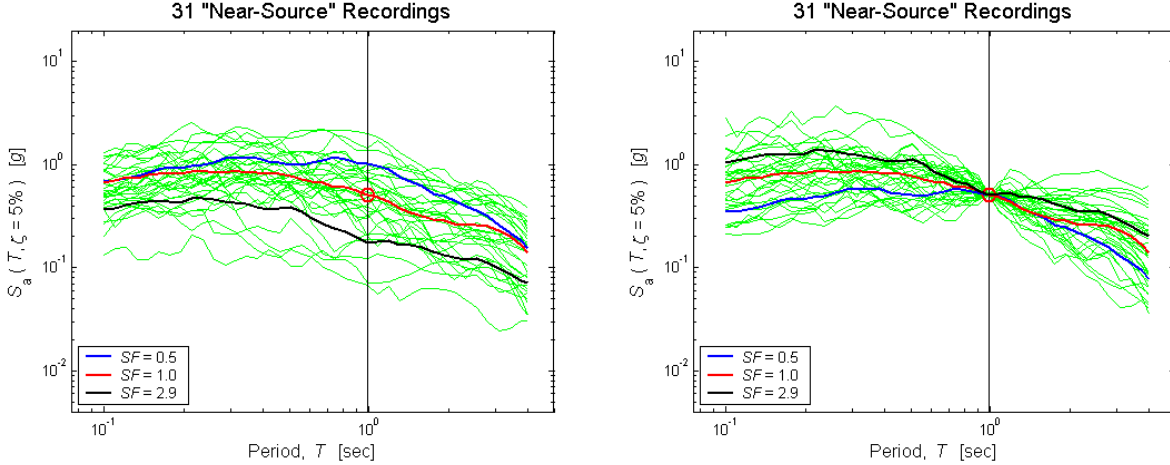


Figure 13. Medians of the elastic response spectra for the 10 largest, the 10 smallest, and the 11 Near-Source earthquake records in between (in terms of their spectral accelerations at $T=1$ sec) **(a)** before and **(b)** after scaling to a target S_a (0.45g in this case). Note how the spectral ordinates at periods longer than the elastic period of the structure are larger for the records that are, on average, scaled up (by a median scale factor of 2.9), and smaller for the ones that are scaled down, both relative to the median response spectrum of the records that are, on average, un-scaled.

Aside:

In Figure 11 above, each data point represents the ratio of (i) the S_d^1 response to a record scaled by the given factor, to (ii) the S_d^1 response to an un-scaled record that is naturally at the target S_a level. Above, this type of data is used to quantify the bias (i.e., average of this ratio) induced by scaling a record by a *single* given factor. Alternatively, one may be interested in quantifying the bias induced by scaling a suite of records, all to a target S_a and hence each by a *different* factor, as a function of the median scale factor. (Again the bias is relative to records that are naturally at the target S_a level.) The same underlying data can be used to investigate this issue, but in a slightly different format, as illustrated in Figure 14 and Figure 15.

The data points shown in Figure 14 are the same ones shown above in Figure 10, namely the $r(S_d^1)$ ratios versus scale factors for the "loop" of the procedure in which the 31 records in the Near-Source Bin are scaled to its median S_a (conventional median, not geometric mean). Also depicted in the figure is the point defined by (i) the median (geometric mean) of the 31 scale factors, and (ii) the median of the 31 $r(S_d^1)$ values.

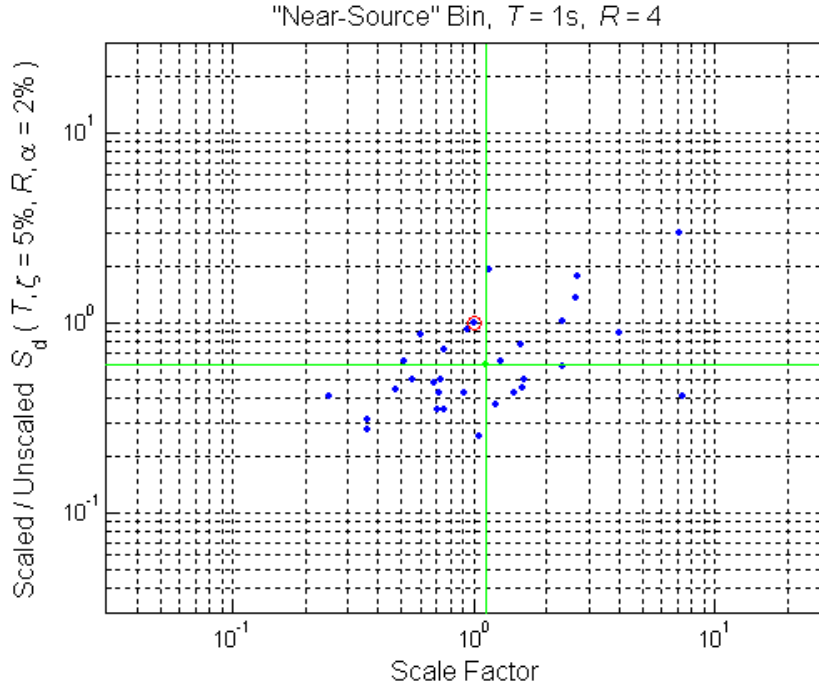


Figure 14. Medians (in green) of the scaled/un-scaled S_d^1 ratios and the corresponding scale factors from Figure 10 above, which illustrated the results of scaling the Near-Source earthquake records to a target spectral acceleration of $0.5g$.

Shown in Figure 15 are the median $r(S_d^1)$ versus median scale factor data points, like the one in Figure 14, obtained after scaling the records in the Near-Source Bin to all 31 of the target S_a levels considered. Also shown in the figure is a log-log linear regression fit to these 31 data points, with its parameters noted. This line gives the bias of the median S_d^1 response for a suite of records that have been scaled, on average, by a given median scale factor. Note from the parameters that this line is precisely the same as that found in Figure 11 using all 31x31 of the underlying data points, as can be expected based upon the nature of (log-log) linear regression. Hence, in summary, the bias of a record scaled by a factor of SF is equivalent in value to bias of the median a suite of records scaled, on average, by a *median* factor of SF .

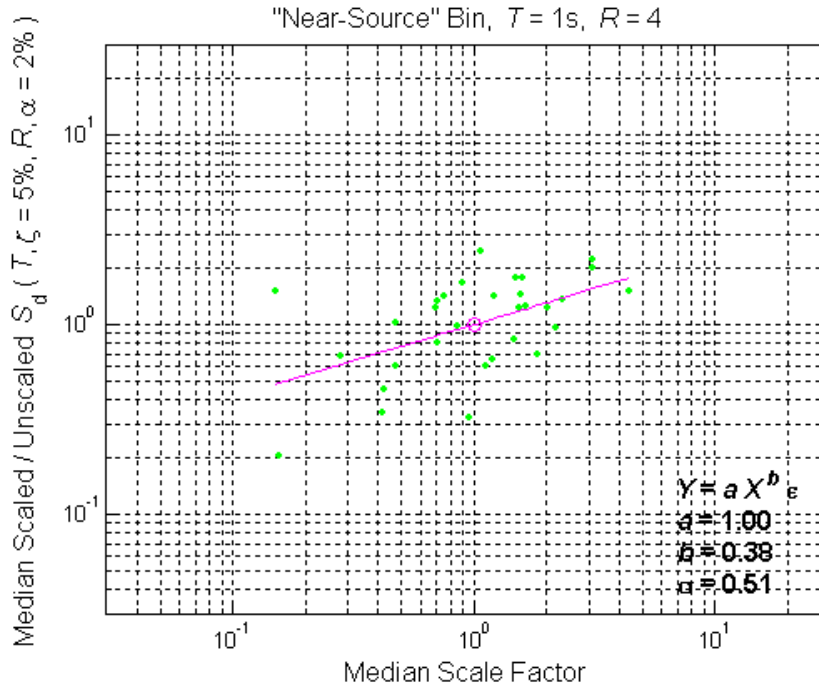


Figure 15. Bias (shown with magenta line) of the median inelastic spectral displacement (at $T=1\text{sec}$ and $R=4$) from the suite of 31 Near-Source earthquake records scaled by the median factor on the abscissa. Note that this is equivalent to the bias for a single Near-Source record scaled by a given factor, which was presented above in Figure 11. One of the green data points shown in the figure is from Figure 14.

8.1.1.2 Bins I-VI, Moderate Period and Strength Structure

Besides the Near-Source Bin, recall that 6 other bins of earthquake records are considered in this study (as described in Section 5). Still for the same $T=1\text{sec}$ and $R=4$ "moderate" oscillator considered in the preceding subsection, the bias versus scale factor regression fits (but not the underlying data) obtained via the same intra-bin scaling procedure demonstrated above are illustrated in Figure 16 for all 7 of the bins. Plots of the data upon which these regression fits are based, as well as the resulting regression parameters (a and b) are provided in the Appendix.

Note from Figure 16 that intra-bin scaling within the Near-Source Bin results in, for this SDOF structure, the largest bias in S_d^1 response for a given scale factor; at the other end of the spectrum, Bin III ($M_w=6.4-6.8$, $R_{\text{close}}=30-50\text{km}$) results in the smallest bias. It is somewhat appropriate that these two bins bracket the results, because one might expect the Near-Source Bin and Bin III to be, respectively, the most aggressive and most benign of those considered in terms of S_d^1 response. The trend over the other 5 bins of records, unfortunately, is not as clear, even in light of the median response spectra for all the bins (shown in Figure 2).

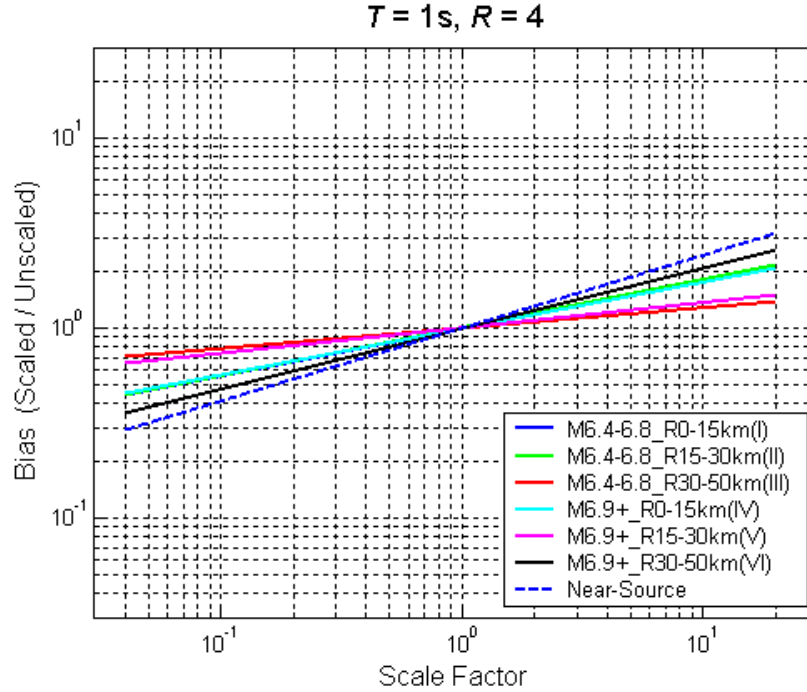


Figure 16. Bias in inelastic spectral displacement (for an SDOF structure with $T=1\text{sec}$, $R=4$) induced by intra-bin scaling within each of the seven different bins of the earthquake records. Note that the lines for Bins I, II, and IV are nearly coincident. The line for the Near-Source Bin is the same as the regression fit in Figure 11.

8.1.1.3 Near-Source Bin, All Structures

To this point, the results presented are for the $T=1\text{sec}$ and $R=4$ oscillator only, but as described above in Section 6.1, SDOF structures of several other periods and strengths are considered in this study. In Figure 17, the log-log linear regression fits based on data like those in Figure 11 (above) are provided for oscillators with (a) a period of $T=1\text{sec}$ but strengths ranging from $R=1$ to 10, and (b) a strength of $R=4$ but periods ranging from $T=0.1$ to 4seconds. Plots of the data upon which these regression fits are based, as well as the resulting regression parameters (a and b) are provided in the Appendix.

From Figure 17a it is apparent that the stronger the oscillator (i.e., the lower the R), the smaller the bias in S_d^1 induced by a given scale factor, at least if $T=1\text{sec}$. In the limit ($R=1$), there is no bias induced for any scale factor because the oscillator is elastic and hence its response is simply equal to the target spectral displacement, which is proportional to the target S_a .

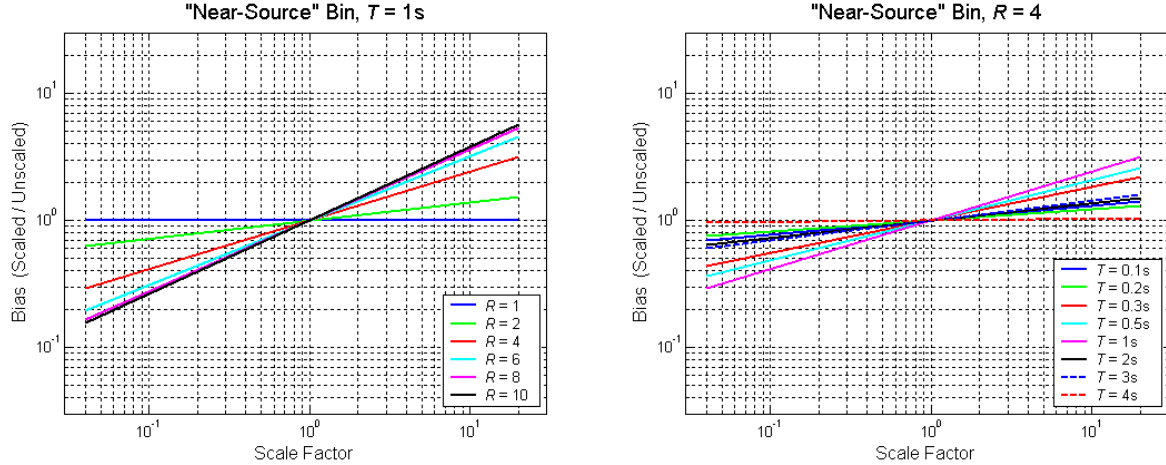


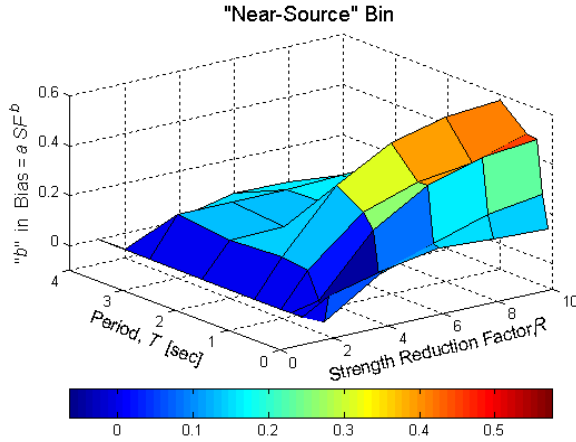
Figure 17. Bias in inelastic spectral displacement induced by intra-bin scaling with the Near-Source Bin for SDOF structures with (a) a period of $T=1$ sec but R ranging from 1 to 10, and (b) T ranging from 0.1 to 4sec but a strength reduction factor of $R=4$.

From Figure 17b we see that, at the $R=4$ strength level, the bias for the $T=1$ sec oscillator considered in preceding subsections is the larger (for a given scale factor) than that for any of the other periods considered. This may be linked to the predominant period of the pulse-like records in the Near-Source Bin. At the other end of the spectrum, note that for the $T=4$ sec oscillator there is nearly no bias in S_d^1 induced at any scale factor. It can be reasoned that at $T=4$ sec the "equal-displacements rule" applies (more so than at the other periods), such that the S_d^1 response is roughly proportional to the target S_a , and hence the results are similar to those for an elastic ($R=1$) oscillator (i.e., no bias, as seen in Figure 17a).

To summarize the results for all 48 combinations of period (T) and strength (R) considered, the slope (in log-log scale) of each bias versus scale factor regression fit, denoted b , is plotted as a function of T and R in Figure 18. (The regression parameter a , which gives the bias for a scale factor of one, is not plotted because it is always equal to unity.) As already observed in Figure 17, the value of b , and thereby the bias at a given scale factor (since $a=1$), is relatively small for the stronger (approaching $R=1$) and longer period (approaching $T=4$ sec) oscillators.

8.1.1.4 Summary

Depending, of course, on the vibration period (T) and strength (R) of the SDOF structure, the results presented above demonstrate that scaling earthquake records up can result in nonlinear structural responses (in this case inelastic spectral displacements) that are biased high, whereas the converse is true for scaling down (i.e., scale factor less than unity). The magnitude of the bias for a given scale factor is smaller for longer period structures and for stronger (closer to elastic) structures; it also depends on the characteristics (e.g., M_w and R_{close}) of the earthquake records that are scaled. More specific comments regarding the magnitude of the bias can be found in Section 9, the overall summary of results.



	"b" in Bias = a*SF^b						Min	Max
	R = 1	R = 2	R = 4	R = 6	R = 8	R = 10		
T = 0.1	0.00	0.06	0.11	0.16	0.14	0.13	0.00	0.16
T = 0.2	0.00	-0.05	0.09	0.17	0.23	0.26	-0.05	0.26
T = 0.3	0.00	0.03	0.26	0.39	0.45	0.48	0.00	0.48
T = 0.5	0.00	0.13	0.31	0.39	0.42	0.48	0.00	0.48
T = 1	0.00	0.14	0.38	0.51	0.56	0.58	0.00	0.58
T = 2	0.00	0.14	0.14	0.16	0.18	0.19	0.00	0.19
T = 3	0.00	0.15	0.16	0.16	0.16	0.17	0.00	0.17
T = 4	0.00	-0.06	0.01	0.06	0.06	0.04	-0.06	0.06
Min	0.00	-0.06	0.01	0.06	0.06	0.04	-0.06	0.06
Max	0.00	0.15	0.38	0.51	0.56	0.58	0.00	0.58

Figure 18. Slope with respect to scale factor (in log-log space) of the bias in inelastic spectral displacement induced by intra-bin scaling within the Near-Source Bin for SDOF structures of a range of periods and strength reduction factors. Note that larger values of the slope b translate into larger biases for a given scale factor (since $a=1$ for intra-bin scaling).

8.1.2 Inter-Bin Scaling

To reiterate, inter-bin scaling involves the scaling of an earthquake record from a "source" M_w - R_{close} bin to a S_a level associated with a different M_w - R_{close} "target" bin. The purpose of inter-bin scaling is to obtain a record for an empty (or sparsely populated) M_w - R_{close} target bin, although here the target bins considered must be adequately populated in order to maintain a basis of comparison. It is assumed that the results presented here can be extrapolated to inter-bin scaling cases for which the number of records in the target bin is minimal (e.g., $M_w > 7.6$).

Detailed results for two different inter-bin scaling scenarios, namely (i) Bin III to Bin I and (ii) Bin I to the Near-Source Bin, are provided here, followed by a summary of results for 8 other inter-bin combinations. The detailed results are for the same moderate period ($T=1$ sec) and strength ($R=4$) oscillator considered above in the detailed intra-bin scaling results (i.e., in Sections 8.1.1.1 and 8.1.1.2), but all of the periods and strengths considered are included in the summary of results.

8.1.2.1 Bin III to Bin I, Moderate Period and Strength Structure

Recall from Section 5 that the "target bin" for this inter-bin scenario, namely Bin I, includes earthquake records with $M_w=6.4-6.8$ and $R_{close}=0-15$ km. The "source bin," Bin III, on the other hand, is also made up of records with $M_w=6.4-6.8$, but with $R_{close}=30-50$ km. Bin I is used as the target bin (and Bin III as the source bin) here because, in general, earthquake records at shorter distances are in shorter supply and hence are more likely to be the target for inter-bin scaling.

Step 1:

As illustrated in Figure 19a, the first target S_a (at $T=1$ sec) considered is $0.4g$. This target S_a is associated with the 1979 Imperial Valley Brawley Airport (H-BCR140) record in Bin I (the target bin), whose elastic response spectrum is highlighted in the figure to distinguish it from the response spectra for the 73 records in Bin III (the source bin).

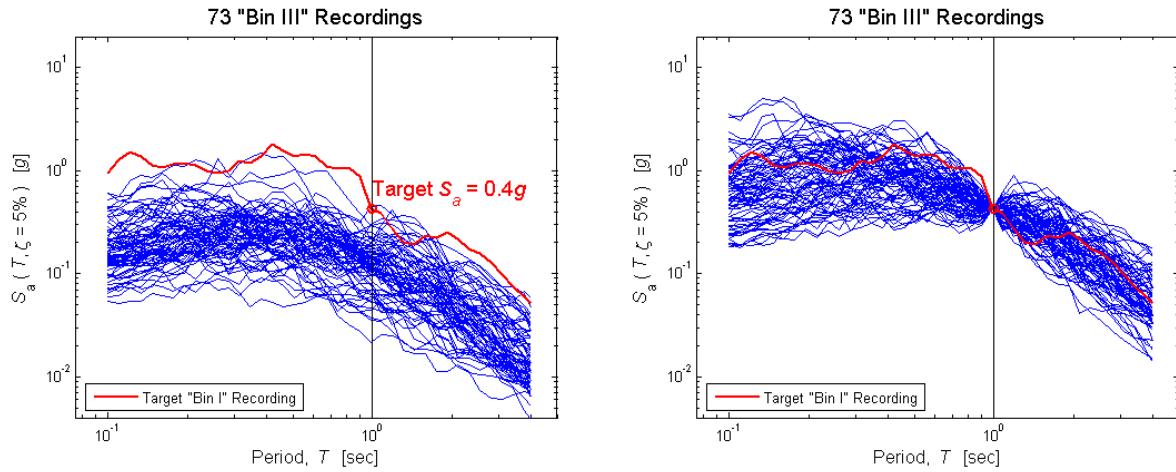


Figure 19. Elastic response spectra (a) before and (b) after scaling (inter-bin) the earthquake records in Bin III ($M_w=6.4-6.8$, $R_{close}=30-50$ km) to a target spectral acceleration associated with Bin I ($M_w=6.4-6.8$, $R_{close}=0-15$ km). The response spectrum in red is for the earthquake record in Bin I (the target bin) that is naturally at the target $S_a=0.4g$.

Step 2:

Recall that the S_d^1 response to the un-scaled target record specified in Step 1 serves as a "true" S_d^1 for this target S_a level; its value (9.2cm) is shown in Figure 20a, along with the S_d^1 values for (i) the other un-scaled records in the target bin (Bin I), and (ii) the source bin (Bin III) records before they are scaled.

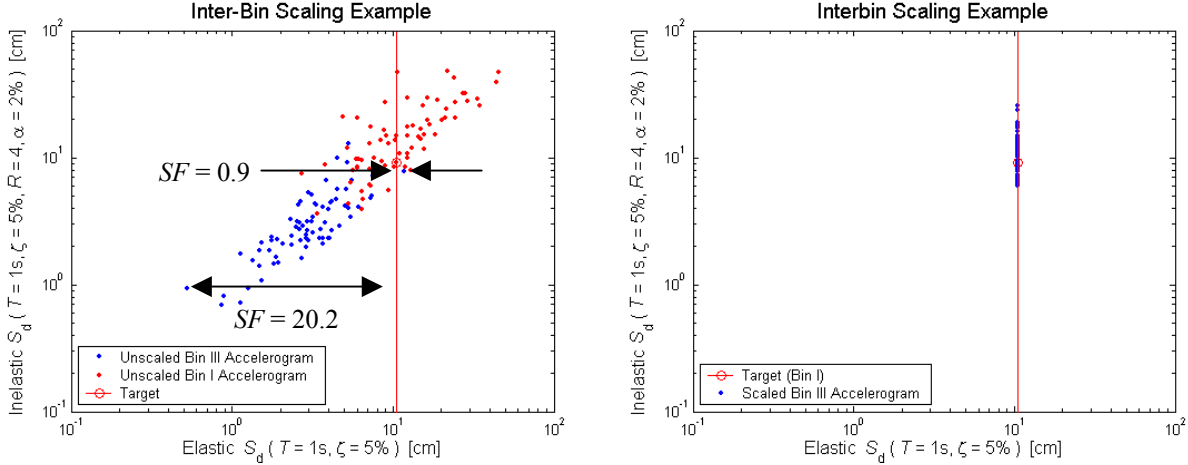


Figure 20. Inelastic spectral displacement responses (a) before and (b) after scaling (inter-bin) the earthquake records in Bin III to a target spectral acceleration associated with Bin I (namely $S_a=0.4g$ or, equivalently, $S_d=10\text{cm}$). For comparison, the S_d^I responses to the un-scaled earthquake records in Bin I (the target bin) are also shown. The S_d^I response to the un-scaled target bin record (circled in red) serves as the "true" response for this iteration of the procedure.

Step 3:

The elastic response spectra after scaling all of the records in the source bin (Bin III) to the target S_a ($0.4g$) are shown in Figure 19b, still with the response spectrum for the target record highlighted. As depicted in Figure 20a, the scale factors in this case range from 0.9 to 20.2.

Step 4:

For all 73 of the source-bin records scaled in Step 3, the S_d^I values are shown in Figure 20b. Note that most of the S_d^I values are larger than the "true" S_d^I of the un-scaled target record.

Step 5:

The ratios of the S_d^I values for the scaled source-bin records (from Step 4) to that for the un-scaled target record (Step 2), which are denoted in the text as $r(S_d^I)$, are plotted against the corresponding scale factors in Figure 21. No trend with the scale factor is apparent, but the average ratio appears to be slightly greater than unity, suggesting that the inter-bin scaled records are biased high, albeit mildly. This, perhaps, can be expected given the shape of the response spectrum for the target record (shown in Figure 19), but recall (e.g., from the intra-bin scaling results that the record-to-record variability of S_d^I for un-scaled records with the same (or similar) values of S_a prevents us from drawing general conclusions before Steps 1-5 are repeated (in Step 6) for the other 72 target records and S_a levels in Bin I.

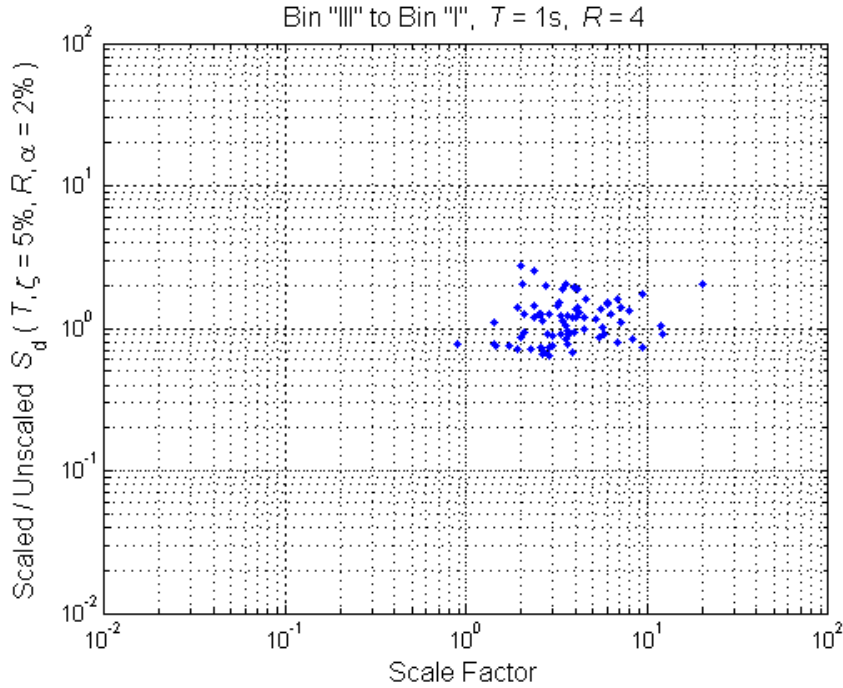


Figure 21. Ratios of the inelastic spectral displacement responses to (i) the Bin III (source bin) records scaled to the target $S_a=2.0g$ versus (ii) the un-scaled Bin I (target bin) record that is naturally at $S_a=2.0g$, both from Figure 20b..

Step 6:

For all 73 of the target S_a values associated with the earthquake records in Bin I, the $r(S_a^I)$ versus scale factor results (including those shown in Figure 21 for the first target S_a) are plotted in Figure 22. Recall that each of the 73 records in the source bin (Bin III) is scaled to each of the 73 target S_a levels associated with the target bin (Bin I), for a total of 5329 data points. Also shown in Figure 22 is the log-log linear regression fit based on all of the data points, and its parameters, a and b. Recall that the regression fit, by definition, provides the average (expected value) of $\ln[r(S_a^I)]$ for a given value of the scale factor, and hence quantifies the "bias" induced by, in this case, inter-bin scaling. The parameters of the regression fit indicate that (i) when the scale factor is equal to unity, the S_a^I response to the scaled records is biased low (i.e., $a=0.61$), and (ii) the bias increases linearly (in log-log scale) with scale factor (i.e., $b=0.19$), as found for intra-bin scaling.

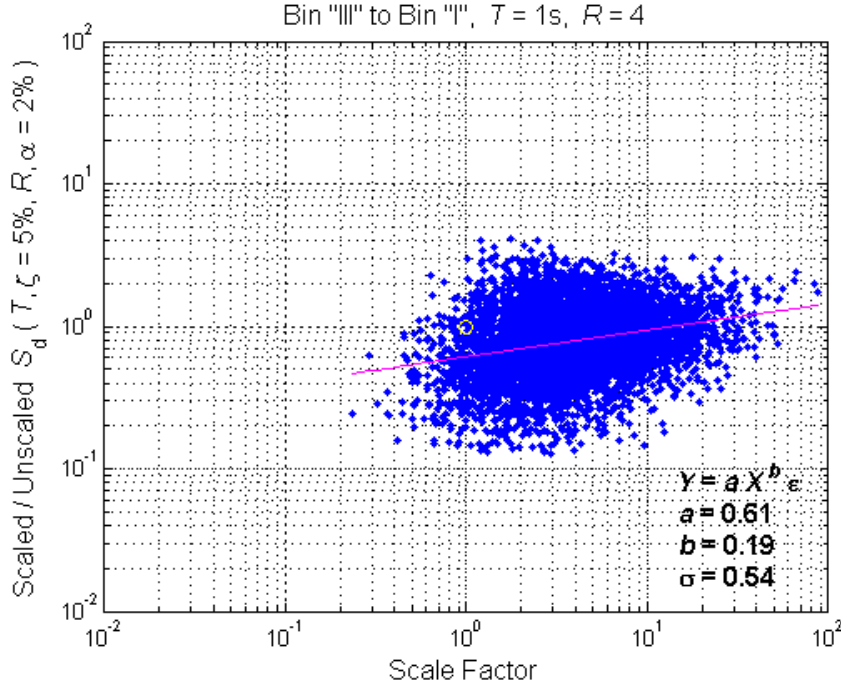


Figure 22. Inter-bin scaling results for the Bin III to Bin I case and the SDOF structure with $T=1\text{sec}$ and $R=4$. The blue data points include those shown in Figure 21 above. The magenta line gives the bias in inelastic spectral displacement response induced by a given inter-bin scale factor.

Explanation of Results:

The same "peak versus pit" concept used to explain the intra-bin scaling results can be used to explain the $r(S_d^1)$ versus scale factor results observed in Figure 22 for inter-bin scaling. As evident from Figure 20a above, scale factors near unity are usually obtained when a source-bin record with a relatively large S_a value for its M_w and R_{close} (likely because there is a peak in its elastic response spectrum at the period under consideration) is scaled to the target S_a level associated with a target-bin record that is naturally at a relatively low S_a value for its M_w and R_{close} (likely because it is in a pit of its response spectrum). Since the "peaked" source-bin record is expected to produce relatively small S_d^1 response, especially as compared to a "pitted" target-bin record, it is expected that the bias in S_d^1 response at a scale factor of unity will be less than one (i.e., biased low S_d^1), as was observed in Figure 22.

Given the explanation above, one might expect to find that the S_d^1 response to inter-bin scaled records is unbiased at a scale factor equal to the average separation (in terms of S_a) between the target and source bins. It is around this scale factor that one would expect to find $r(S_d^1)$ results for "peaked" source-bin records scaled to "peaked" target-bin records, for example. After scaling the source-bin (Bin III) records by the ratio of the median S_a for the target (Bin I) and source bins (before scaling), the S_a (actually, $S_a = S_a * (T/2\pi)^2$) and S_d^1 values for the two bins are illustrated in

Figure 23. In this case, the ratio of the median S_a values, denoted here as $r(m[S_a])$, is equal to 3.8.

To check whether the S_d^I response to inter-bin scaled source-bin records is unbiased at a scale factor equal to $r(m[S_a])$, the scale factor axis in Figure 22 is divided by $r(m[S_a])=3.8$ and re-plotted in Figure 24. From the figure we see that there is still a bias at an "adjusted" scale factor of one, although it is smaller than before (i.e., $a=0.79$ versus 0.61 in Figure 22). As will be demonstrated in the subsequent section (for the second inter-bin scaling scenario), the remaining bias can be explained by considering the differences in the shapes of the elastic response spectra for the source and target bins.

Note that in all of the inter-bin scaling results to follow, the scale factors reported have already been divided by the ratio of the median S_a values for the target and source bins, $r(m[S_a])$. In other words, what is reported hereafter is the scale factor after the source-bin has been pre-scaled by the average S_a separation between the source and target bins, or $r(m[S_a])$. This factor for pre-scaling can be quantified using an attenuation relation, but here it is calculated based upon the specific records in each bin.

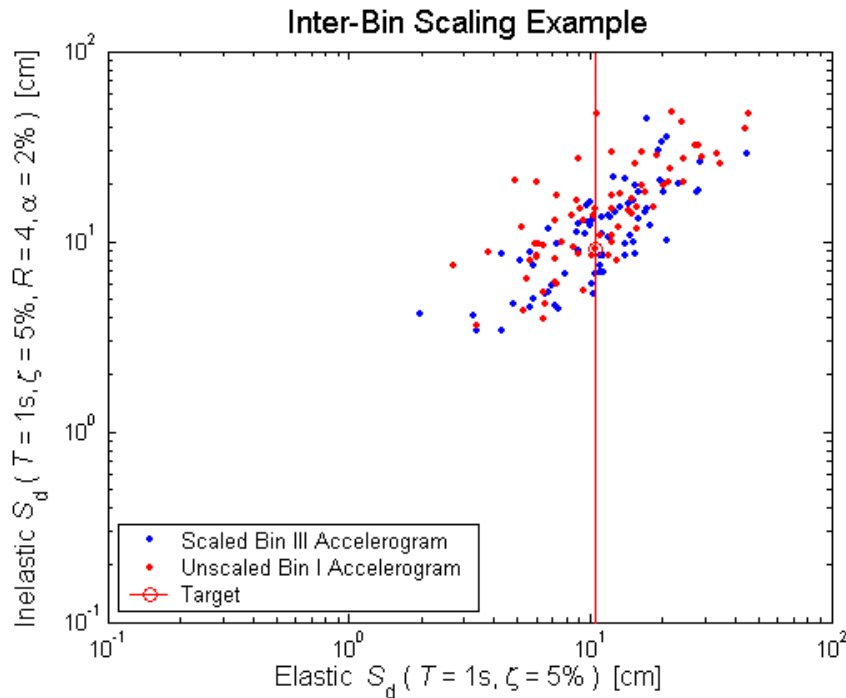


Figure 23. Illustration of "pre-scaling" the earthquake records in the source bin (Bin III) by a common factor such that their median spectral acceleration (or spectral displacement) matches that of the target bin (Bin I). This pre-scaling factor is removed (by division) from the scale factors in Figure 22 to obtain Figure 24.

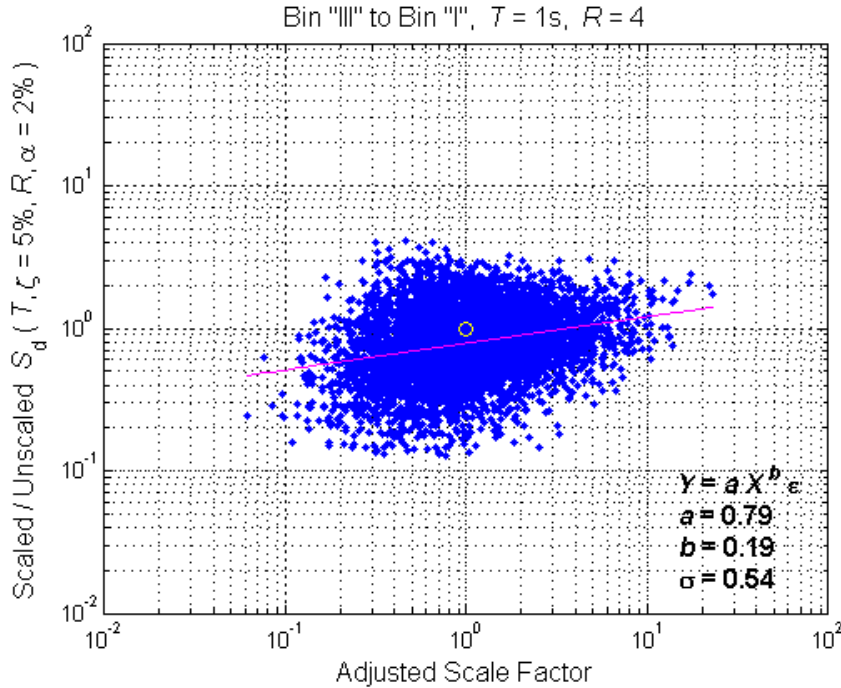


Figure 24. Inter-bin scaling results *after* removing the "pre-scaling" factor illustrated in Figure 23 from the un-adjusted results shown in Figure 22. The ratio of the median spectral accelerations for the target and source bins is *not* included in the adjusted scale factor.

8.1.2.2 Bin I to Near-Source Bin, Moderate Period and Strength Structure

The results detailed here consider the same target ground motion scenario ("Near-Source") and SDOF structure ($T=1s$, $R=4$) that was considered in Section 8.1.1.1 on intra-bin scaling. In order to consider inter-bin scaling, here earthquake records from a different "source" bin are scaled, namely those from "Bin I". Recall from the descriptions in Section 5 that Bin I is similar in M_w and R_{close} to the Near-Source bin, but Bin I includes records from backward as well as forward directivity conditions, and is comprised of random horizontal components rather than strictly strike-normal components. As a result, Bin I includes fewer pulse-like records as compared to the Near-Source bin.

The ratios of the S_d^I responses to scaled source-bin records versus un-scaled target bin records (i.e., $r(S_d^I)$ values) are plotted in Figure 25 as a function of the scale factor. Recall that each of the 73 records in Bin I, the source bin, is scaled to each of the 31 target S_a levels associated with the target Near-Source Bin, for a total of 2263 data points. The log-log linear regression fit to all of these data points and its parameters, a and b , are also shown in Figure 25.

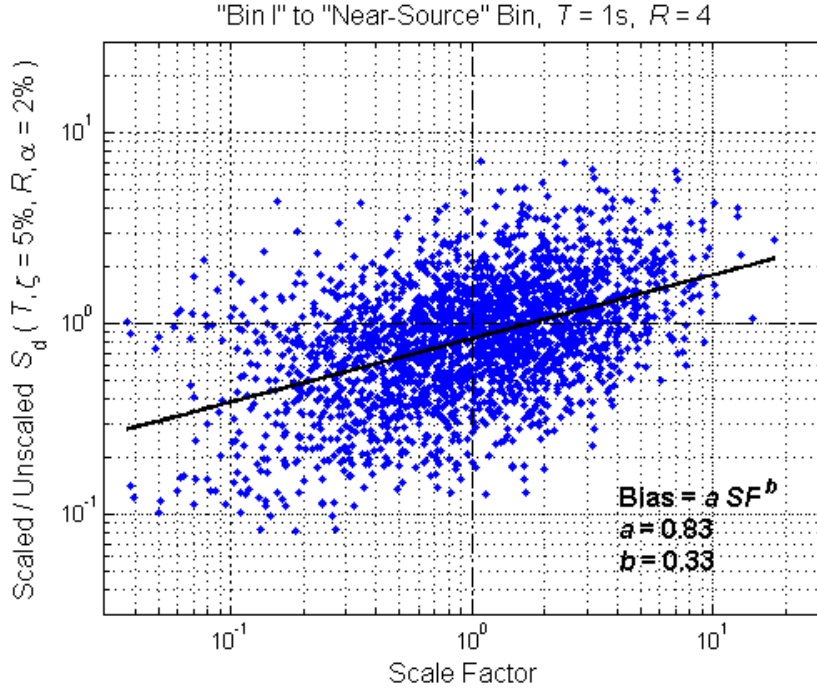


Figure 25. Inter-bin scaling results for the Bin I to Near-Source Bin case, still for the SDOF structure with $T=1.0$ sec and $R=4$. The scale factor presented here (and hereafter) has already been divided by the pre-scaling factor that brings the median S_a of the source bin (Bin I) to that of the target bin (Near-Source).

Similar to the results for the Bin III to Bin I scenario considered in the preceding subsection, note from Figure 25 that there is a bias at a scale factor of unity (i.e., $a=0.83$). Recall that here the source-bin records have been pre-scaled, all by a single factor, such that the median of their S_a values is equal to that of the target bin. The median elastic response spectrum for (i) Bin I (the source bin), after the pre-scaling, and (ii) the Near-Source Bin (the target bin), is illustrated in Figure 26. Note that at periods longer than that of the structure under consideration here (i.e., $T=1$ sec), the median response spectrum for Bin I drops off more quickly than that for the Near-Source Bin. As a result, it is expected that the S_d^I response to the Bin I records will, on average, be smaller than that to the records in the Near-Source Bin. This is precisely what was observed in Figure 25, which indicated that after the pre-scaling alone (i.e., at a scale factor of unity in the figure), the S_d^I response of the source-bin (Bin I) records is biased low relative to the target Near-Source Bin. If one looks back at the median response spectra (before any scaling) for Bin III and Bin I shown in Figure 4, the same explanation can also be made for the inter-bin scaling results reported in the preceding section.

Another observation to note from Figure 25 above is that the log-log slope of the bias versus scale factor, $b=0.33$, is rather similar to that observed from the intra-bin scaling results for the same target bin and structure, namely $b=0.39$ from Figure 11. This similarity will be commented on further in the subsequent subsection.

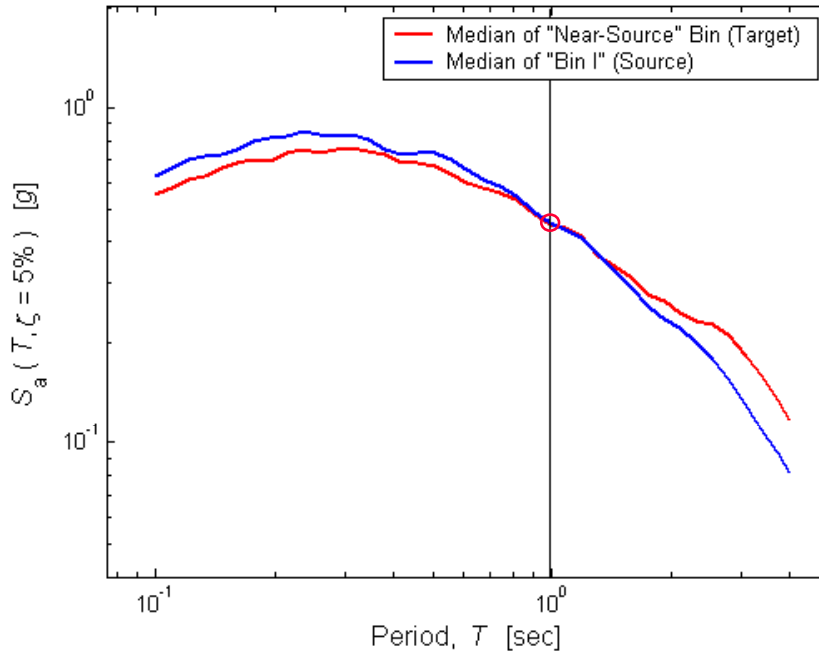
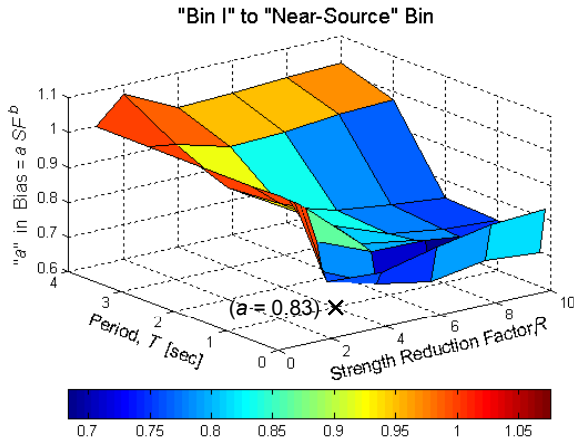


Figure 26. Median elastic response spectra for the earthquake records in Bin I (the source bin) and the Near-Source Bin (the target). Note that the median spectra happen to match at $T=1.0$ sec (the period of the structure under consideration), so no "pre-scaling" is necessary. The higher spectral amplitudes at periods above 1.0sec suggest that the inelastic response to the near-source records will be larger than that to the records in Bin I.

8.1.2.3 Bin I to Near-Source Bin, All Structures

For all of the SDOF structures considered in this study, but still for the Bin I to Near-Source Bin inter-bin scaling scenario considered in the preceding subsection, a graphical summary of the regression parameters a and b is provided in Figure 27 (for a) and Figure 28 (for b). Recall that the parameter a quantifies the bias in S_d^1 induced by merely pre-scaling the source-bin records by a single factor such that their median S_a (at the particular T) is equal to that of the records in the target bin (i.e., "adjusted" scale factor $SF=1$). The parameter b , on the other hand, quantifies how quickly the bias increases (or decreases) with increasing (or decreasing) scale factor (not including, or after, the pre-scaling).

Similar to what was observed for the b values in the intra-bin scaling results, the values of a for inter-bin scaling (shown in Figure 27) approach unity (no bias) for longer period and stronger structures (e.g., $T=4$ sec and $R=1$). For shorter period and weaker structures, the bias quantified by a appears to increase. The smallest value of a (and most bias) observed is 0.68, for $T=0.2$ sec and $R=6$.



		"a" in Bias = a*SF^b							
		R = 1	R = 2	R = 4	R = 6	R = 8	R = 10	Min	Max
T = 0.1		1.00	0.76	0.75	0.79	0.82	0.83	0.75	1.00
T = 0.2		1.00	0.78	0.71	0.68	0.71	0.70	0.68	1.00
T = 0.3		1.00	0.86	0.80	0.80	0.78	0.76	0.76	1.00
T = 0.5		1.00	0.95	0.81	0.79	0.75	0.73	0.73	1.00
T = 1		1.00	0.93	0.83	0.78	0.75	0.74	0.74	1.00
T = 2		1.00	0.92	0.83	0.79	0.77	0.75	0.75	1.00
T = 3		1.00	0.99	0.95	0.95	0.97	0.98	0.95	1.00
T = 4		1.00	1.08	1.00	1.01	1.02	1.02	1.00	1.08
Min		1.00	0.76	0.71	0.68	0.71	0.70	0.68	1.00
Max		1.00	1.08	1.00	1.01	1.02	1.02	1.00	1.08

Figure 27. Bias at a scale factor of unity (after pre-scaling), given by a , for the Bin I to Near-Source Bin case and SDOF structures of a range of periods and strengths. For the most part, this bias can be explained by the differences between the median elastic response spectra of the source and target bins.

The values of b shown in Figure 28a are very similar to those observed in the intra-bin scaling results for the same target bin (the Near-Source Bin). The difference between the two sets of b values is plotted in Figure 28b, which shows that the two are nearly the same at all but very short periods.

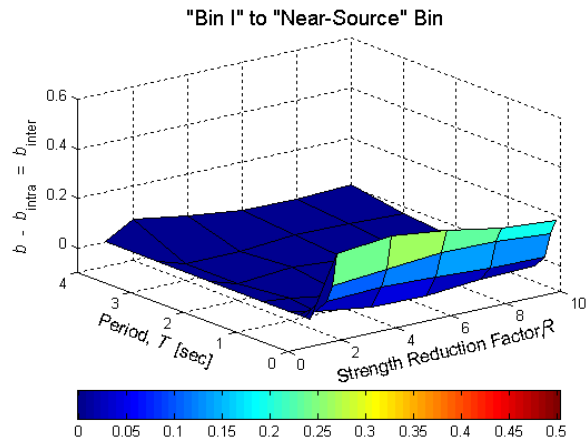
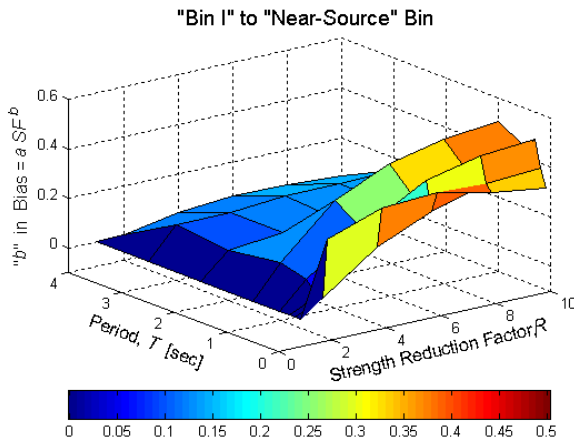


Figure 28. Slope with respect to scale factor (in log-log space) of the bias in inelastic spectral displacement induced by inter-bin scaling from Bin I to the Near-Source Bin for SDOF structures of a range of periods and strength reduction factors. The figure on the right shows that the difference in minimal between the slope b for this inter-bin scaling case and that for intra-bin scaling within the target (Near-Source) bin, except perhaps at short periods.

8.1.2.4 Other Inter-Bin Combinations, All Structures

Including the combinations described above (i.e., Bin III to Bin I, and Bin I to Near-Source Bin), a total of 10 different inter-bin scaling scenarios are considered, as listed in Table 2. Plots like Figure 27 of the regression fit parameter a for these scenarios are left to the appendix. The associated regression parameters, b , for the most part, are similar to those found for intra-bin scaling within the target bin; the latter results are also provided in the appendix.

Table 2. Inter-bin scaling scenarios considered in this study. Detailed results for these scenarios can be found in the appendix.

Scenario #	Source Bin	Target Bin
1	"I" ($M_w=6.4-6.8$, $R_{close}=0-15\text{km}$)	"Near-Source"
2	"Near-Source"	"I" ($M_w=6.4-6.8$, $R_{close}=0-15\text{km}$)
3	"I" ($M_w=6.4-6.8$, $R_{close}=0-15\text{km}$)	"IV" ($M_w=6.9-7.6$, $R_{close}=0-15\text{km}$)
4	"II" ($M_w=6.4-6.8$, $R_{close}=15-30\text{km}$)	"IV" ($M_w=6.9-7.6$, $R_{close}=0-15\text{km}$)
5	"V" ($M_w=6.9-7.6$, $R_{close}=15-30\text{km}$)	"IV" ($M_w=6.9-7.6$, $R_{close}=0-15\text{km}$)
6	"II" ($M_w=6.4-6.8$, $R_{close}=15-30\text{km}$)	"V" ($M_w=6.9-7.6$, $R_{close}=15-30\text{km}$)
7	"III" ($M_w=6.4-6.8$, $R_{close}=30-50\text{km}$)	"V" ($M_w=6.9-7.6$, $R_{close}=15-30\text{km}$)
8	"VI" ($M_w=6.9-7.6$, $R_{close}=30-50\text{km}$)	"V" ($M_w=6.9-7.6$, $R_{close}=15-30\text{km}$)
9	"III" ($M_w=6.4-6.8$, $R_{close}=30-50\text{km}$)	"VI" ($M_w=6.9-7.6$, $R_{close}=30-50\text{km}$)
10	"III" ($M_w=6.4-6.8$, $R_{close}=30-50\text{km}$)	"I" ($M_w=6.4-6.8$, $R_{close}=0-15\text{km}$)

Note that the majority of the scenarios, i.e., #3-9, considered use one of the three larger magnitude bins (IV-VI) as a target and scale records from bins with smaller magnitudes and similar or larger distances. These scenarios are motivated by the fact that the existing database contains fewer records from larger earthquake magnitudes and closer source-to-site distances. In practice, therefore, it is more likely that records from smaller M_w and larger R_{close} bins are scaled to represent larger M_w and smaller R_{close} bins, not vice-versa. (The primary goal of inter-bin scaling, recall, is extrapolation to larger M_w and shorter R_{close} bins.)

It is also assumed here that scaling from "adjacent" bins is more likely than scaling across bins that are more different in magnitude and/or distance (e.g., $R_{close}=30-50\text{km}$ to $R_{close}=0-15\text{km}$). In any case, in this respect only two scenarios are left out: Bin III and VI to Bin IV. Recall that the inter-bin scenario detailed above Section 8.1.2.1 (i.e., #10), however, does consider scaling across two bins in distance (i.e., from Bin III to I), because it is intended to check the most extreme inter-bin scaling within the lower magnitude bins.

Finally, note that scenario #2 (Near-Source Bin to Bin I) is merely included to check that its results are equal and opposite those from the first scenario (which they are).

8.1.2.5 Summary

Inter-bin scaling appears to introduce a bias in inelastic spectral displacement that varies with scale factor in a manner similar to that induced by intra-bin scaling within the target bin. For a given scale factor, this bias is smaller for longer period and stronger (i.e., closer to elastic) oscillators. Unlike intra-bin scaling, however, an additional bias that is roughly independent of scale factor is also introduced. The degree of this bias can be related to the difference between the shapes of the median elastic response spectra for the source and target bins. More specific comments regarding the magnitude of the bias are left to the overall summary in Section 9.

8.2 MDOF Structures

The same procedure for quantifying the effects of intra- and inter-bin scaling that is applied for the SDOF structure in Section 8.1 (as outlined in Section 7) is followed here for the MDOF structures considered in this study, namely the elastic and the ductile 2-D models of a 9-story steel moment-resisting frame building.

Analogous the peak relative displacement response considered for the SDOF structures (i.e., inelastic spectral displacement, S_d^I), the following three drift response measures are considered for the MDOF structures:

θ_{roof} = the peak roof drift ratio (i.e., peak roof displacement relative to the ground, normalized by the height of the roof),

θ_{max} = the maximum, over all stories, peak (over time) inter-story drift ratio, and

θ_i = the peak inter-story drift ratio for story i ($= 1$ to 9).

Like in Sections 8.1.1.1 and 8.1.2.2 for intra- and inter-bin scaling, respectively, the Near-Source Bin is used here as the target (for both intra- and inter-bin scaling), and Bin I is used as the source of earthquake records to scale (for inter-bin scaling). Due to the computational intensity of analyzing the MDOF structures, these are the only intra- and inter-bin scaling cases considered in this study. However, the analogy between the SDOF and MDOF results described below can, perhaps, be used to extrapolate the effects of scaling for the MDOF structures to other intra- and inter-bin cases.

One conceptual difference between the SDOF and MDOF results to note is that the strength of the ductile MDOF structure is *not* modified relative to each target S_a value (which, for the SDOF structure, created "constant R " results). Instead, here the strength of the ductile MDOF structure remains fixed, and hence "constant strength" results are produced. This is done because modifying the strength of an MDOF structure in a realistic fashion is not a straightforward and unique process like it is for SDOF structures. The implications of this difference are described in what follows.

8.2.1 Intra-Bin Scaling

As mentioned above, intra-bin scaling with the Near-Source Bin of earthquake records is considered here, for both the elastic and ductile models of the 9-story SMRF building.

8.2.1.1 Elastic Model

Analogous to Figure 11 above for an SDOF structure with vibration period $T=1$ sec and strength reduction factor $R=4$, the intra-bin scaling results in terms of θ_{roof} and θ_{max} are shown in Figure 29 for the elastic model of the 9-story SMRF building. Since θ_{roof} is dominated by the first mode of response and hence is nearly proportional to first-mode spectral acceleration, it is expected, and observed (in Figure 29a), that intra-bin scaling does not induce a bias in elastic θ_{roof} response (i.e., $a=1$ and $b=0$). In contrast, a bias (albeit relatively minor) in θ_{max} is observed that is proportional in log-log space to the earthquake record scale factor (e.g., a bias of 9% and 32% for scale factors of 2 and 10, respectively). Recall that the bias increases with scale factor for the SDOF structures as well, but for differing reasons, since here the MDOF response is elastic. As one might expect (and as detailed below), the bias in the θ_{max} response is a result of the fact that more than just the first mode contributes significantly to it.

For the second, fifth, and eighth stories of the elastic building model, the intra-bin scaling results for θ_i (i.e., the ratio of the scaled versus un-scaled θ_i results as a function of the scale factor) are shown in Figure 30, alongside those for the ductile building model results to be discussed in the next subsection. The θ_i results for the other six stories, which follow the same trends observed here, are included in the appendix.

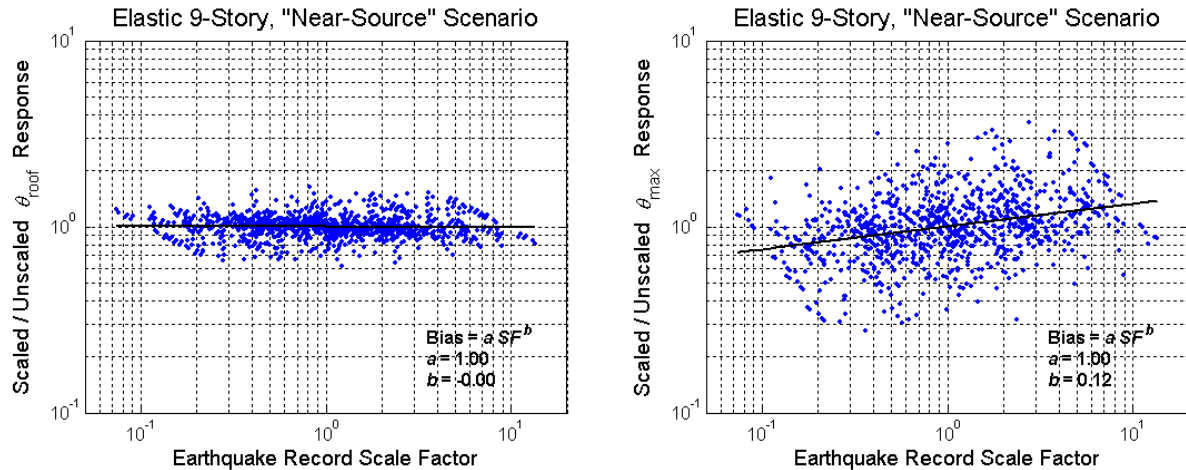


Figure 29. Intra-bin scaling results in terms of (a) peak roof drift ratio (θ_{roof}), and (b) maximum (over all stories) peak inter-story drift ratio (θ_{max}) for the elastic model of the 9-story building considered and the Near-Source Bin of earthquake records.

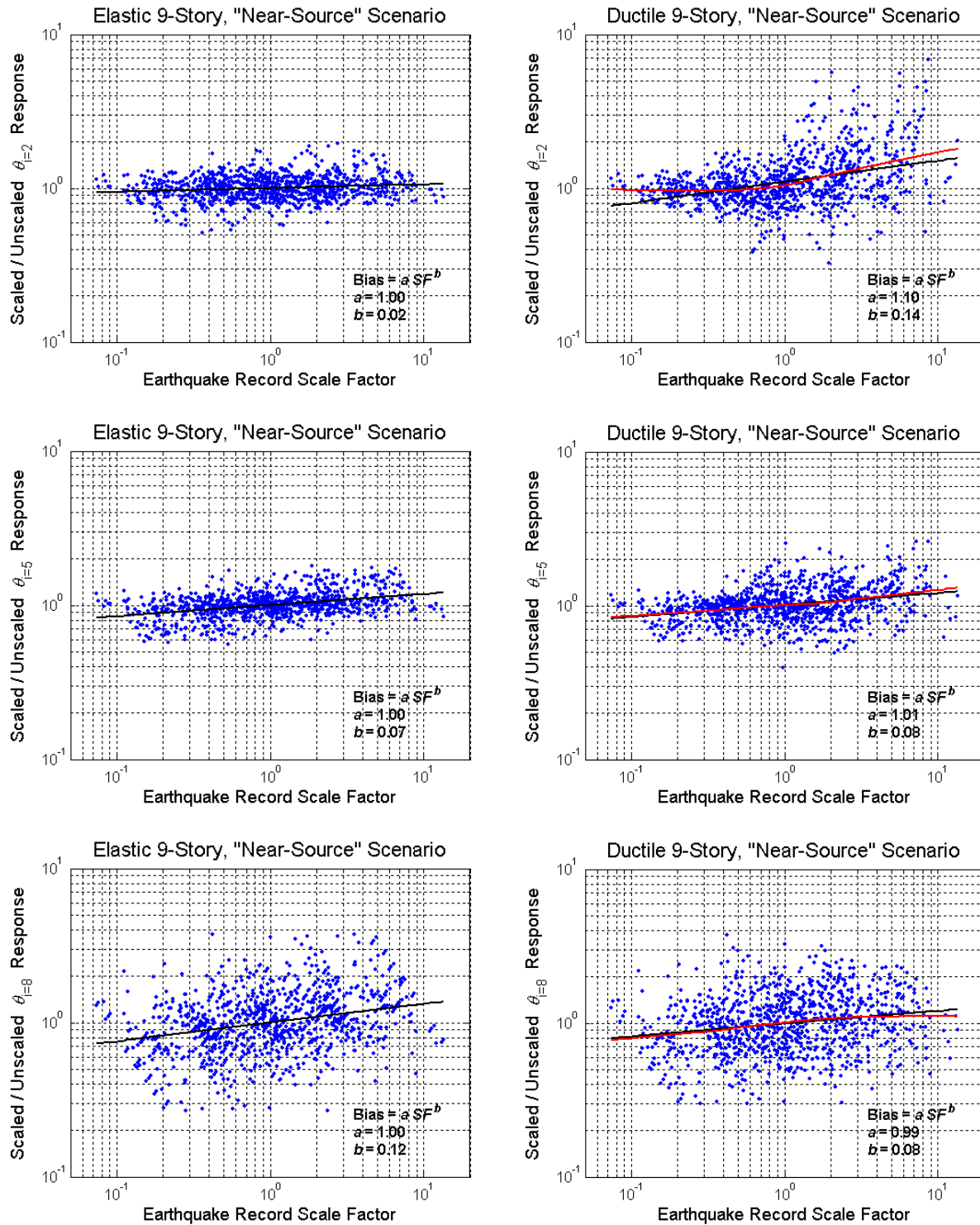


Figure 30. Intra-bin scaling results in terms of the peak inter-story drift ratios (θ_i) at the 2nd story (top row), 5th story (middle row), and 8th story (bottom row), for the elastic (left column) and ductile (right column) models of the 9-story building considered. The curve fit shown in red on the ductile results is obtained via a non-parametric local regression (LOESS). The analogous results for the other 6 of the 9 stories are provided in the appendix.

At the 2nd story, practically no scaling-induced bias in θ_2 is observed in Figure 30 (top left panel, $a=1$ and $b=0.02$) because, like for θ_{roof} , the contribution of higher modes to θ_2 is relatively minor. In contrast, higher modes contribute significantly to the response at the 8th story, θ_8 , and a bias is observed (albeit relatively minor). Note that the extent of the bias in θ_8 is identical to that in θ_{max} (i.e., $b=0.12$) because the maximum inter-story drift ratio typically occurs in the upper stories. The bias in θ_5 is intermediate to those at θ_2 and θ_8 .

The scaling-induced bias observed for the θ_{max} and θ_8 response (in Figure 29a and Figure 30) can be explained by looking at the shapes of the elastic response spectra for records that are scaled up versus down. The same approach was taken to explain the observed bias in inelastic spectral displacement for the SDOF structures, with one fundamental difference: instead of looking at the spectral amplitudes at periods longer than the fundamental period of the structure (to reflect inelasticity), here we look at shorter periods, specifically the second-mode period, since response spectrum analysis concepts apply.

In Figure 31a the median of the elastic response spectra associated with (i) the 10 earthquake records in the Near-Source Bin that have the largest S_a values (at $T=2.3\text{sec}$), (ii) the 10 that have the smallest, and (iii) the remaining 11 records that have S_a values in between. As noted in the figure, the median of the scale factors needed to reach the target S_a level ($0.23g$ in this case) for each of these three subsets of records is (i) 0.5, (ii) 2.6, and (iii) 1.0. After scaling all of the earthquake records to the target S_a , the median response spectra for the same three subsets of records are plotted in Figure 31b. Note how, on average, the records that are scaled up have larger spectral amplitudes at the second-mode period (0.9sec), and those that are scaled down have smaller, relative to the un-scaled records. It is therefore expected, as observed, that the second mode contribution to θ_{max} and θ_8 (and hence the overall response, since the first-mode component is normalized) will be biased high/low for scale factors larger/less than unity.

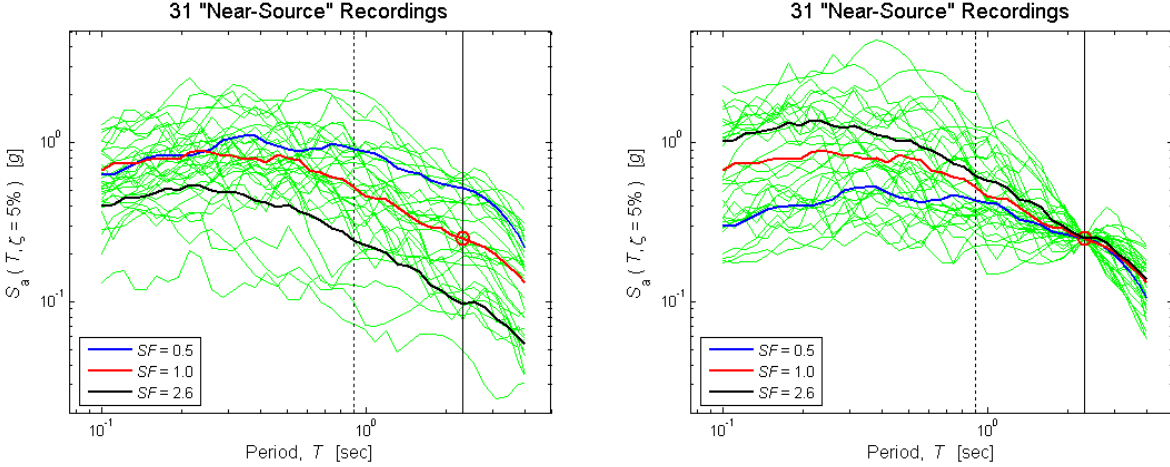


Figure 31. Medians of the elastic response spectra for the 10 largest, the 10 smallest, and the 11 Near-Source earthquake records in between (in terms of their spectral accelerations at $T=2.3$ sec, the fundamental period of the 9-story building) **(a)** before and **(b)** after scaling to a target S_a ($0.23g$ in this case). Note how the spectral ordinate at the second-mode period, $T=0.9$ sec, is larger for the records that are, on average, scaled up (by a median scale factor of 2.6), and smaller for the ones that are scaled down, both relative to the median response spectrum of the records that are, on average, un-scaled.

8.2.1.2 Ductile Model

The analogous results presented in the preceding subsection for the elastic building model are presented here for the ductile model of the building. In Figure 32, the intra-bin scaling results in terms of θ_{roof} and θ_{max} are presented. For θ_{roof} , the data shown in the figure appear to be very similar to that for the elastic building model (shown in Figure 29), up to a scale factor near unity. At higher scale factors, there is a slight "upward swing" in the data, suggesting that the θ_{roof} response to the scaled records is biased high. The change near a scale factor of unity can be explained as a gradual shift from linear elastic to nonlinear inelastic results. It happens to be the case that the overall strength of the ductile building model, in terms of the spectral acceleration that induces notable nonlinearity, is roughly near the median S_a (at $T=2.3$ sec) of the target Near-Source Bin, namely $0.23g$. So, when the target S_a is near $0.23g$, and hence the median scale factor is near unity (not including, recall, the "pre-scaling" factor), the θ_{roof} (or θ_{max} , θ_i) response is in the transition between elastic and nonlinear behavior. At lower scale factors the response is essentially elastic, whereas at higher scale factors it is progressively more nonlinear.

As is clear in Figure 32, the "upward swing" in the data described above cannot be captured by a log-log linear regression fit. Hence, a non-parametric LOESS (Cleveland 1979) local regression fit is also plotted in the figure, using a "windowing fraction" of 0.75. The LOESS fit indicates that the scaled records provide an unbiased θ_{roof} response at scale factors lower than unity (roughly), as was observed for the elastic building model in the preceding section. At higher scale factors, however, the θ_{roof} response to the scaled records is somewhat biased high (e.g., by 30% at a scale factor). This bias can be explained via (again) the illustration in Figure 31

(above) of the median response spectra for records that are scaled up versus down. Although difficult to discern, there the median response spectrum of the records scale by a median factor of $SF=2.6$ is shown to be higher at periods longer than the fundamental period of the MDOF structures ($T=2.3\text{sec}$), as compared to the median spectrum of the un-scaled records ($SF=1$). Hence, as the fundamental period effectively elongates due to nonlinearity, it is expected (as observed) that the θ_{roof} response to the records that are scaled up will be biased high.

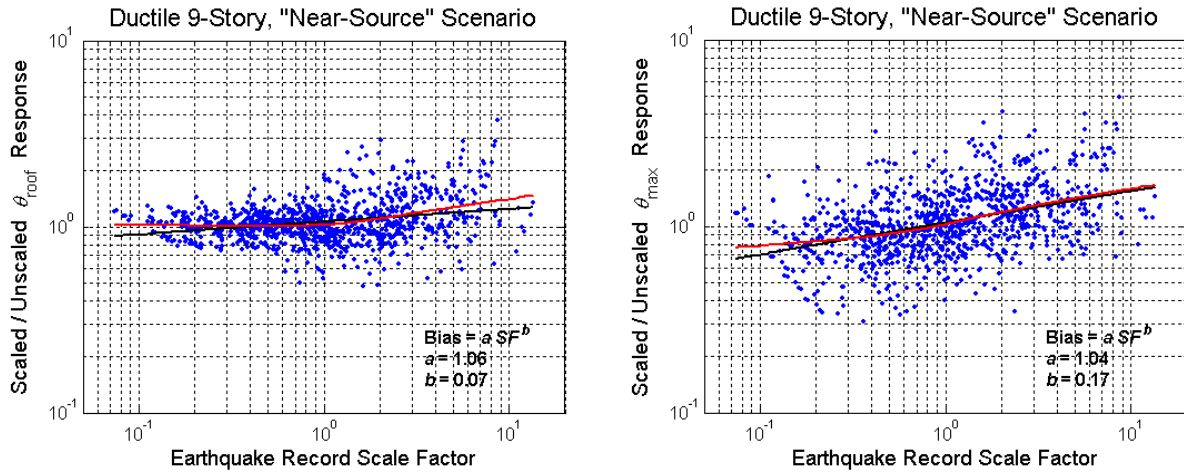


Figure 32. Intra-bin scaling results in terms of (a) peak roof drift ratio (θ_{roof}), and (b) maximum (over all stories) peak inter-story drift ratio (θ_{max}) for the *ductile* model of the 9-story building considered and the Near-Source Bin of earthquake records. The curve fits shown in red are obtained via a non-parametric local regression (LOESS).

Unlike the θ_{roof} results, the θ_{max} results shown in Figure 32b are very much similar to those for the elastic building model, even at large scale factors (and hence, most likely, large target S_a values) for which the structural response is notably nonlinear. At the large scale factors is not readily apparent whether the θ_{max} response to the scaled records is biased high because of (i) the same higher mode contributions to θ_{max} the resulted in a bias for the elastic building model (in Figure 29b), or (ii) the same effect of nonlinearity observed for the θ_{roof} response (in Figure 32a). As a final remark on the θ_{max} results, it is noted that the linear and LOESS fits (in log-log space) are almost identical, except at the very low end of the data (i.e., lowest scale factors).

For the 2nd, 5th, and 8th stories, the θ_i results for the ductile building model are presented alongside the corresponding results for the elastic building model in Figure 30 (above). Comments similar to those made for the elastic results, as well as those for the θ_{roof} and θ_{max} response of the ductile model, apply.

8.2.1.3 Summary

Intra-bin scaling of the elastic MDOF building model introduces a bias in the drift response measures that are sensitive to multiple modes (e.g., θ_{\max}), but not those that are first-mode-dominated (e.g., θ_{roof}). For both of these response measures, intra-bin scaling introduces a bias for the ductile building model, except for the responses that are first-mode-dominated and essentially elastic due to the small target S_a level (typically corresponding to small scale factors).

At lower (than unity) scale factors, the response of even the ductile building model considered is more-or-less elastic, and hence no bias is observed in drift responses that are dominated by the first mode of vibration (e.g., θ_{roof}), whereas the response of multi-mode-sensitive drift responses (e.g., θ_{\max}) is biased low. The latter can be explained by the shape of the response spectra for records with relatively low scale factors.

At higher scale factors, the multi-mode-sensitive (but not the first-mode-dominated) drift responses of the elastic building model are biased high, consistent with the response spectral shape for records with relatively large scale factors. For the ductile building model, on the other hand, both the first-mode-dominated and multi-mode-sensitive responses are biased high are larger scale factors, to varying degrees. Again, both can be explained by the shape of the response spectra for records with relatively high scale factors, at periods either smaller (for higher modes) or larger (for the effects of nonlinearity).

For more specific comments regarding the extent of the biases observed for the MDOF structures and intra-bin scaling, as well as a comparison with the SDOF results presented above, the reader is referred to the overall summary in Section 9.

8.2.2 Inter-Bin Scaling

The inter-bin scaling results presented here are for the same "target bin" considered in the preceding intra-bin scaling section, namely the Near-Source Bin, but a different "source bin," i.e., Bin I.

8.2.2.1 Elastic Model

For the elastic model of the 9-story SMRF building considered, the inter-bin scaling results in terms of θ_{roof} and θ_{\max} are plotted in Figure 33. As expected, practically no bias in θ_{roof} is observed ($a=1.03$, $b=0.02$) because the first-mode-dominated θ_{roof} is effectively proportional to the target S_a values to which all the source bin records are scaled. For the multi-mode-sensitive θ_{\max} response, however, a bias proportional (in log-log space) to scale factor is observed ($b=0.17$), similar to the intra-bin scaling results ($b=0.12$). The pre-scaling of the source bin (Bin I) records such that their median S_a is equal to that of the target (Near-Source) bin does not appear to introduce a significant bias (i.e., $a=1.03$). Given the differences between the median response spectra for the pre-scaled Bin I and the Near-Source Bin records, shown in Figure 34, this lack of bias is somewhat unexpected. Perhaps other differences between the target and source bins not reflected in the response spectra (e.g. time-domain features of the records) compensate for the disparity in spectral shape.

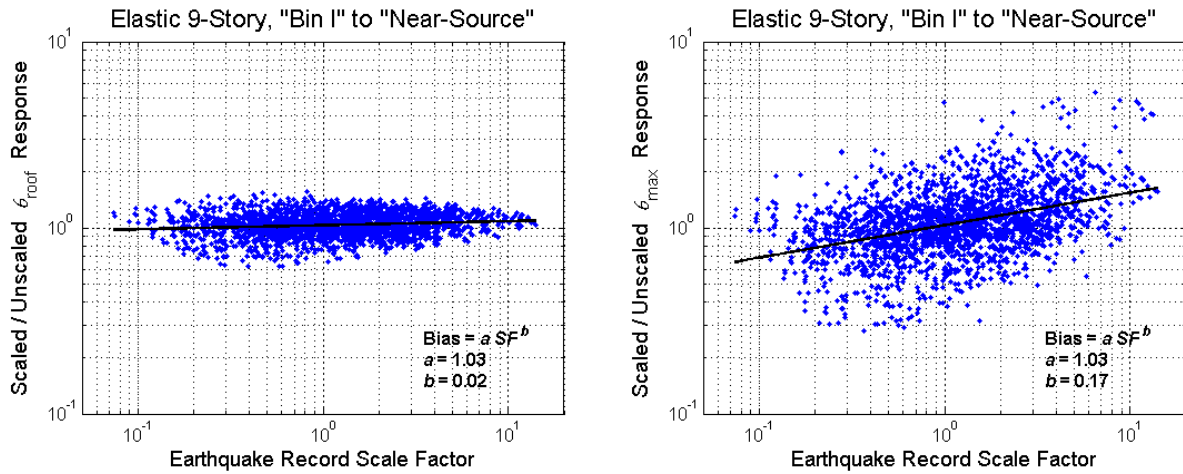


Figure 33. *Inter-bin scaling results in terms of (a) peak roof drift ratio (θ_{roof}), and (b) maximum (over all stories) peak inter-story drift ratio (θ_{max}) for the elastic model of the 9-story building considered and the Bin I to Near-Source Bin scenario.*

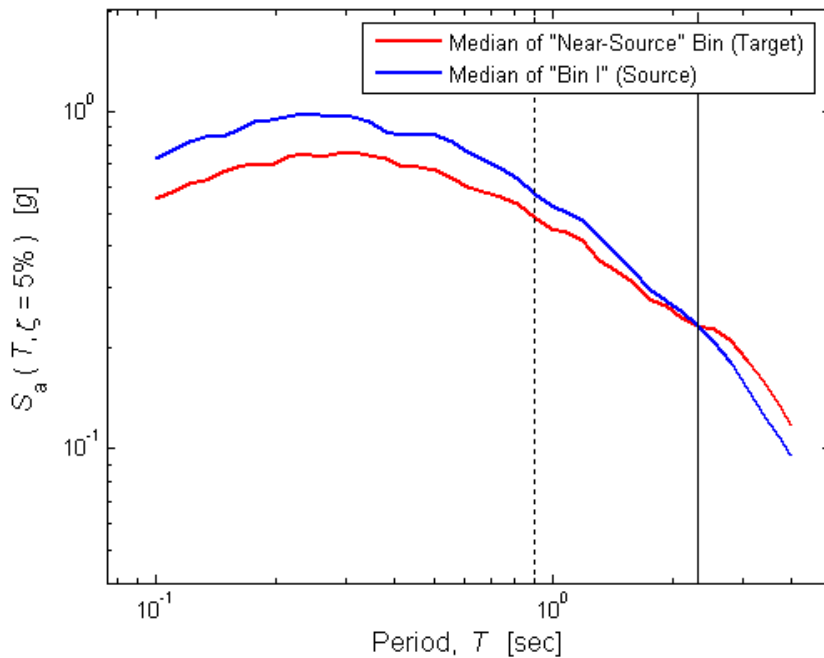


Figure 34. Median elastic response spectra for the Near-Source Bin and the earthquake records in Bin I scaled by a common factor such that their median S_a matches that of the Near-Source Bin at a period of $T=2.3\text{sec}$ (the fundamental period of the 9-story building considered). Note that while the spectral ordinates at periods longer than 2.3sec are larger for the Near-Source Bin, the opposite is true at the second-mode period 0.9sec .

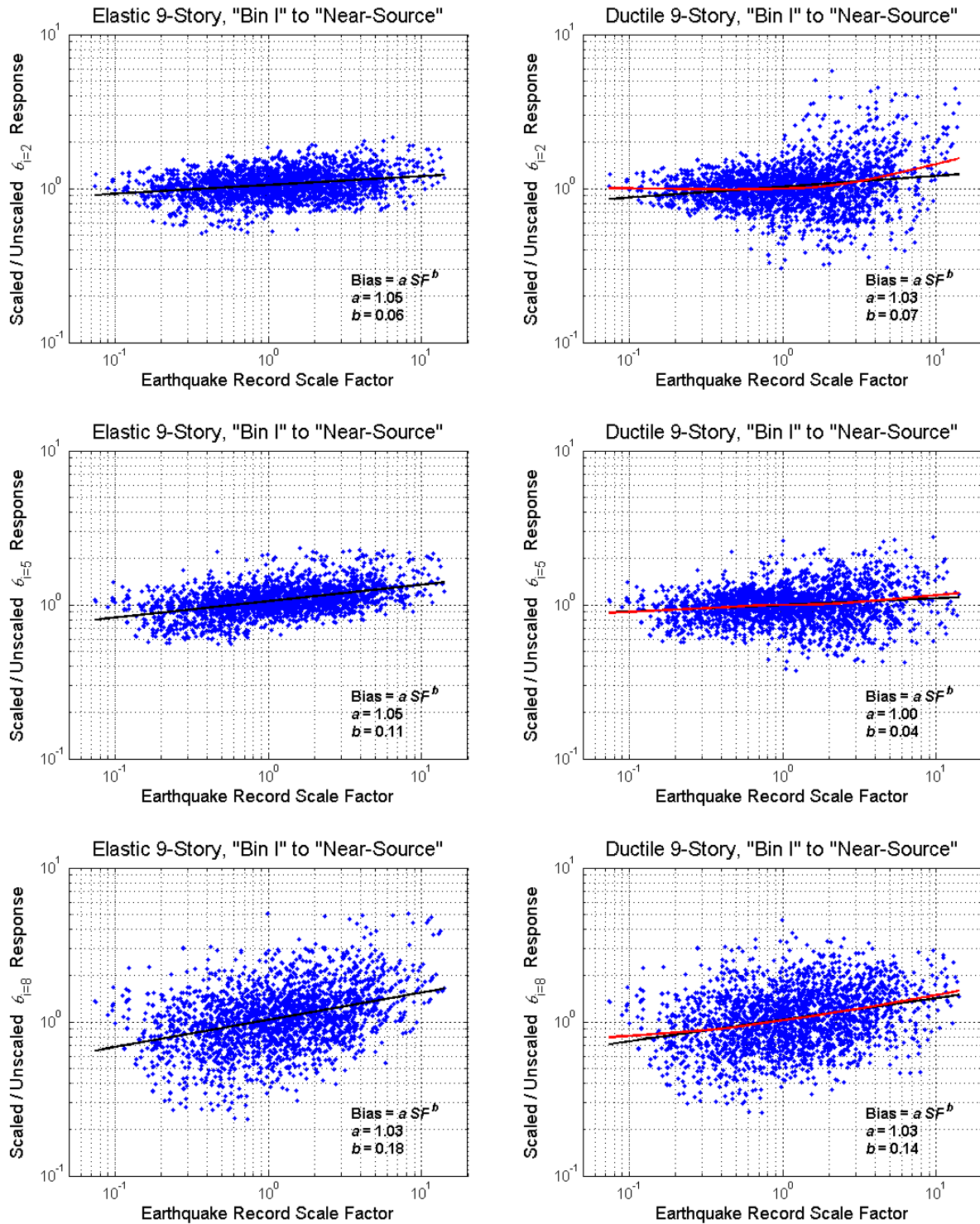


Figure 35. *Inter-bin scaling results in terms of the peak inter-story drift ratios (θ_i) at the 2nd story (top row), 5th story (middle row), and 8th story (bottom row), for the elastic (left column) and ductile (right column) models of the 9-story building considered. The curve fit shown in red on the ductile results is obtained via a non-parametric local regression (LOESS). The analogous results for the other 6 of the 9 stories are provided in the appendix.*

Like the intra-bin results shown in Figure 30, the inter-bin scaling results for the elastic building model are plotted in terms of θ_2 , θ_5 , and θ_8 in Figure 35, alongside the analogous results for the ductile building model. Comments similar to those already stated for the intra-bin results and the inter-bin results for θ_{roof} and θ_{max} apply to this figure as well.

8.2.2.2 Ductile Model

Lastly, for the ductile model of the 9-story SMRF building, the inter-bin scaling results for θ_{roof} and θ_{max} are plotted in Figure 36. For θ_{roof} , the log-log linear regression fit to the data suggests that practically no bias is introduced by scaling ($a=1.02$, $b=0.03$), which is confirmed by the LOEES fit at the smaller scale factors. At larger scale factors the LOEES fit (and the data itself) indicates that the scaled θ_{roof} response is biased high (e.g., by about 20% at a scale factor of 10), as was observed (and explained) for the intra-bin scaling results presented above.

For θ_{max} , the ductile results shown in Figure 36b are very similar to those for the elastic building model (shown in Figure 33b), and in turn the intra-bin scaling results for both the elastic and ductile building models. Also note that the differences between the linear and LOESS regression fits to the θ_{max} results are relatively minor, even at the extreme scale factors.

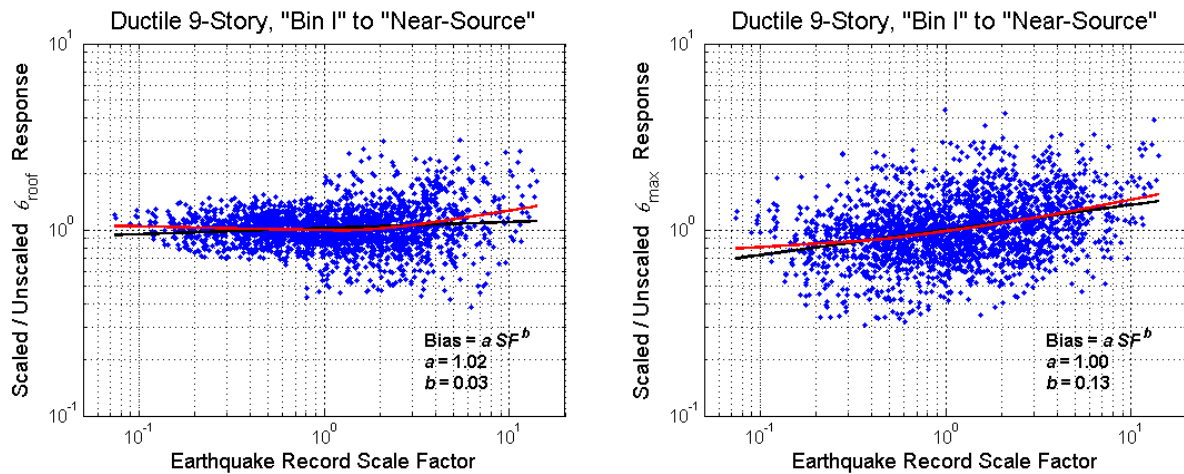


Figure 36. Inter-bin scaling results in terms of (a) peak roof drift ratio (θ_{roof}), and (b) maximum (over all stories) peak inter-story drift ratio (θ_{max}) for the *ductile* model of the 9-story building and the Bin I to Near-Source Bin scenario. The curve fits shown in red are obtained via a non-parametric local regression (LOESS).

8.2.2.3 Summary

Inter-bin scaling appears to have a very similar effect, in terms of the bias in linear or nonlinear MDOF response it introduces, to that of *intra*-bin scaling. In both cases there is (practically) no bias in θ_{roof} , θ_{max} , or θ_i at a scale factor of unity. For the inter-bin case, recall, this indicates that

"pre-scaling" the source bin records such that their median S_a matches that of the target bin does not induce a bias, which is somewhat unexpected given the differences between the (median) response spectra for the source and target bins. For lower and higher scale factors, the bias introduced is as described for intra-bin scaling (in Section **Error! Reference source not found.**). The magnitude of these biases for inter-bin scaling and the MDOF structures, as well as those for the other cases considered, are summarized in the next section.

9 Summary

An overall summary of the detailed results presented above for both the SDOF and MDOF structures is provided here for intra- and inter-bin scaling separately. A comparison of the results for the two types of scaling is made in the inter-bin section (Section 9.2.1.1).

9.2.1.1 Intra-Bin Scaling

The intra-bin scaling results for the SDOF structures covering a range of periods and strengths, and considering the seven different bins of earthquake records, indicate the following:

- For elastic or mildly inelastic SDOF structures (i.e., $R \leq 2$), the bias in drift response (i.e., S_d^d) that is introduced by intra-bin scaling is at most 15% and 60% (i.e., factors of 1.15 and 1.60) for scale factors of 2 and 10 (or 1/1.15 and 1/1.60 for 1/2 and 1/10), respectively, with the exception of a few short-period cases ($T \leq 0.2$ sec).
- For relatively long period SDOF structures (i.e., $T \geq 3$ sec), the bias introduced is also less than 15% and 60% for scale factors of 2 and 10, respectively, except for Bin VI containing large M_w and long R_{close} records, in which case the bias is large as 27% and 119% (respectively).
- For relatively short periods (i.e., $T \leq 0.5$ sec), the bias is *at least* 15% and 60%, and can be as large as 90% and 690%, for scale factors of 2 and 10, respectively. This is true even at the $R=2$ strength level (with only one exception), but with a few lower-bias exceptions (i) at the $R=4$ strength level and (ii) for the Near-Source Bin containing "pulse-like" records.
- At moderate periods (i.e., $T=1$ or 2sec), the magnitude of the bias is dependent on the characteristics (e.g., M_w , R_{close}) of the bin of records that are scaled. For $T=1$ sec, the bias is less than 15% and 60% for scale factors of 2 and 10, respectively, for Bin III and IV, but for the other five bins the bias is larger, up to 50% and 280% (respectively). For $T=2$ sec, the bias is less than 15%/60% for all but Bin II, IV, and VI, for which it is still less than 30%/150% (for scale factors of 2/10).

For the MDOF structure, even the elastic model exhibits a scaling-induced bias, but only for those drift responses that are sensitive to higher modes of vibration (e.g., θ_9 , θ_{max}). At most, this bias is about 15% and 60% at scale factors of 2 and 10, respectively (i.e., $b < 0.20$). The ductile building model exhibits a comparable bias for the multi-mode-sensitive responses, but also displays a bias for first-mode-dominated responses (e.g., θ_1 , θ_{roof}). The latter is as large as 25% and 80% for scale factors of 2 and 10, respectively, but at scale factors less than about unity there is nearly no bias because the response is essentially elastic (and first-mode-dominated).

9.2.1.2 Inter-Bin Scaling

The inter-bin scaling results, recall, are very similar to those for intra-bin scaling in terms of the variation of bias with scale factor (described above), except perhaps at very short periods (e.g., $T \leq 0.5$ sec). Inter-bin scaling, however, can also introduce a bias in nonlinear structural response at an "adjusted" scale factor of one, i.e., merely by pre-scaling the earthquake records in the source bin by a common factor such that their median spectral acceleration (S_a) is equal to the median S_a of the target bin. The magnitude of this additional bias for the SDOF structures and 10 different inter-bin scaling cases considered shows the following trends:

- For elastic or mildly inelastic SDOF structures (i.e., $R \leq 2$), the bias in drift response (i.e., S_d^I) that is introduced by inter-bin "pre-scaling" is less than 15% (i.e., between a factor of $1/1.15=0.87$ and 1.15), except at short periods ($T \leq 0.3$ sec) in some cases.
- Roughly speaking, the bias tends to increase with decreasing strength (i.e., increasing R), and can be as large as 80%.
- For Bin I to IV (from smaller to larger M_w , for shorter R_{close}), Bin V to VI (from intermediate to shorter R_{close} , for larger M_w), and Bin VI to V (from longer to shorter R_{close} , for larger M_w), however, the bias is less than 15% for all but a few of the period-strength combinations (always with $T \leq 1$), in which case the bias is still less than 40%.
- For the most part, the largest biases are observed for shorter period ($T \leq 0.2$) structures, except in the Bin III to V case (largest biases at $T \geq 3$ sec), the Bin VI to V case (largest biases at $T=1$ sec), and Bin III to I case (largest biases at $T=0.5$ or 1 sec).
- Bin V to IV case (for which the bias is less than 18% across all T - R combination), the

Note that for most (but not all) of the inter-bin cases described above, the S_d^I response to the pre-scaled records is biased low because the earthquake records in the source bin are generally more "benign," in terms of the S_d^I response that they induce for a given S_a level, than those in the target bin. In practice, it is typically the more "aggressive" target bin (often of larger M_w and shorter R_{close}) that is of interest, for which fewer (if any) existing records are available.

Unlike for the SDOF structures, the inter-bin pre-scaling induces practically no bias in the drift response of the MDOF structures. Hence, the inter-bin scaling results for the MDOF structures are very similar to those for intra-bin scaling.

10 Conclusions

For a range of SDOF structures of different periods and strengths, as well as two MDOF structures of different strengths (one elastic), we have quantified the bias in nonlinear structural response induced by scaling input earthquake records to a target spectral acceleration level. The bias is measured with respect to the response to un-scaled records that are naturally at the spectral acceleration of interest. In the case of intra-bin scaling, these un-scaled records have, by definition, the same general characteristics (in terms of M_w , R_{close} , etc.) as the records that are scaled. In inter-bin scaling, on the other hand, the un-scaled records lie in a "target bin" with different characteristics than the "source bin" of earthquake records to scale. Of course, in practice this target bin is devoid of records, but we assume that the inter-bin scaling results

presented here can be extrapolated to such cases. The nonlinear structural response measures considered are inelastic spectral displacement for the SDOF structures, and inter-story and roof drift for the MDOF structures.

The results of this study demonstrate that scaling earthquake records can introduce a bias in nonlinear structural response that increases with the degree of scaling. As detailed in the preceding section, the magnitude of this bias depends on (i) the fundamental period of vibration of the structure, (ii) the overall strength of the structure, and (iii) the sensitivity of the nonlinear structural response to higher (than the first) modes of vibration. The bias is also observed to depend on the characteristics (e.g., M_w , R_{close}) of the earthquake records that are scaled. In the case of inter-bin scaling, however, the characteristics of these "source records" mainly effects the bias (if any) introduced by first "pre-scaling" them such that their median spectral acceleration matches that of the target bin (e.g., as obtained from an attenuation relation). Any additional bias induced by scaling to a target spectral acceleration level is observed to depend primarily on the characteristics of the target bin.

The biases quantified in this study can be used to place limits on the amount scaling that is acceptable for comparable structures, once one has decided on a tolerable amount of bias. Alternatively, one could, in an approximate fashion, "correct" for a scaling-induced bias by using results like those presented in this paper.

11 Future Work

In this study the bias in nonlinear structural response induced by scaling is quantified as a function of the scale factor only, irrespective of whether it comes from scaling an earthquake record with a relatively small spectral acceleration (S_a) up to a moderate S_a level, for example, or a moderate S_a record to a high S_a level. Whether it is necessary to distinguish between these two cases (as examples) deserves future consideration.

Given that scaling to a spectral acceleration level can, in fact, introduce a bias in nonlinear structural response, other approaches to scaling are worthy of investigation. If, for example, some measure of the shape of the elastic response spectrum at the target spectral acceleration level is considered, can the scaling-induced bias be reduced? Can the effects of scaling be avoided altogether by instead interpolating (or extrapolating) the nonlinear structural responses to un-scaled earthquake records?

12 Acknowledgements

The PEER Lifelines Program funded the work presented in this paper (under an addendum to Task 1G00). The content benefited from discussions with the following individuals: Brian Chiou and Cliff Roblee of Caltrans, Maury Power of Geomatrix, Allin Cornell, Jack backer, Gee-Liek Yeo, and Polsak Tothong of Stanford University.

Appendix

Tables A1-2. Lists of the 73 earthquake records in "Bin I" ($M_w=6.4-6.8$, $R_{close}=0-15\text{km}$), on the left, and "Bin II" ($M_w=6.4-6.8$, $R_{close}=15-30\text{km}$), on the right.

	EARTHQUAKE NAME	YEAR	M	R	RECORD NAME
1	Imperial Valley	1979	6.5	8.5	H-AEP045.AT2.txt
2	Imperial Valley	1979	6.5	8.5	H-AEP315.AT2.txt
3	Imperial Valley	1979	6.5	2.5	H-BCR140.AT2.txt
4	Imperial Valley	1979	6.5	2.5	H-BCR230.AT2.txt
5	Imperial Valley	1979	6.5	8.5	H-BRA225.AT2.txt
6	Imperial Valley	1979	6.5	8.5	H-BRA315.AT2.txt
7	Imperial Valley	1979	6.5	10.6	H-CXO315.AT2.txt
8	Imperial Valley	1979	6.5	10.6	H-CXO315.AT2.txt
9	Imperial Valley	1979	6.5	10.4	H-E02140.AT2.txt
10	Imperial Valley	1979	6.5	4.2	H-E04140.AT2.txt
11	Imperial Valley	1979	6.5	4.2	H-E04230.AT2.txt
12	Imperial Valley	1979	6.5	1.0	H-E05140.AT2.txt
13	Imperial Valley	1979	6.5	1.0	H-E05230.AT2.txt
14	Imperial Valley	1979	6.5	1.0	H-E06140.AT2.txt
15	Imperial Valley	1979	6.5	1.0	H-E06230.AT2.txt
16	Imperial Valley	1979	6.5	0.6	H-E07140.AT2.txt
17	Imperial Valley	1979	6.5	0.6	H-E07230.AT2.txt
18	Imperial Valley	1979	6.5	3.8	H-E08140.AT2.txt
19	Imperial Valley	1979	6.5	3.8	H-E08230.AT2.txt
20	Imperial Valley	1979	6.5	8.6	H-E10050.AT2.txt
21	Imperial Valley	1979	6.5	8.6	H-E10320.AT2.txt
22	Imperial Valley	1979	6.5	12.6	H-E11140.AT2.txt
23	Imperial Valley	1979	6.5	12.6	H-E11230.AT2.txt
24	Imperial Valley	1979	6.5	7.6	H-ECC002.AT2.txt
25	Imperial Valley	1979	6.5	7.6	H-ECC092.AT2.txt
26	Imperial Valley	1979	6.5	5.3	H-EDA270.AT2.txt
27	Imperial Valley	1979	6.5	5.3	H-EDA360.AT2.txt
28	Imperial Valley	1979	6.5	0.5	H-EMO000.AT2.txt
29	Imperial Valley	1979	6.5	0.5	H-EMO270.AT2.txt
30	Imperial Valley	1979	6.5	7.5	H-HVP225.AT2.txt
31	Imperial Valley	1979	6.5	7.5	H-HVP315.AT2.txt
32	Imperial Valley	1979	6.5	14.2	H-PTS225.AT2.txt
33	Imperial Valley	1979	6.5	14.2	H-PTS315.AT2.txt
34	Imperial Valley	1979	6.5	11.1	H-SHP000.AT2.txt
35	Imperial Valley	1979	6.5	11.1	H-SHP270.AT2.txt
36	Coalinga	1983	6.4	8.5	H-PVY045.AT2.txt
37	Coalinga	1983	6.4	8.5	H-PVY135.AT2.txt
38	Superstition Hills	1987	6.7	13.9	B-ICC000.AT2.txt
39	Superstition Hills	1987	6.7	13.9	B-ICC090.AT2.txt
40	Superstition Hills	1987	6.7	0.7	B-PTS225.AT2.txt
41	Superstition Hills	1987	6.7	0.7	B-PTS315.AT2.txt
42	Superstition Hills	1987	6.7	13.3	B-WSM090.AT2.txt
43	Superstition Hills	1987	6.7	13.3	B-WSM180.AT2.txt
44	Northridge	1994	6.7	9.2	ARL090.AT2.txt
45	Northridge	1994	6.7	9.2	ARL360.AT2.txt
46	Northridge	1994	6.7	14.6	CWC180.AT2.txt
47	Northridge	1994	6.7	14.6	CWC270.AT2.txt
48	Northridge	1994	6.7	6.2	JEN022.AT2.txt
49	Northridge	1994	6.7	6.2	JEN292.AT2.txt
50	Northridge	1994	6.7	13.0	LOS000.AT2.txt
51	Northridge	1994	6.7	13.0	LOS270.AT2.txt
52	Northridge	1994	6.7	7.1	NWH090.AT2.txt
53	Northridge	1994	6.7	7.1	NWH360.AT2.txt
54	Northridge	1994	6.7	8.2	PKC090.AT2.txt
55	Northridge	1994	6.7	8.2	PKC360.AT2.txt
56	Northridge	1994	6.7	12.3	RO3000.AT2.txt
57	Northridge	1994	6.7	12.3	RO3090.AT2.txt
58	Northridge	1994	6.7	7.1	RRS228.AT2.txt
59	Northridge	1994	6.7	7.1	RRS318.AT2.txt
60	Northridge	1994	6.7	6.1	SCE018.AT2.txt
61	Northridge	1994	6.7	6.1	SCE288.AT2.txt
62	Northridge	1994	6.7	6.2	SCS052.AT2.txt
63	Northridge	1994	6.7	6.2	SCS142.AT2.txt
64	Northridge	1994	6.7	8.9	SPV270.AT2.txt
65	Northridge	1994	6.7	8.9	SPV360.AT2.txt
66	Northridge	1994	6.7	13.3	STC090.AT2.txt
67	Northridge	1994	6.7	13.3	STC180.AT2.txt
68	Northridge	1994	6.7	6.4	SYL090.AT2.txt
69	Northridge	1994	6.7	6.4	SYL360.AT2.txt
70	Northridge	1994	6.7	14.9	UCL090.AT2.txt
71	Northridge	1994	6.7	14.9	UCL360.AT2.txt
72	Northridge	1994	6.7	7.1	WPI046.AT2.txt
73	Northridge	1994	6.7	7.1	WPI316.AT2.txt
	Min		6.4	0.5	
	Max		6.7	14.9	

	EARTHQUAKE NAME	YEAR	M	R	RECORD NAME
1	San Fernando	1971	6.6	21.2	PEL090.AT2.txt
2	San Fernando	1971	6.6	21.2	PEL180.AT2.txt
3	Imperial Valley	1979	6.5	23.8	H-CAL225.AT2.txt
4	Imperial Valley	1979	6.5	23.8	H-CAL315.AT2.txt
5	Imperial Valley	1979	6.5	28.7	H-CH012.AT2.txt
6	Imperial Valley	1979	6.5	28.7	H-CHI282.AT2.txt
7	Imperial Valley	1979	6.5	26.5	H-CPE147.AT2.txt
8	Imperial Valley	1979	6.5	26.5	H-CPE237.AT2.txt
9	Imperial Valley	1979	6.5	15.5	H-E01140.AT2.txt
10	Imperial Valley	1979	6.5	15.5	H-E01230.AT2.txt
11	Imperial Valley	1979	6.5	18.2	H-E12140.AT2.txt
12	Imperial Valley	1979	6.5	18.2	H-E12230.AT2.txt
13	Imperial Valley	1979	6.5	21.9	H-E13140.AT2.txt
14	Imperial Valley	1979	6.5	21.9	H-E13230.AT2.txt
15	Imperial Valley	1979	6.5	23.6	H-QKP085.AT2.txt
16	Imperial Valley	1979	6.5	26.0	H-SUP045.AT2.txt
17	Imperial Valley	1979	6.5	26.0	H-SUP135.AT2.txt
18	Imperial Valley	1979	6.5	15.1	H-WSM090.AT2.txt
19	Imperial Valley	1979	6.5	15.1	H-WSM180.AT2.txt
20	Coalinga	1983	6.4	25.5	H-CAK270.AT2.txt
21	Coalinga	1983	6.4	25.5	H-CAK360.AT2.txt
22	Coalinga	1983	6.4	29.2	H-GH3000.AT2.txt
23	Coalinga	1983	6.4	29.2	H-GH3090.AT2.txt
24	Coalinga	1983	6.4	29.5	H-PRK090.AT2.txt
25	Coalinga	1983	6.4	29.5	H-PRK180.AT2.txt
26	Coalinga	1983	6.4	26.7	H-PV1000.AT2.txt
27	Coalinga	1983	6.4	26.7	H-PV1090.AT2.txt
28	Coalinga	1983	6.4	29.6	H-Z08000.AT2.txt
29	Coalinga	1983	6.4	29.6	H-Z08090.AT2.txt
30	Coalinga	1983	6.4	28.4	H-Z11000.AT2.txt
31	Coalinga	1983	6.4	28.4	H-Z11090.AT2.txt
32	Coalinga	1983	6.4	29.9	H-Z14000.AT2.txt
33	Coalinga	1983	6.4	29.9	H-Z14090.AT2.txt
34	Coalinga	1983	6.4	29.9	H-Z15000.AT2.txt
35	Coalinga	1983	6.4	29.9	H-Z15090.AT2.txt
36	Coalinga	1983	6.4	28.1	H-Z16000.AT2.txt
37	Coalinga	1983	6.4	28.1	H-Z16090.AT2.txt
38	Superstition Hills	1987	6.7	18.2	B-BRA225.AT2.txt
39	Superstition Hills	1987	6.7	18.2	B-BRA315.AT2.txt
40	Superstition Hills	1987	6.7	28.3	B-CAL225.AT2.txt
41	Superstition Hills	1987	6.7	28.3	B-CAL315.AT2.txt
42	Superstition Hills	1987	6.7	21.0	B-PLS135.AT2.txt
43	Northridge	1994	6.7	25.7	CCN090.AT2.txt
44	Northridge	1994	6.7	25.7	CCN360.AT2.txt
45	Northridge	1994	6.7	15.8	CNP106.AT2.txt
46	Northridge	1994	6.7	15.8	CNP106.AT2.txt
47	Northridge	1994	6.7	23.9	FAR000.AT2.txt
48	Northridge	1994	6.7	23.9	FAR090.AT2.txt
49	Northridge	1994	6.7	17.7	GLE170.AT2.txt
50	Northridge	1994	6.7	17.7	GLE260.AT2.txt
51	Northridge	1994	6.7	20.8	MU2035.AT2.txt
52	Northridge	1994	6.7	20.8	MU2125.AT2.txt
53	Northridge	1994	6.7	19.6	MUL009.AT2.txt
54	Northridge	1994	6.7	19.6	MUL279.AT2.txt
55	Northridge	1994	6.7	22.6	ORR090.AT2.txt
56	Northridge	1994	6.7	22.6	ORR360.AT2.txt
57	Northridge	1994	6.7	25.4	PDL120.AT2.txt
58	Northridge	1994	6.7	25.4	PDL210.AT2.txt
59	Northridge	1994	6.7	19.3	SSU000.AT2.txt
60	Northridge	1994	6.7	19.3	SSU090.AT2.txt
61	Northridge	1994	6.7	27.6	STM090.AT2.txt
62	Northridge	1994	6.7	27.6	STM360.AT2.txt
63	Northridge	1994	6.7	30.0	STN020.AT2.txt
64	Northridge	1994	6.7	30.0	STN110.AT2.txt
65	Northridge	1994	6.7	26.2	SUN190.AT2.txt
66	Northridge	1994	6.7	26.2	SUN280.AT2.txt
67	Northridge	1994	6.7		TPF000.AT2.txt
68	Northridge	1994	6.7	24.2	VAS000.AT2.txt
69	Northridge	1994	6.7	24.2	VAS090.AT2.txt
70	Northridge	1994	6.7	25.7	WIL090.AT2.txt
71	Northridge	1994	6.7	25.7	WIL180.AT2.txt
72	Northridge	1994	6.7	29.0	WST000.AT2.txt
73	Northridge	1994	6.7	29.0	WST270.AT2.txt
	Min		6.4	15.1	
	Max		6.7	30	

Tables A3-4. Lists of the 73 earthquake records in "Bin III" ($M_w=6.4-6.8$, $R_{close}=30-50km$), on the left, and "Bin IV" ($M_w=6.9-7.6$, $R_{close}=0-15km$), on the right.

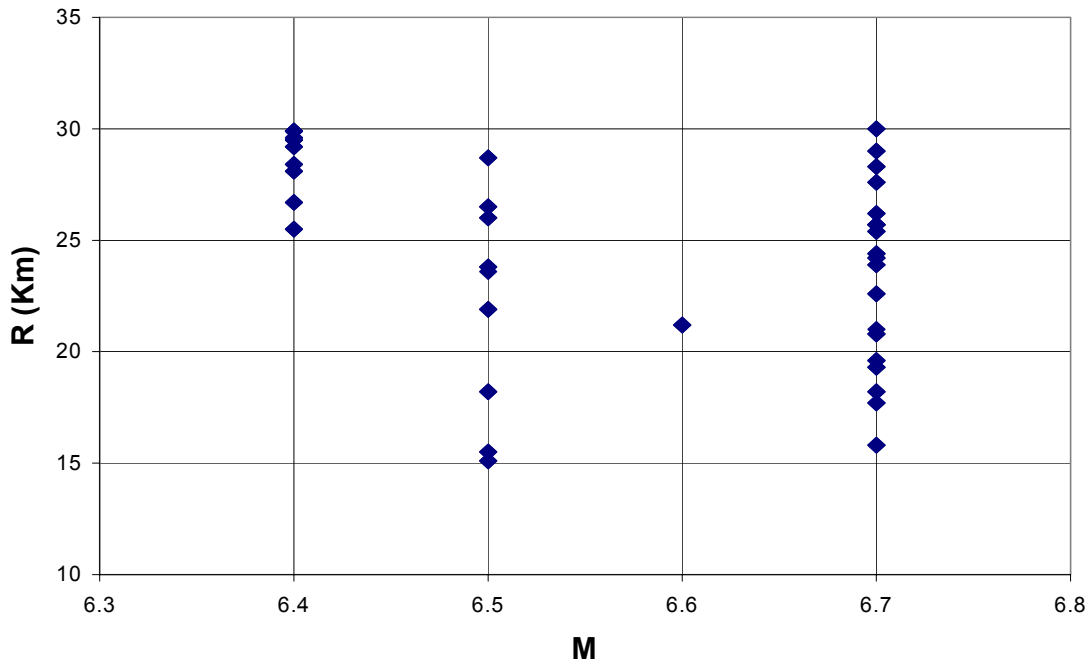
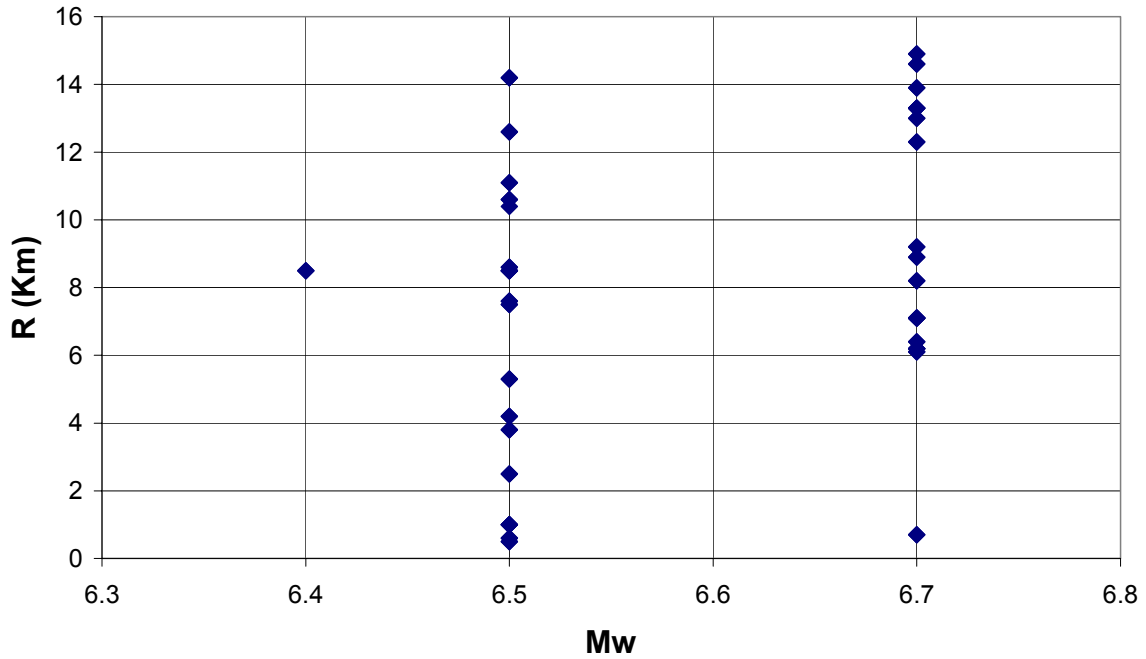
	EARTHQUAKE NAME	YEAR	M	R	RECORD NAME
1	Borrego Mountain	1968	6.8	46.0	A-ELC180.AT2.txt
2	Borrego Mountain	1968	6.8	46.0	A-ELC270.AT2.txt
3	San Fernando	1971	6.6	48.1	OPP000.AT2.txt
4	San Fernando	1971	6.6	48.1	OPP270.AT2.txt
5	San Fernando	1971	6.6	31.7	PAS090.AT2.txt
6	San Fernando	1971	6.6	38.9	PPP000.AT2.txt
7	San Fernando	1971	6.6	38.9	PPP270.AT2.txt
8	Fruiti	1976	6.5	34.6	A-COD000.AT2.txt
9	Fruiti	1976	6.5	34.6	A-COD270.AT2.txt
10	Fruiti	1976	6.5	37.7	A-TMZ000.AT2.txt
11	Fruiti	1976	6.5	37.7	A-TMZ270.AT2.txt
12	Imperial Valley	1979	6.5	49.3	H-CC4045.AT2.txt
13	Imperial Valley	1979	6.5	49.3	H-CC4135.AT2.txt
14	Imperial Valley	1979	6.5	32.6	H-CMP015.AT2.txt
15	Imperial Valley	1979	6.5	32.6	H-CMP285.AT2.txt
16	Imperial Valley	1979	6.5	35.9	H-NIL090.AT2.txt
17	Imperial Valley	1979	6.5	35.9	H-NIL360.AT2.txt
18	Imperial Valley	1979	6.5	31.7	H-PLS045.AT2.txt
19	Imperial Valley	1979	6.5	31.7	H-PLS135.AT2.txt
20	Coalinga	1983	6.4	41.6	H-C01000.AT2.txt
21	Coalinga	1983	6.4	41.6	H-C01090.AT2.txt
22	Coalinga	1983	6.4	43.9	H-C03000.AT2.txt
23	Coalinga	1983	6.4	43.9	H-C03090.AT2.txt
24	Coalinga	1983	6.4	44.7	H-C04000.AT2.txt
25	Coalinga	1983	6.4	44.7	H-C04090.AT2.txt
26	Coalinga	1983	6.4	49.0	H-C06090.AT2.txt
27	Coalinga	1983	6.4	46.0	H-C4A000.AT2.txt
28	Coalinga	1983	6.4	46.0	H-C4A090.AT2.txt
29	Coalinga	1983	6.4	40.4	H-COW000.AT2.txt
30	Coalinga	1983	6.4	40.4	H-COW090.AT2.txt
31	Coalinga	1983	6.4	40.5	H-TM2090.AT2.txt
32	Coalinga	1983	6.4	37.9	H-Z02000.AT2.txt
33	Coalinga	1983	6.4	37.9	H-Z02090.AT2.txt
34	Coalinga	1983	6.4	34.3	H-Z04000.AT2.txt
35	Coalinga	1983	6.4	34.3	H-Z04090.AT2.txt
36	Coalinga	1983	6.4	32.8	H-Z06000.AT2.txt
37	Coalinga	1983	6.4	32.8	H-Z06090.AT2.txt
38	Coalinga	1983	6.4	31.0	H-Z07000.AT2.txt
39	Coalinga	1983	6.4	31.0	H-Z07090.AT2.txt
40	Coalinga	1983	6.4	30.4	H-Z10000.AT2.txt
41	Coalinga	1983	6.4	30.4	H-Z10090.AT2.txt
42	Northridge	1994	6.7	41.9	116090.AT2.txt
43	Northridge	1994	6.7	41.9	116360.AT2.txt
44	Northridge	1994	6.7	35.7	ALH090.AT2.txt
45	Northridge	1994	6.7	35.7	ALH360.AT2.txt
46	Northridge	1994	6.7	38.4	ANA090.AT2.txt
47	Northridge	1994	6.7	38.4	ANA180.AT2.txt
48	Northridge	1994	6.7	31.3	BLD090.AT2.txt
49	Northridge	1994	6.7	31.3	BLD360.AT2.txt
50	Northridge	1994	6.7	44.2	CAM279.AT2.txt
51	Northridge	1994	6.7	49.6	CAS000.AT2.txt
52	Northridge	1994	6.7	49.6	CAS270.AT2.txt
53	Northridge	1994	6.7	37.2	ELI090.AT2.txt
54	Northridge	1994	6.7	37.2	ELI180.AT2.txt
55	Northridge	1994	6.7	47.4	FAI095.AT2.txt
56	Northridge	1994	6.7	32.3	L4B000.AT2.txt
57	Northridge	1994	6.7	32.3	L4B090.AT2.txt
58	Northridge	1994	6.7	42.4	LOA092.AT2.txt
59	Northridge	1994	6.7	42.4	LOA182.AT2.txt
60	Northridge	1994	6.7	38.5	LV6090.AT2.txt
61	Northridge	1994	6.7	38.5	LV6360.AT2.txt
62	Northridge	1994	6.7	43.6	PHP000.AT2.txt
63	Northridge	1994	6.7	43.6	PHP270.AT2.txt
64	Northridge	1994	6.7	46.6	RHE090.AT2.txt
65	Northridge	1994	6.7	46.6	RHE360.AT2.txt
66	Northridge	1994	6.7	32.3	TEM090.AT2.txt
67	Northridge	1994	6.7	32.3	TEM180.AT2.txt
68	Northridge	1994	6.7	34.6	UNI005.AT2.txt
69	Northridge	1994	6.7	34.6	UNI095.AT2.txt
70	Northridge	1994	6.7	39.3	VER090.AT2.txt
71	Northridge	1994	6.7	39.3	VER180.AT2.txt
72	Northridge	1994	6.7	32.4	W15090.AT2.txt
73	Northridge	1994	6.7	32.4	W15180.AT2.txt
	Min		6.4	30.4	
	Max		6.8	49.6	

	EARTHQUAKE NAME	YEAR	M	R	RECORD NAME
1	Imperial Valley	1940	7	8.3	I-ELC180.AT2.txt
2	Imperial Valley	1940	7	8.3	I-ELC270.AT2.txt
3	Tabas	1978	7.4	14.0	DAY-LN.AT2.txt
4	Tabas	1978	7.4	14.0	DAY-TR.AT2.txt
5	Tabas	1978	7.4	3.0	TAB-LN.AT2.txt
6	Tabas	1978	7.4	3.0	TAB-TR.AT2.txt
7	Irpinia 1	1980	6.9	13.0	A-CTR000.AT2.txt
8	Irpinia 1	1980	6.9	13.0	A-CTR270.AT2.txt
9	Irpinia 2	1980	6.9	13.0	B-CTR000.AT2.txt
10	Irpinia 2	1980	6.9	13.0	B-CTR270.AT2.txt
11	Loma Prieta	1989	6.9	14.5	CAP000.AT2.txt
12	Loma Prieta	1989	6.9	14.5	CAP090.AT2.txt
13	Loma Prieta	1989	6.9	5.1	CLS000.AT2.txt
14	Loma Prieta	1989	6.9	5.1	CLS090.AT2.txt
15	Loma Prieta	1989	6.9	12.7	G02000.AT2.txt
16	Loma Prieta	1989	6.9	12.7	G02090.AT2.txt
17	Loma Prieta	1989	6.9	14.4	G03000.AT2.txt
18	Loma Prieta	1989	6.9	14.4	G03090.AT2.txt
19	Loma Prieta	1989	6.9	11.6	GL067.AT2.txt
20	Loma Prieta	1989	6.9	11.6	GL137.AT2.txt
21	Loma Prieta	1989	6.9	13.0	STG000.AT2.txt
22	Loma Prieta	1989	6.9	13.0	STG090.AT2.txt
23	Loma Prieta	1989	6.9	13.7	WVC000.AT2.txt
24	Loma Prieta	1989	6.9	13.7	WVC270.AT2.txt
25	Erzincan	1992	6.9	2.0	ERZ-EW.AT2.txt
26	Erzincan	1992	6.9	2.0	ERZ-NS.AT2.txt
27	Landers	1992	7.3	11.6	JOS000.AT2.txt
28	Landers	1992	7.3	11.6	JOS090.AT2.txt
29	Kobe	1995	6.9	10.2	AMA000.AT2.txt
30	Kobe	1995	6.9	10.2	AMA090.AT2.txt
31	Kobe	1995	6.9	0.6	KJM000.AT2.txt
32	Kobe	1995	6.9	0.6	KJM090.AT2.txt
33	Kobe	1995	6.9	1.2	TAZ000.AT2.txt
34	Kobe	1995	6.9	1.2	TAZ090.AT2.txt
35	Kocaeli	1999	7.4	12.7	DZC180.AT2.txt
36	Kocaeli	1999	7.4	12.7	DZC270.AT2.txt
37	Kocaeli	1999	7.4	3.1	SKR090.AT2.txt
38	Kocaeli	1999	7.4	2.6	YPT060.AT2.txt
39	Kocaeli	1999	7.4	2.6	YPT330.AT2.txt
40	Chi Chi	1999	7.6	7.3	CHY028-N.AT2.txt
41	Chi Chi	1999	7.6	7.3	CHY028-W.AT2.txt
42	Chi Chi	1999	7.6	6.9	CHY080-N.AT2.txt
43	Chi Chi	1999	7.6	6.9	CHY080-W.AT2.txt
44	Chi Chi	1999	7.6	9.7	NSY-E.AT2.txt
45	Chi Chi	1999	7.6	9.7	NSY-N.AT2.txt
46	Chi Chi	1999	7.6	5.7	TCU-E.AT2.txt
47	Chi Chi	1999	7.6	5.7	TCU-N.AT2.txt
48	Chi Chi	1999	7.6	0.3	TCU067-N.AT2.txt
49	Chi Chi	1999	7.6	0.3	TCU067-W.AT2.txt
50	Chi Chi	1999	7.6	4.9	TCU071-N.AT2.txt
51	Chi Chi	1999	7.6	4.9	TCU071-W.AT2.txt
52	Chi Chi	1999	7.6	13.7	TCU074-N.AT2.txt
53	Chi Chi	1999	7.6	13.7	TCU074-W.AT2.txt
54	Chi Chi	1999	7.6	10.0	TCU079-N.AT2.txt
55	Chi Chi	1999	7.6	10.0	TCU079-W.AT2.txt
56	Chi Chi	1999	7.6	8.2	TCU089-N.AT2.txt
57	Chi Chi	1999	7.6	8.2	TCU089-W.AT2.txt
58	Chi Chi	1999	7.6	13.6	TCU104-N.AT2.txt
59	Chi Chi	1999	7.6	13.6	TCU104-W.AT2.txt
60	Chi Chi	1999	7.6	13.1	TCU109-N.AT2.txt
61	Chi Chi	1999	7.6	13.1	TCU109-W.AT2.txt
62	Chi Chi	1999	7.6	9.0	TCU136-E.AT2.txt
63	Chi Chi	1999	7.6	9.0	TCU136-N.AT2.txt
64	Duzce	1999	7.1	0.9	1058-E.AT2.txt
65	Duzce	1999	7.1	0.9	1058-N.AT2.txt
66	Duzce	1999	7.1	8.5	1059-E.AT2.txt
67	Duzce	1999	7.1	8.5	1059-N.AT2.txt
68	Duzce	1999	7.1	13.3	1062-E.AT2.txt
69	Duzce	1999	7.1	13.3	1062-N.AT2.txt
70	Duzce	1999	7.1	8.2	375-E.AT2.txt
71	Duzce	1999	7.1	8.2	375-N.AT2.txt
72	Duzce	1999	7.1	8.2	DZC180.AT2.txt
73	Duzce	1999	7.1	8.2	DZC270.AT2.txt
	Min		6.9	0.3	
	Max		7.6	14.5	

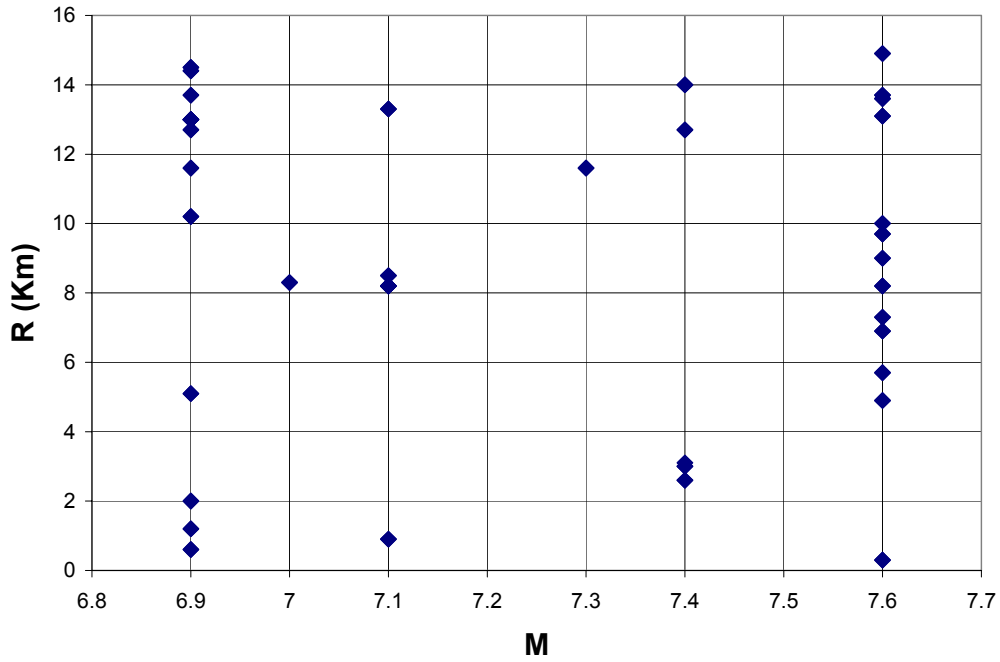
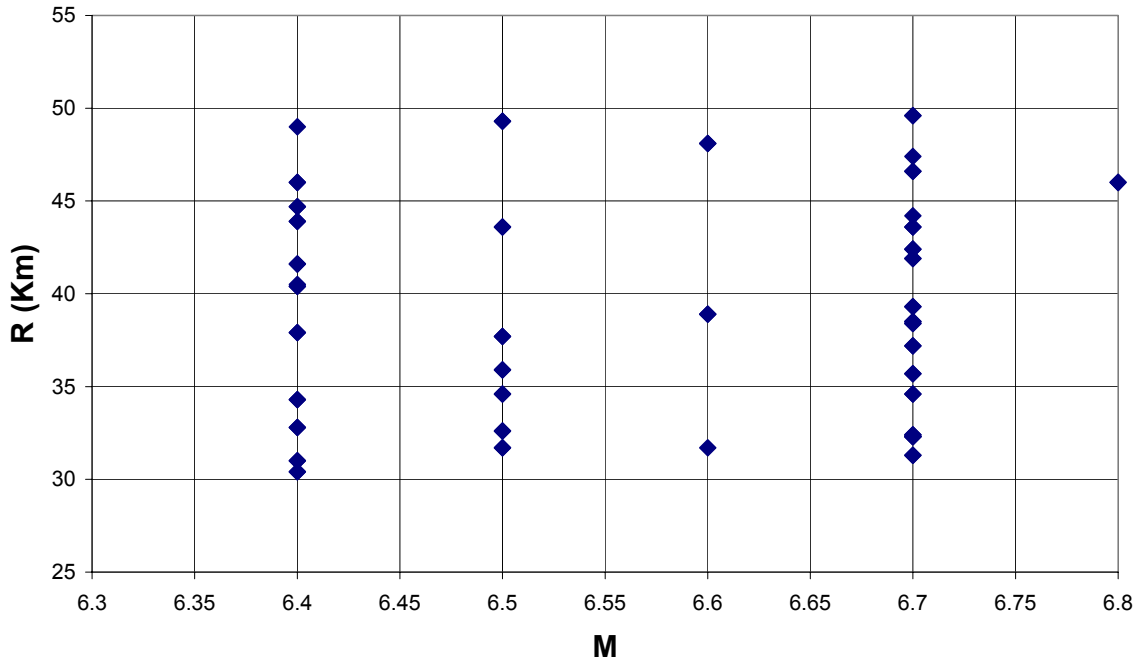
Table A5-6. Lists of the 73 earthquake records in "Bin V" ($M_w=6.9-7.6$, $R_{close}=15-30\text{km}$), on the left, and "Bin VI" ($M_w=6.9-7.6$, $R_{close}=30-50\text{km}$), on the right.

	EARTHQUAKE NAME	YEAR	M	R	RECORD NAME
1	Tabas	1978	7.4	26.1	BOS-L1.AT2.txt
2	Tabas	1978	7.4	26.1	BOS-T1.AT2.txt
3	Irpina 1	1980	6.9	23.0	A-BRZ000.AT2.txt
4	Irpina 1	1980	6.9	23.0	A-BRZ270.AT2.txt
5	Irpina 2	1980	6.9	23.0	B-BRZ000.AT2.txt
6	Irpina 2	1980	6.9	23.0	B-BRZ270.AT2.txt
7	Loma Prieta	1989	6.9	21.4	ADL250.AT2.txt
8	Loma Prieta	1989	6.9	21.4	ADL340.AT2.txt
9	Loma Prieta	1989	6.9	28.2	AGW000.AT2.txt
10	Loma Prieta	1989	6.9	28.2	AGW090.AT2.txt
11	Loma Prieta	1989	6.9	21.4	AND270.AT2.txt
12	Loma Prieta	1989	6.9	21.4	AND360.AT2.txt
13	Loma Prieta	1989	6.9	22.3	CLD195.AT2.txt
14	Loma Prieta	1989	6.9	22.3	CLD285.AT2.txt
15	Loma Prieta	1989	6.9	16.1	G04000.AT2.txt
16	Loma Prieta	1989	6.9	16.1	G04090.AT2.txt
17	Loma Prieta	1989	6.9	19.9	G06000.AT2.txt
18	Loma Prieta	1989	6.9	19.9	G06090.AT2.txt
19	Loma Prieta	1989	6.9	24.2	GMR000.AT2.txt
20	Loma Prieta	1989	6.9	24.2	GMR090.AT2.txt
21	Loma Prieta	1989	6.9	28.2	HCH090.AT2.txt
22	Loma Prieta	1989	6.9	28.2	HCH180.AT2.txt
23	Loma Prieta	1989	6.9	28.8	SVL270.AT2.txt
24	Loma Prieta	1989	6.9	28.8	SVL360.AT2.txt
25	Landers	1992	7.3	21.2	CLW-LN.AT2.txt
26	Landers	1992	7.3	21.2	CLW-TR.AT2.txt
27	Landers	1992	7.3	23.2	DSP000.AT2.txt
28	Landers	1992	7.3	23.2	DSP090.AT2.txt
29	Landers	1992	7.3	19.3	MVH000.AT2.txt
30	Landers	1992	7.3	19.3	MVH090.AT2.txt
31	Landers	1992	7.3	24.2	NPS000.AT2.txt
32	Landers	1992	7.3	24.2	NPS090.AT2.txt
33	Landers	1992	7.3	24.9	YER270.AT2.txt
34	Landers	1992	7.3	24.9	YER360.AT2.txt
35	Kobe	1995	6.9	23.8	ABN000.AT2.txt
36	Kobe	1995	6.9	23.8	ABN090.AT2.txt
37	Kocaeli	1999	7.4	17.0	ARC000.AT2.txt
38	Kocaeli	1999	7.4	17.0	ARC090.AT2.txt
39	Chi Chi	1999	7.6	25.4	CHY010-E.AT2.txt
40	Chi Chi	1999	7.6	25.4	CHY010-N.AT2.txt
41	Chi Chi	1999	7.6	15.3	CHY029-N.AT2.txt
42	Chi Chi	1999	7.6	15.3	CHY029-W.AT2.txt
43	Chi Chi	1999	7.6	18.1	CHY035-N.AT2.txt
44	Chi Chi	1999	7.6	20.4	CHY036-N.AT2.txt
45	Chi Chi	1999	7.6	20.4	CHY036-W.AT2.txt
46	Chi Chi	1999	7.6	29.5	CHY046-N.AT2.txt
47	Chi Chi	1999	7.6	29.5	CHY046-W.AT2.txt
48	Chi Chi	1999	7.6	24.7	TCU029-N.AT2.txt
49	Chi Chi	1999	7.6	24.7	TCU029-W.AT2.txt
50	Chi Chi	1999	7.6	26.8	TCU031-N.AT2.txt
51	Chi Chi	1999	7.6	26.8	TCU031-W.AT2.txt
52	Chi Chi	1999	7.6	16.7	TCU036-N.AT2.txt
53	Chi Chi	1999	7.6	16.7	TCU036-W.AT2.txt
54	Chi Chi	1999	7.6	16.7	TCU039-N.AT2.txt
55	Chi Chi	1999	7.6	16.7	TCU039-W.AT2.txt
56	Chi Chi	1999	7.6	24.1	TCU045-N.AT2.txt
57	Chi Chi	1999	7.6	24.1	TCU045-W.AT2.txt
58	Chi Chi	1999	7.6	17.8	TCU059-N.AT2.txt
59	Chi Chi	1999	7.6	17.8	TCU059-W.AT2.txt
60	Chi Chi	1999	7.6	17.7	TCU061-N.AT2.txt
61	Chi Chi	1999	7.6	17.7	TCU061-W.AT2.txt
62	Chi Chi	1999	7.6	19.1	TCU070-N.AT2.txt
63	Chi Chi	1999	7.6	19.1	TCU070-W.AT2.txt
64	Chi Chi	1999	7.6	20.3	TCU107-N.AT2.txt
65	Chi Chi	1999	7.6	20.3	TCU107-W.AT2.txt
66	Chi Chi	1999	7.6	15.1	TCU123-N.AT2.txt
67	Chi Chi	1999	7.6	15.1	TCU123-W.AT2.txt
68	Duzce	1999	7.1	15.6	1061-E.AT2.txt
69	Duzce	1999	7.1	15.6	1061-N.AT2.txt
70	Duzce	1999	7.1	27.4	362-E.AT2.txt
71	Duzce	1999	7.1	27.4	362-N.AT2.txt
72	Duzce	1999	7.1	17.6	BOL000.AT2.txt
73	Duzce	1999	7.1	17.6	BOL090.AT2.txt
	Min		6.9	15.1	
	Max		7.6	29.5	

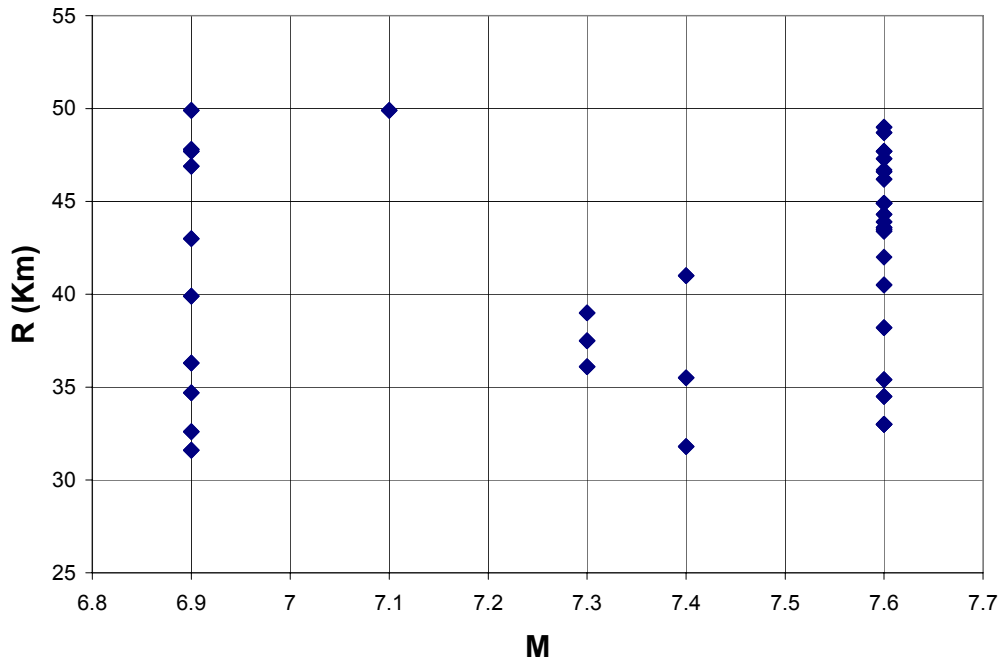
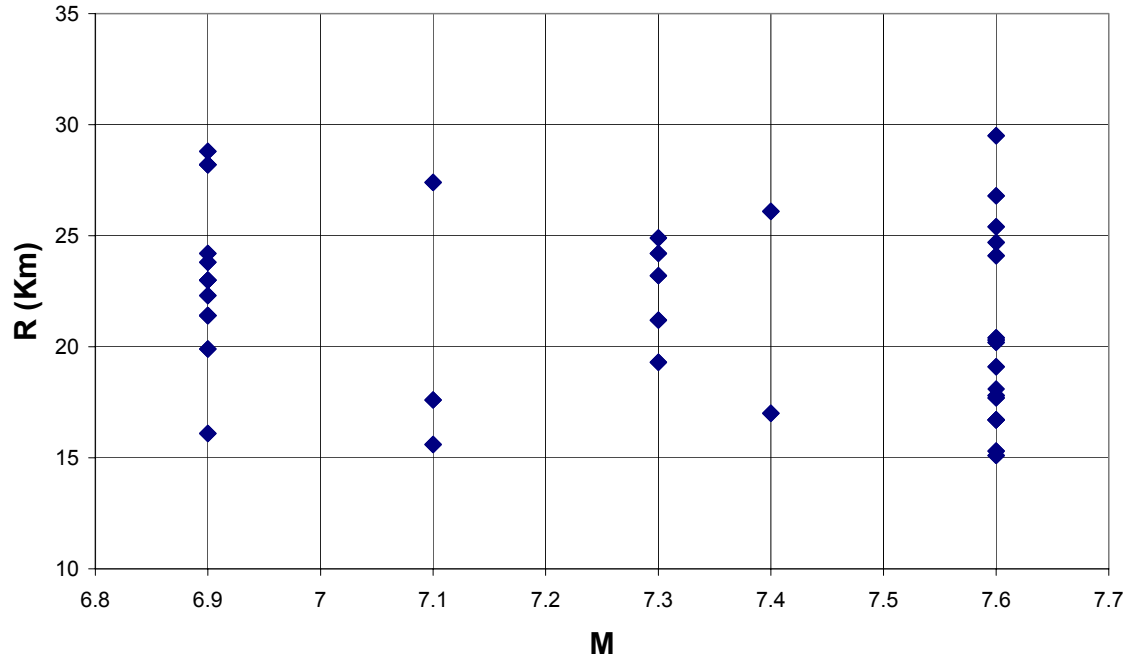
	EARTHQUAKE NAME	YEAR	M	R	RECORD NAME
1	Kern County	1952	7.4	41.0	TAF021.AT2.txt
2	Kern County	1952	7.4	41.0	TAF111.AT2.txt
3	Taiwan Smart 1	1986	7.3	39.0	45C00EW.AT2.txt
4	Taiwan Smart 1	1986	7.3	39.0	45C00NS.AT2.txt
5	Loma Prieta	1989	6.9	47.7	A07000.AT2.txt
6	Loma Prieta	1989	6.9	47.7	A07090.AT2.txt
7	Loma Prieta	1989	6.9	46.9	A09137.AT2.txt
8	Loma Prieta	1989	6.9	46.9	A09227.AT2.txt
9	Loma Prieta	1989	6.9	47.8	A10000.AT2.txt
10	Loma Prieta	1989	6.9	47.8	A10090.AT2.txt
11	Loma Prieta	1989	6.9	49.9	BES000.AT2.txt
12	Loma Prieta	1989	6.9	49.9	BES090.AT2.txt
13	Loma Prieta	1989	6.9	43.0	FRE000.AT2.txt
14	Loma Prieta	1989	6.9	43.0	FRE090.AT2.txt
15	Loma Prieta	1989	6.9	31.6	HVR000.AT2.txt
16	Loma Prieta	1989	6.9	31.6	HVR090.AT2.txt
17	Loma Prieta	1989	6.9	34.7	SG3261.AT2.txt
18	Loma Prieta	1989	6.9	34.7	SG3351.AT2.txt
19	Loma Prieta	1989	6.9	32.6	SJW160.AT2.txt
20	Loma Prieta	1989	6.9	32.6	SJW250.AT2.txt
21	Loma Prieta	1989	6.9	36.3	SLC270.AT2.txt
22	Loma Prieta	1989	6.9	36.3	SLC360.AT2.txt
23	Loma Prieta	1989	6.9	39.9	WDS000.AT2.txt
24	Loma Prieta	1989	6.9	39.9	WDS090.AT2.txt
25	Landers	1992	7.3	36.1	BRS000.AT2.txt
26	Landers	1992	7.3	36.1	BRS090.AT2.txt
27	Landers	1992	7.3	37.5	PSA000.AT2.txt
28	Landers	1992	7.3	37.5	PSA090.AT2.txt
29	Kocaeli	1999	7.4	35.5	GYN000.AT2.txt
30	Kocaeli	1999	7.4	35.5	GYN090.AT2.txt
31	Kocaeli	1999	7.4	31.8	IZN090.AT2.txt
32	Kocaeli	1999	7.4	31.8	IZN180.AT2.txt
33	Chi Chi	1999	7.6	47.7	CHY081-N.AT2.txt
34	Chi Chi	1999	7.6	47.7	CHY081-W.AT2.txt
35	Chi Chi	1999	7.6	35.4	CHY086-N.AT2.txt
36	Chi Chi	1999	7.6	35.4	CHY086-W.AT2.txt
37	Chi Chi	1999	7.6	34.5	CHY087-N.AT2.txt
38	Chi Chi	1999	7.6	34.5	CHY087-W.AT2.txt
39	Chi Chi	1999	7.6	46.2	CHY102-N.AT2.txt
40	Chi Chi	1999	7.6	46.2	CHY102-W.AT2.txt
41	Chi Chi	1999	7.6	44.9	ESL-E.AT2.txt
42	Chi Chi	1999	7.6	44.9	ESL-N.AT2.txt
43	Chi Chi	1999	7.6	43.9	HWA005-E.AT2.txt
44	Chi Chi	1999	7.6	43.9	HWA005-N.AT2.txt
45	Chi Chi	1999	7.6	44.9	HWA020-N.AT2.txt
46	Chi Chi	1999	7.6	44.9	HWA020-W.AT2.txt
47	Chi Chi	1999	7.6	44.3	HWA024-N.AT2.txt
48	Chi Chi	1999	7.6	44.3	HWA024-W.AT2.txt
49	Chi Chi	1999	7.6	49.0	HWA033-N.AT2.txt
50	Chi Chi	1999	7.6	49.0	HWA033-W.AT2.txt
51	Chi Chi	1999	7.6	42.0	HWA034-W.AT2.txt
52	Chi Chi	1999	7.6	43.6	HWA036-N.AT2.txt
53	Chi Chi	1999	7.6	43.6	HWA036-W.AT2.txt
54	Chi Chi	1999	7.6	46.6	HWA037-N.AT2.txt
55	Chi Chi	1999	7.6	46.6	HWA037-W.AT2.txt
56	Chi Chi	1999	7.6	46.7	HWA039-N.AT2.txt
57	Chi Chi	1999	7.6	47.7	HWA039-W.AT2.txt
58	Chi Chi	1999	7.6	48.7	HWA055-E.AT2.txt
59	Chi Chi	1999	7.6	48.7	HWA055-N.AT2.txt
60	Chi Chi	1999	7.6	40.5	KAU054-N.AT2.txt
61	Chi Chi	1999	7.6	40.5	KAU054-W.AT2.txt
62	Chi Chi	1999	7.6	47.3	TCU015-N.AT2.txt
63	Chi Chi	1999	7.6	47.3	TCU015-W.AT2.txt
64	Chi Chi	1999	7.6	38.2	TCU033-N.AT2.txt
65	Chi Chi	1999	7.6	38.2	TCU033-W.AT2.txt
66	Chi Chi	1999	7.6	33.0	TCU034-N.AT2.txt
67	Chi Chi	1999	7.6	33.0	TCU034-W.AT2.txt
68	Chi Chi	1999	7.6	33.0	TCU047-N.AT2.txt
69	Chi Chi	1999	7.6	33.0	TCU047-W.AT2.txt
70	Chi Chi	1999	7.6	43.4	TCU095-N.AT2.txt
71	Chi Chi	1999	7.6	43.4	TCU095-W.AT2.txt
72	Duzce	1999	7.1	49.9	SKR090.AT2.txt
73	Duzce	1999	7.1	49.9	SKR180.AT2.txt
	Min		6.9	31.6	
	Max		7.6	49.9	



Figures A1-2. Scatter plots of earthquake magnitude (M_w) versus closest source-to-site distance (R_{close}) for the earthquake records in "Bin I" ($M_w=6.4-6.8$, $R_{close}=0-15$ km), on the top, and "Bin II" ($M_w=6.4-6.8$, $R_{close}=15-30$ km), on the bottom.



Figures A3-4. Scatter plots of earthquake magnitude (M_w) versus closest source-to-site distance (R_{close}) for the earthquake records in "Bin III" ($M_w=6.4-6.8$, $R_{close}=30-50$ km), on the top, and "Bin IV" ($M_w=6.9-7.6$, $R_{close}=0-15$ km), on the bottom.



Figures A5-6. Scatter plots of earthquake magnitude (M_w) versus closest source-to-site distance (R_{close}) for the earthquake records in "Bin V" ($M_w=6.9-7.6$, $R_{close}=15-30\text{km}$), on the top, and "Bin VI" ($M_w=6.9-7.6$, $R_{close}=30-50\text{km}$), on the bottom.

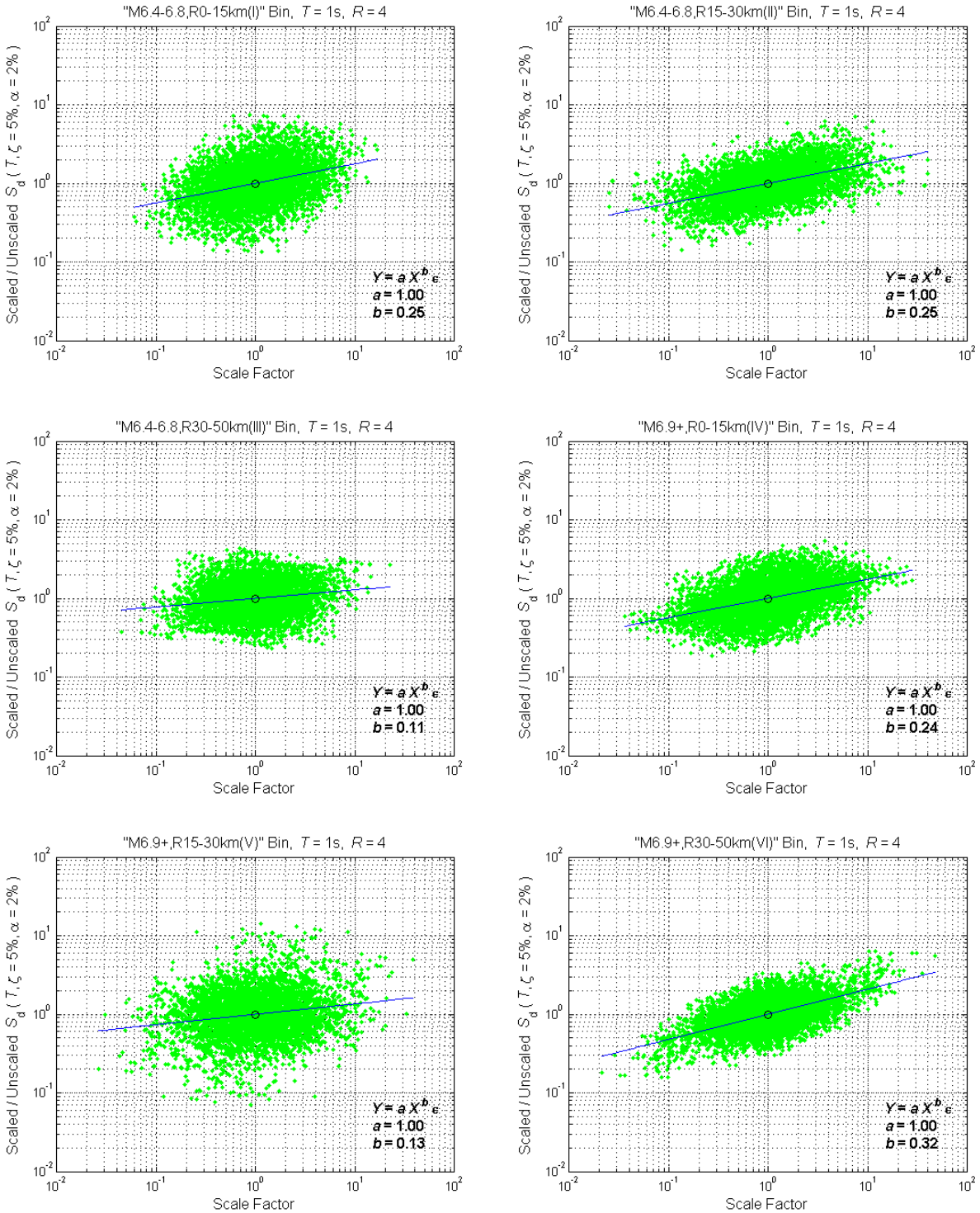


Figure A7. Intra-bin scaling results for a bilinear SDOF structure of period $T=1$ sec and strength reduction factor $R=4$ for the six M_w - R_{close} bins of earthquake records considered. The analogous results for the Near-Source Bin are shown in Figure 11 of the main text.

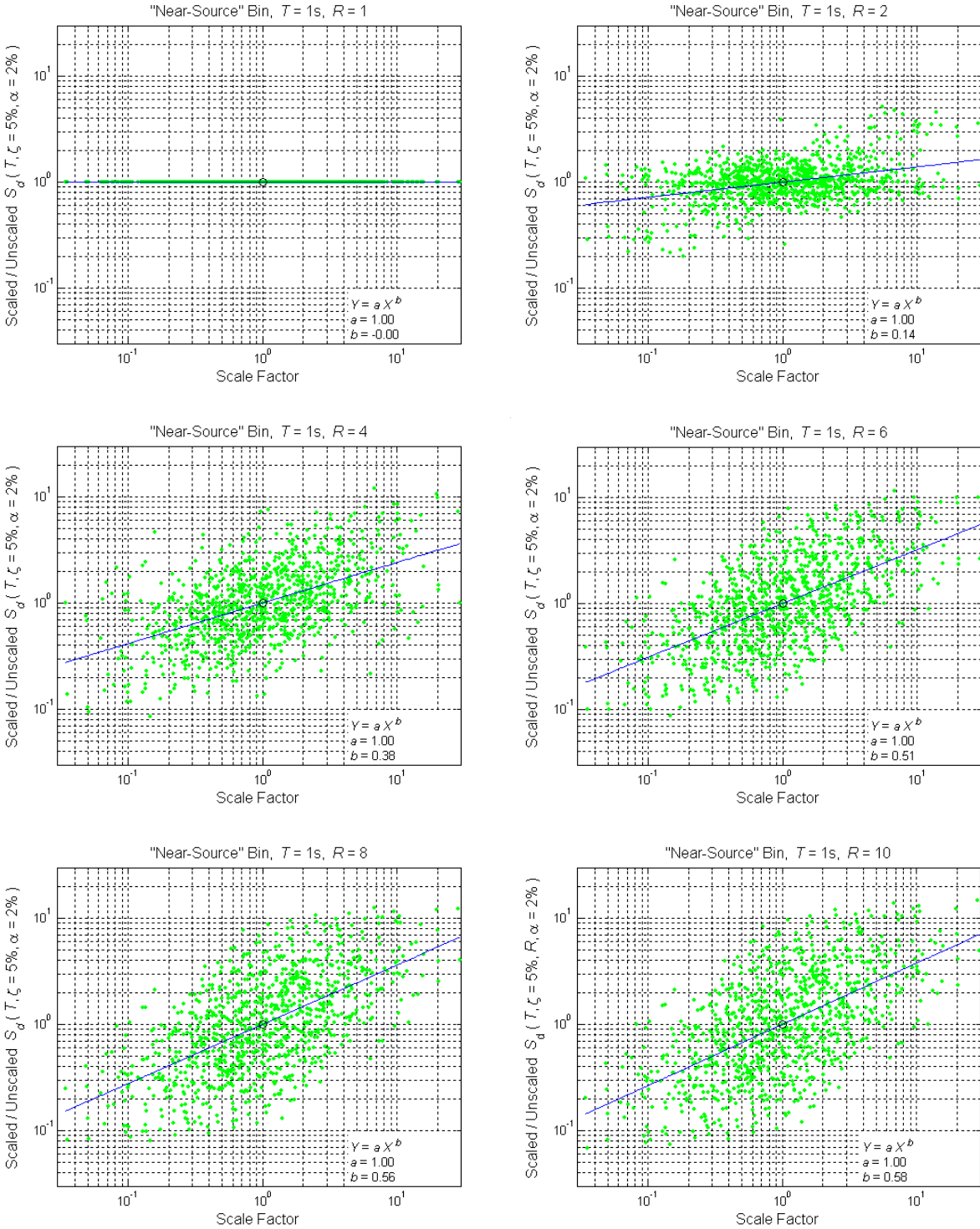


Figure A8. Intra-bin scaling results for the Near-Source Bin and a bilinear SDOF structure of period $T=1$ sec but strength reduction factors ranging from $R=1$ to 10. The results for $R=4$ are the same as those shown in Figure 11 of the main text.

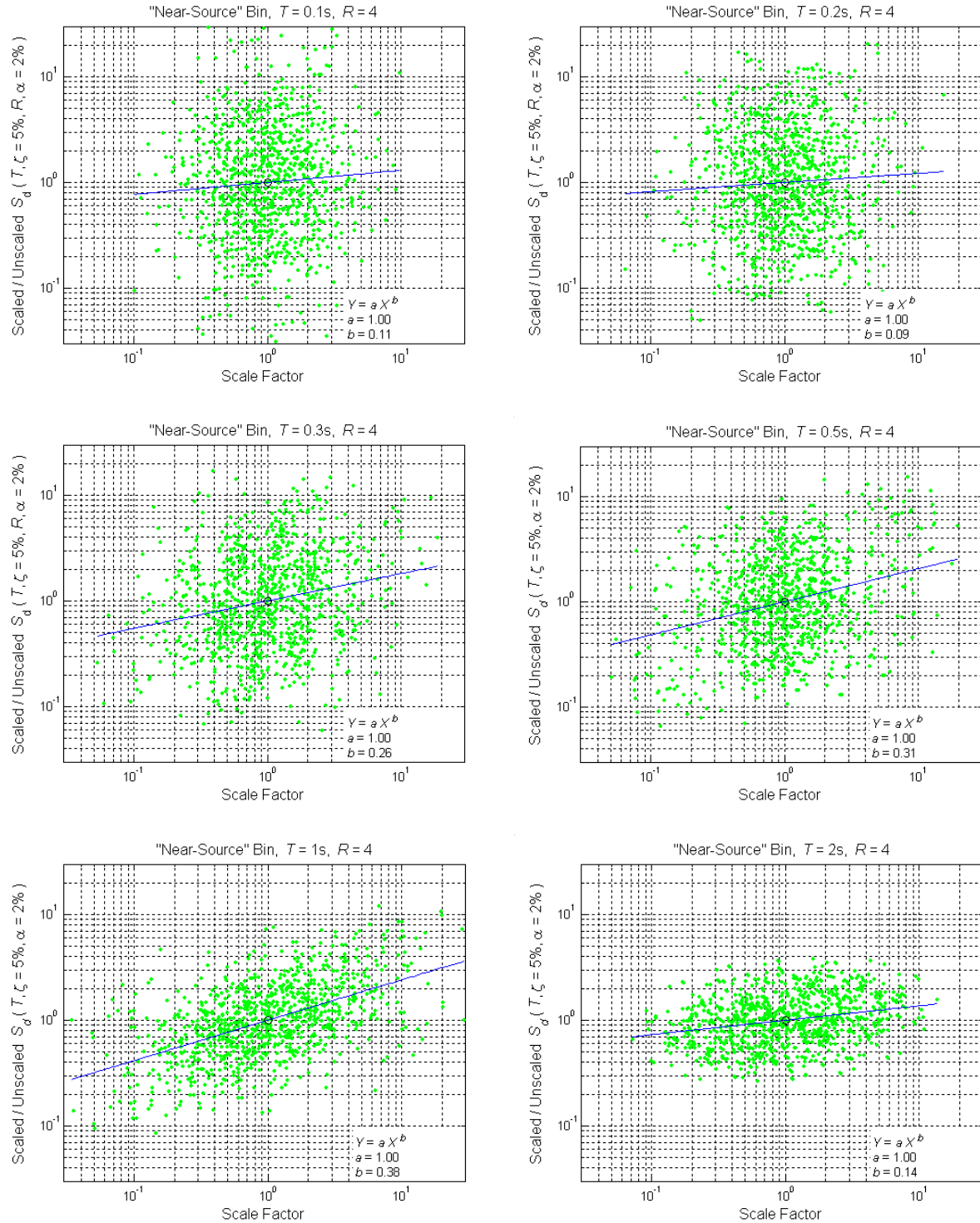


Figure A9(a). Intra-bin scaling results for the Near-Source Bin and a bilinear SDOF structure with periods ranging from $T=0.1$ sec to 2sec and a strength reduction factor of $R=4$. The results for $T=1$ sec are the same as those shown in Figure 11 of the main text.

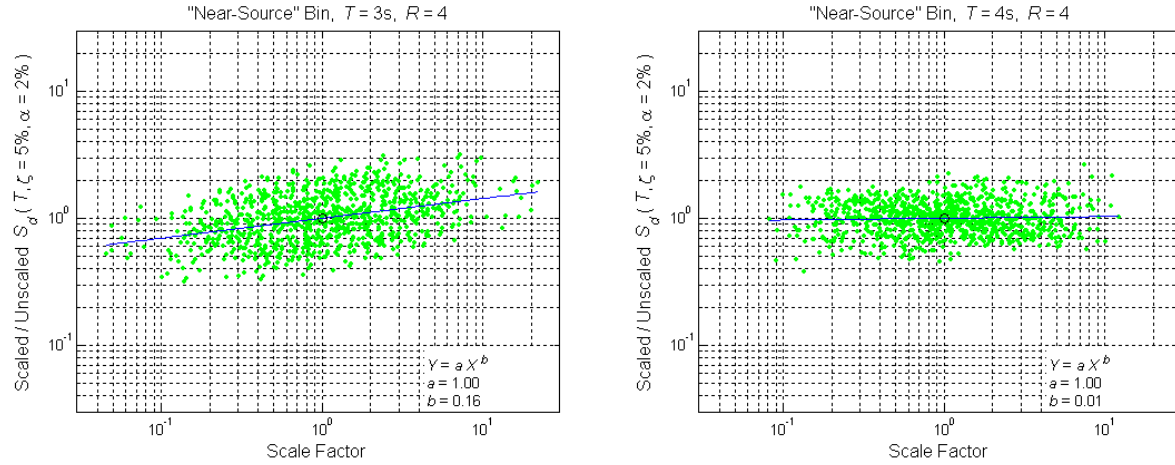
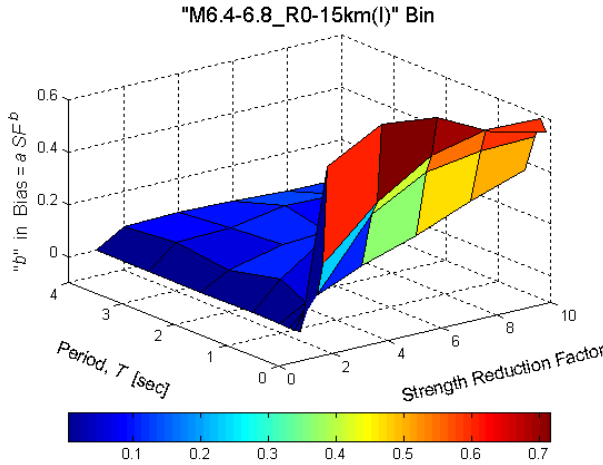
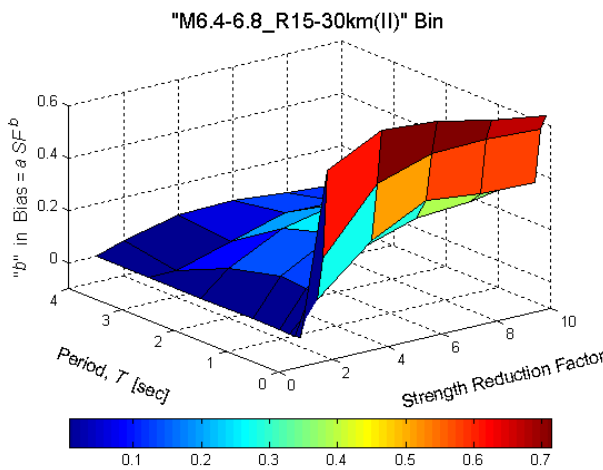


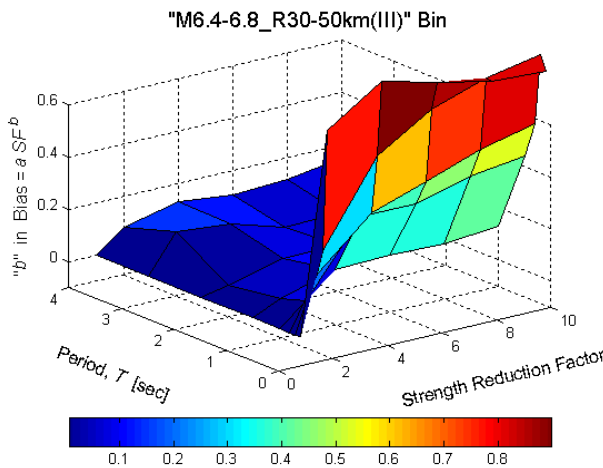
Figure A9(b). Intra-bin scaling results for the Near-Source Bin and a bilinear SDOF structure of period $T=3$ sec or 4 sec and a strength reduction factor of $R=4$. The results for periods less than 3 sec are shown in Figure A9(a).



		"b" in Bias = a*SF^b							
		R = 1	R = 2	R = 4	R = 6	R = 8	R = 10	Min	Max
T = 0.1		0.00	0.61	0.72	0.70	0.59	0.54	0.00	0.72
T = 0.2		0.00	0.23	0.42	0.55	0.59	0.58	0.00	0.59
T = 0.3		0.00	0.10	0.36	0.47	0.50	0.51	0.00	0.51
T = 0.5		0.00	0.06	0.15	0.21	0.30	0.37	0.00	0.37
T = 1		0.00	0.11	0.25	0.31	0.36	0.38	0.00	0.38
T = 2		0.00	0.06	0.11	0.09	0.09	0.09	0.00	0.11
T = 3		0.00	0.09	0.09	0.13	0.12	0.11	0.00	0.13
T = 4		0.00	0.07	0.07	0.07	0.06	0.05	0.00	0.07
Min		0.00	0.06	0.07	0.07	0.06	0.05	0.00	0.07
Max		0.00	0.61	0.72	0.70	0.59	0.58	0.00	0.72

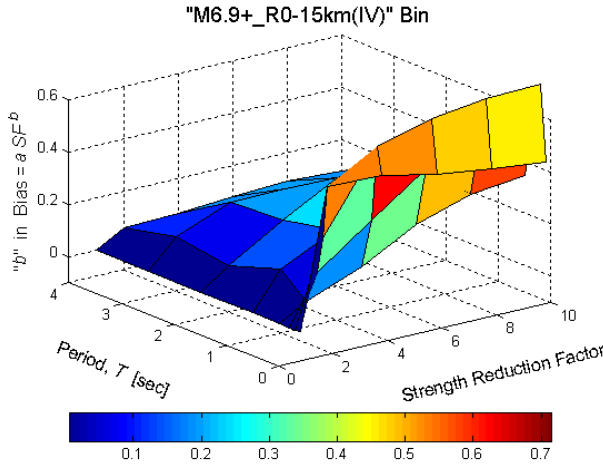


		"b" in Bias = a*SF^b							
		R = 1	R = 2	R = 4	R = 6	R = 8	R = 10	Min	Max
T = 0.1		0.00	0.62	0.72	0.71	0.66	0.63	0.00	0.72
T = 0.2		0.00	0.27	0.51	0.58	0.58	0.57	0.00	0.58
T = 0.3		0.00	0.11	0.28	0.39	0.36	0.36	0.00	0.39
T = 0.5		0.00	0.13	0.24	0.30	0.32	0.35	0.00	0.35
T = 1		0.00	0.14	0.25	0.35	0.39	0.42	0.00	0.42
T = 2		0.00	0.09	0.20	0.24	0.27	0.26	0.00	0.27
T = 3		0.00	0.00	0.06	0.12	0.12	0.11	0.00	0.12
T = 4		0.00	0.04	0.08	0.09	0.07	0.06	0.00	0.09
Min		0.00	0.00	0.06	0.09	0.07	0.06	0.00	0.09
Max		0.00	0.62	0.72	0.71	0.66	0.63	0.00	0.72

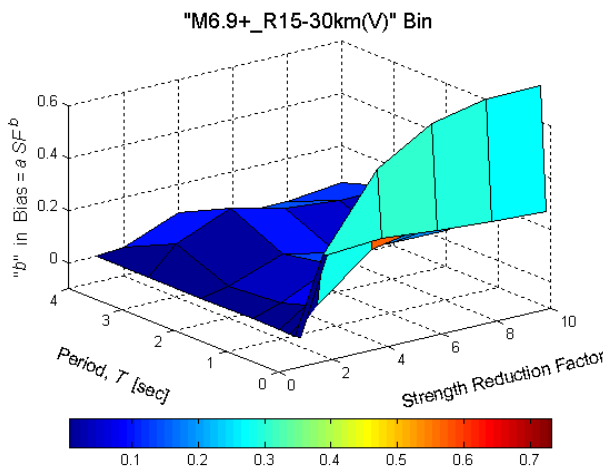


		"b" in Bias = a*SF^b							
		R = 1	R = 2	R = 4	R = 6	R = 8	R = 10	Min	Max
T = 0.1		0.00	0.77	0.90	0.85	0.81	0.79	0.00	0.90
T = 0.2		0.00	0.30	0.61	0.74	0.81	0.85	0.00	0.85
T = 0.3		0.00	0.20	0.39	0.45	0.53	0.58	0.00	0.58
T = 0.5		0.00	0.08	0.36	0.35	0.41	0.44	0.00	0.44
T = 1		0.00	0.05	0.11	0.12	0.11	0.13	0.00	0.13
T = 2		0.00	0.02	0.07	0.08	0.06	0.06	0.00	0.08
T = 3		0.00	0.14	0.13	0.06	0.07	0.08	0.00	0.14
T = 4		0.00	0.08	0.13	0.11	0.12	0.15	0.00	0.15
Min		0.00	0.02	0.07	0.06	0.06	0.06	0.00	0.08
Max		0.00	0.77	0.90	0.85	0.81	0.85	0.00	0.90

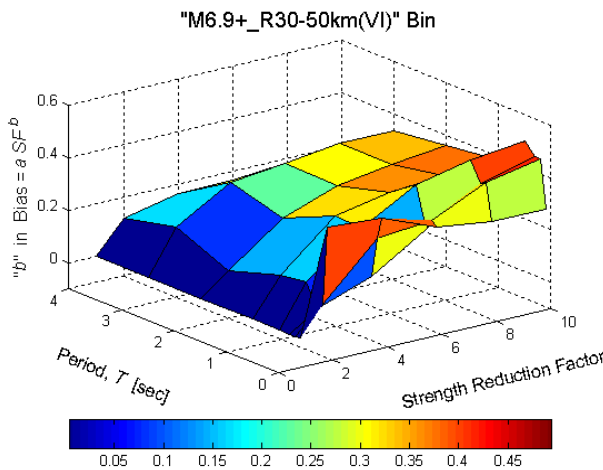
Figures A10-12. Intra-bin scaling results for Bins I-III and the range of SDOF periods and strength reduction factors considered. Note that the parameter "a" is found to equal unity for intra-bin scaling (and the SDOF structures), so a larger value of b translates to a larger bias for a given scale factor.



		"b" in Bias = $a \cdot SF^b$							
		$R = 1$	$R = 2$	$R = 4$	$R = 6$	$R = 8$	$R = 10$	Min	Max
$T = 0.1$		0.00	0.53	0.53	0.48	0.45	0.43	0.00	0.53
$T = 0.2$		0.00	0.33	0.63	0.69	0.71	0.72	0.00	0.72
$T = 0.3$		0.00	0.19	0.34	0.48	0.58	0.61	0.00	0.61
$T = 0.5$		0.00	0.06	0.14	0.25	0.32	0.34	0.00	0.34
$T = 1$		0.00	0.14	0.24	0.32	0.33	0.35	0.00	0.35
$T = 2$		0.00	0.08	0.20	0.32	0.37	0.40	0.00	0.40
$T = 3$		0.00	0.11	0.19	0.19	0.18	0.19	0.00	0.19
$T = 4$		0.00	0.06	0.07	0.08	0.09	0.08	0.00	0.09
Min		0.00	0.06	0.07	0.08	0.09	0.08	0.00	0.09
Max		0.00	0.53	0.63	0.69	0.71	0.72	0.00	0.72

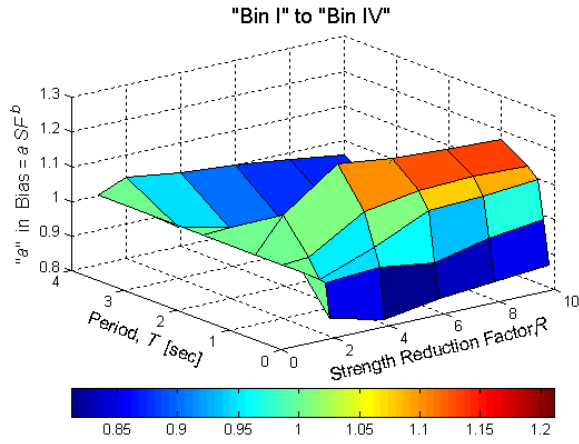


		"b" in Bias = $a \cdot SF^b$							
		$R = 1$	$R = 2$	$R = 4$	$R = 6$	$R = 8$	$R = 10$	Min	Max
$T = 0.1$		0.00	0.29	0.31	0.29	0.27	0.26	0.00	0.31
$T = 0.2$		0.00	0.29	0.57	0.69	0.74	0.74	0.00	0.74
$T = 0.3$		0.00	0.08	0.25	0.29	0.42	0.48	0.00	0.48
$T = 0.5$		0.00	0.07	0.25	0.29	0.38	0.41	0.00	0.41
$T = 1$		0.00	0.04	0.13	0.19	0.19	0.20	0.00	0.20
$T = 2$		0.00	0.02	0.09	0.05	0.04	0.04	0.00	0.09
$T = 3$		0.00	0.10	0.19	0.14	0.12	0.12	0.00	0.19
$T = 4$		0.00	0.01	0.09	0.03	0.04	0.06	0.00	0.09
Min		0.00	0.01	0.09	0.03	0.04	0.04	0.00	0.09
Max		0.00	0.29	0.57	0.69	0.74	0.74	0.00	0.74

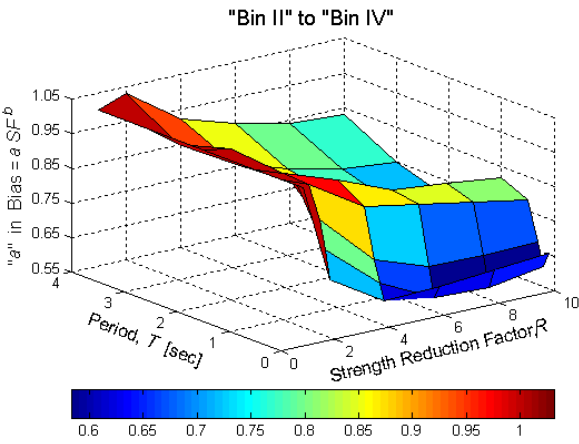


		"b" in Bias = $a \cdot SF^b$							
		$R = 1$	$R = 2$	$R = 4$	$R = 6$	$R = 8$	$R = 10$	Min	Max
$T = 0.1$		0.00	0.40	0.38	0.30	0.27	0.27	0.00	0.40
$T = 0.2$		0.00	0.10	0.30	0.32	0.41	0.45	0.00	0.45
$T = 0.3$		0.00	0.07	0.14	0.28	0.40	0.45	0.00	0.45
$T = 0.5$		0.00	0.16	0.31	0.43	0.48	0.50	0.00	0.50
$T = 1$		0.00	0.14	0.32	0.36	0.38	0.39	0.00	0.39
$T = 2$		0.00	0.08	0.23	0.30	0.34	0.36	0.00	0.36
$T = 3$		0.00	0.16	0.29	0.31	0.34	0.34	0.00	0.34
$T = 4$		0.00	0.12	0.17	0.17	0.13	0.13	0.00	0.17
Min		0.00	0.07	0.14	0.17	0.13	0.13	0.00	0.17
Max		0.00	0.40	0.38	0.43	0.48	0.50	0.00	0.50

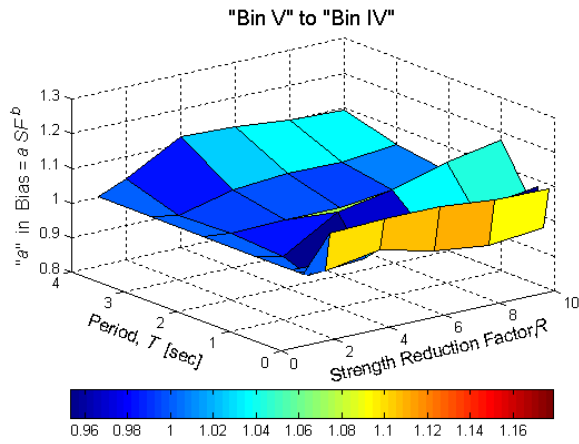
Figure A13-15. Intra-bin scaling results for Bins IV-VI and the range of SDOF periods and strength reduction factors considered. Note that the parameter " a " is found to equal unity for intra-bin scaling (and the SDOF structures), so a larger value of b translates to a larger bias for a given scale factor.



		"a" in Bias = $a \cdot SF^b$							
		$R = 1$	$R = 2$	$R = 4$	$R = 6$	$R = 8$	$R = 10$	Min	Max
$T = 0.1$		1.00	0.85	0.81	0.84	0.85	0.86	0.81	1.00
$T = 0.2$		1.00	0.95	0.96	0.93	0.97	0.99	0.93	1.00
$T = 0.3$		1.00	0.95	1.01	1.08	1.09	1.10	0.95	1.10
$T = 0.5$		1.00	1.01	1.10	1.13	1.13	1.13	1.00	1.13
$T = 1$		1.00	1.10	1.21	1.19	1.18	1.17	1.00	1.21
$T = 2$		1.00	1.01	0.93	0.89	0.86	0.85	0.85	1.01
$T = 3$		1.00	0.95	0.90	0.88	0.87	0.86	0.86	1.00
$T = 4$		1.00	1.03	1.01	1.00	0.98	0.96	0.96	1.03
Min		1.00	0.85	0.81	0.84	0.85	0.85	0.81	1.00
Max		1.00	1.10	1.21	1.19	1.18	1.17	1.00	1.21

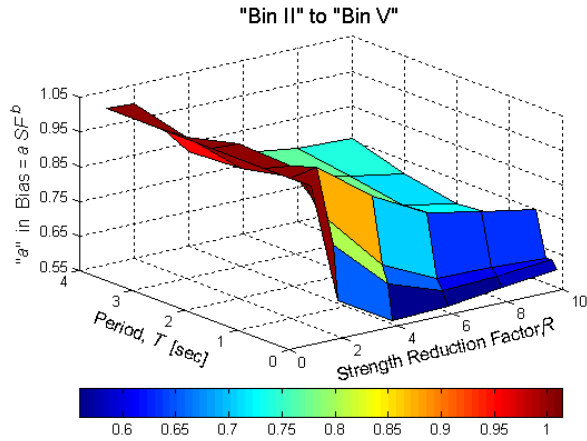


		"a" in Bias = $a \cdot SF^b$							
		$R = 1$	$R = 2$	$R = 4$	$R = 6$	$R = 8$	$R = 10$	Min	Max
$T = 0.1$		1.00	0.72	0.62	0.63	0.64	0.65	0.62	1.00
$T = 0.2$		1.00	0.80	0.67	0.59	0.58	0.61	0.58	1.00
$T = 0.3$		1.00	0.88	0.73	0.67	0.67	0.67	0.67	1.00
$T = 0.5$		1.00	0.97	0.87	0.84	0.81	0.78	0.78	1.00
$T = 1$		1.00	0.97	0.92	0.85	0.84	0.82	0.82	1.00
$T = 2$		1.00	0.99	0.86	0.77	0.72	0.70	0.70	1.00
$T = 3$		1.00	0.94	0.85	0.80	0.77	0.75	0.75	1.00
$T = 4$		1.00	1.03	0.92	0.87	0.84	0.83	0.83	1.03
Min		1.00	0.72	0.62	0.59	0.58	0.61	0.58	1.00
Max		1.00	1.03	0.92	0.87	0.84	0.83	0.83	1.03

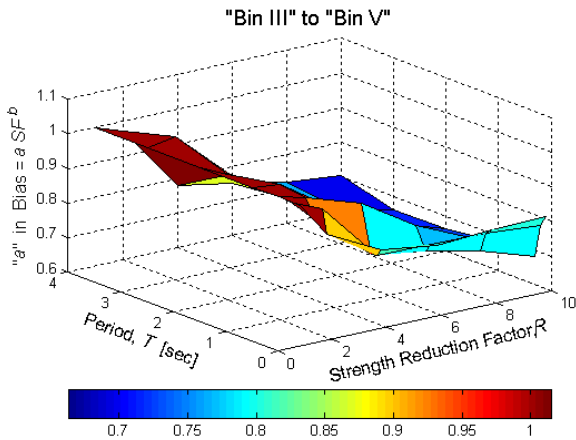


		"a" in Bias = $a \cdot SF^b$							
		$R = 1$	$R = 2$	$R = 4$	$R = 6$	$R = 8$	$R = 10$	Min	Max
$T = 0.1$		1.00	1.10	1.11	1.11	1.09	1.09	1.00	1.11
$T = 0.2$		1.00	0.99	1.01	0.97	0.95	0.97	0.95	1.01
$T = 0.3$		1.00	1.00	1.03	1.06	1.06	1.08	1.00	1.08
$T = 0.5$		1.00	0.96	0.97	1.04	1.04	1.05	0.96	1.05
$T = 1$		1.00	0.98	1.08	1.10	1.15	1.18	0.98	1.18
$T = 2$		1.00	0.99	1.00	1.00	1.01	1.03	0.99	1.03
$T = 3$		1.00	0.99	1.02	1.04	1.03	1.05	0.99	1.05
$T = 4$		1.00	1.03	1.12	1.11	1.10	1.09	1.00	1.12
Min		1.00	0.96	0.97	0.97	0.95	0.97	0.95	1.01
Max		1.00	1.10	1.12	1.11	1.15	1.18	1.00	1.18

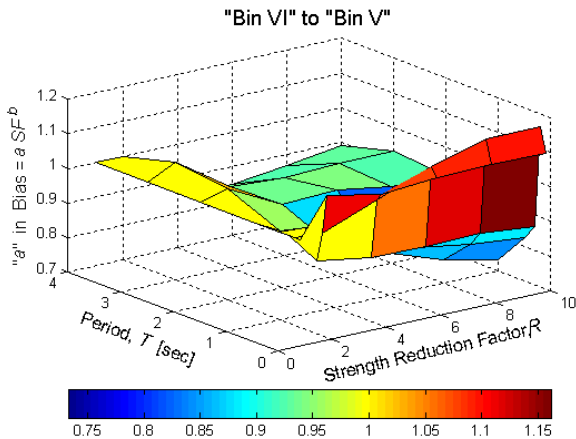
Figures A16-18. Inter-bin scaling results for the Bin I ($M_w=6.4-6.8$, $R_{close}=0-15km$) to Bin IV ($M_w=6.9-7.6$, $R_{close}=0-15km$), the Bin II ($M_w=6.4-6.8$, $R_{close}=15-30km$) to Bin IV, and the Bin V ($M_w=6.9-7.6$, $R_{close}=15-30km$) to Bin IV scenarios. The corresponding values of "b" are very similar to those observed for intra-bin scaling within the target bin (shown in Figure A13).



		"a" in Bias = a*SF^b							
		R = 1	R = 2	R = 4	R = 6	R = 8	R = 10	Min	Max
T = 0.1		1.00	0.65	0.56	0.56	0.59	0.60	0.56	1.00
T = 0.2		1.00	0.81	0.66	0.61	0.61	0.62	0.61	1.00
T = 0.3		1.00	0.88	0.71	0.63	0.63	0.62	0.62	1.00
T = 0.5		1.00	1.01	0.90	0.81	0.78	0.75	0.75	1.01
T = 1		1.00	0.99	0.85	0.77	0.73	0.70	0.70	1.00
T = 2		1.00	0.99	0.86	0.78	0.71	0.68	0.68	1.00
T = 3		1.00	0.96	0.83	0.77	0.74	0.71	0.71	1.00
T = 4		1.00	1.00	0.82	0.78	0.76	0.76	0.76	1.00
Min		1.00	0.65	0.56	0.56	0.59	0.60	0.56	1.00
Max		1.00	1.01	0.90	0.81	0.78	0.76	0.76	1.01

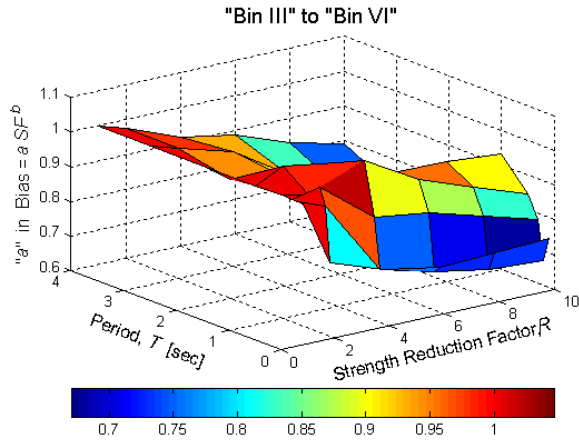


		"a" in Bias = a*SF^b							
		R = 1	R = 2	R = 4	R = 6	R = 8	R = 10	Min	Max
T = 0.1		1.00	0.90	0.82	0.79	0.80	0.81	0.79	1.00
T = 0.2		1.00	0.96	0.79	0.79	0.79	0.78	0.78	1.00
T = 0.3		1.00	0.92	0.79	0.77	0.73	0.68	0.68	1.00
T = 0.5		1.00	0.98	0.93	0.83	0.76	0.70	0.70	1.00
T = 1		1.00	0.99	0.88	0.78	0.73	0.68	0.68	1.00
T = 2		1.00	0.96	0.86	0.79	0.72	0.66	0.66	1.00
T = 3		1.00	1.01	0.87	0.77	0.70	0.66	0.66	1.01
T = 4		1.00	0.97	0.78	0.75	0.72	0.70	0.70	1.00
Min		1.00	0.90	0.78	0.75	0.70	0.66	0.66	1.00
Max		1.00	1.01	0.93	0.83	0.80	0.81	0.79	1.01

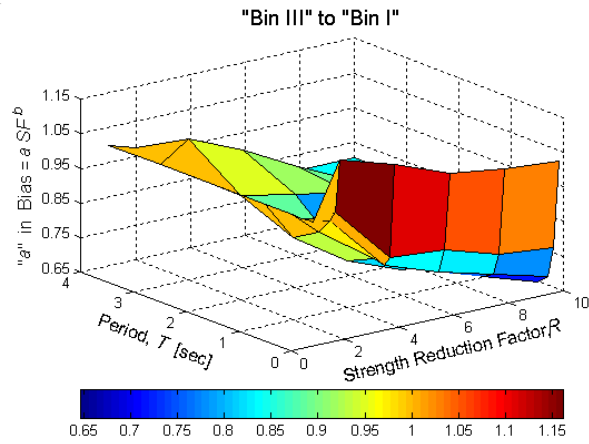


		"a" in Bias = a*SF^b							
		R = 1	R = 2	R = 4	R = 6	R = 8	R = 10	Min	Max
T = 0.1		1.00	1.11	1.08	1.09	1.09	1.09	1.00	1.11
T = 0.2		1.00	0.99	1.06	1.12	1.16	1.16	0.99	1.16
T = 0.3		1.00	0.91	0.88	0.88	0.88	0.87	0.87	1.00
T = 0.5		1.00	1.00	0.89	0.87	0.84	0.82	0.82	1.00
T = 1		1.00	0.96	0.87	0.82	0.77	0.73	0.73	1.00
T = 2		1.00	1.02	0.94	0.95	0.92	0.92	0.92	1.02
T = 3		1.00	1.04	0.93	0.92	0.93	0.93	0.92	1.04
T = 4		1.00	1.00	0.85	0.85	0.87	0.89	0.85	1.00
Min		1.00	0.91	0.85	0.82	0.77	0.73	0.73	1.00
Max		1.00	1.11	1.08	1.12	1.16	1.16	1.00	1.16

Figures A19-21. Inter-bin scaling results for the Bin II ($M_w=6.4-6.8$, $R_{close}=15-30\text{km}$) to Bin V ($M_w=6.9-7.6$, $R_{close}=15-30\text{km}$), the Bin III ($M_w=6.4-6.8$, $R_{close}=30-50\text{km}$) to Bin V, and the Bin VI ($M_w=6.9-7.6$, $R_{close}=30-50\text{km}$) to Bin V scenarios. The corresponding values of "b" are very similar to those observed for intra-bin scaling within the target bin (shown in Figure A14).



"a" in Bias = a ^a SF ^b								
	R = 1	R = 2	R = 4	R = 6	R = 8	R = 10	Min	Max
T = 0.1	1.00	0.81	0.76	0.73	0.73	0.74	0.73	1.00
T = 0.2	1.00	0.97	0.75	0.71	0.68	0.67	0.67	1.00
T = 0.3	1.00	1.02	0.90	0.87	0.83	0.79	0.79	1.02
T = 0.5	1.00	0.98	1.05	0.96	0.90	0.85	0.85	1.05
T = 1	1.00	1.04	1.01	0.95	0.95	0.93	0.93	1.04
T = 2	1.00	0.94	0.92	0.84	0.78	0.72	0.72	1.00
T = 3	1.00	0.98	0.93	0.83	0.75	0.71	0.71	1.00
T = 4	1.00	0.98	0.91	0.88	0.83	0.79	0.79	1.00
Min	1.00	0.81	0.75	0.71	0.68	0.67	0.67	1.00
Max	1.00	1.04	1.05	0.96	0.95	0.93	0.93	1.05



	R = 1	R = 2	R = 4	R = 6	R = 8	R = 10	Min	Max
T = 0.1	1.00	1.16	1.11	1.05	1.03	1.02	1.00	1.16
T = 0.2	1.00	1.01	0.84	0.83	0.78	0.76	0.76	1.01
T = 0.3	1.00	0.97	0.81	0.76	0.72	0.67	0.67	1.00
T = 0.5	1.00	0.93	0.82	0.76	0.70	0.65	0.65	1.00
T = 1	1.00	0.89	0.79	0.72	0.71	0.69	0.69	1.00
T = 2	1.00	0.95	0.92	0.89	0.84	0.81	0.81	1.00
T = 3	1.00	1.06	0.99	0.91	0.83	0.81	0.81	1.06
T = 4	1.00	0.97	0.86	0.84	0.81	0.80	0.80	1.00
Min	1.00	0.89	0.79	0.72	0.70	0.65	0.65	1.00
Max	1.00	1.16	1.11	1.05	1.03	1.02	1.00	1.16

Figures A22-23. Inter-bin scaling results for the Bin III ($M_w=6.4-6.8$, $R_{close}=30-50km$) to Bin VI ($M_w=6.9-7.6$, $R_{close}=30-50km$) and the Bin III to Bin I ($M_w=6.4-6.8$, $R_{close}=0-15km$) scenarios. The corresponding values of "b" are very similar to those observed for intra-bin scaling within the target bin (shown in Figures A15 and A10, respectively).

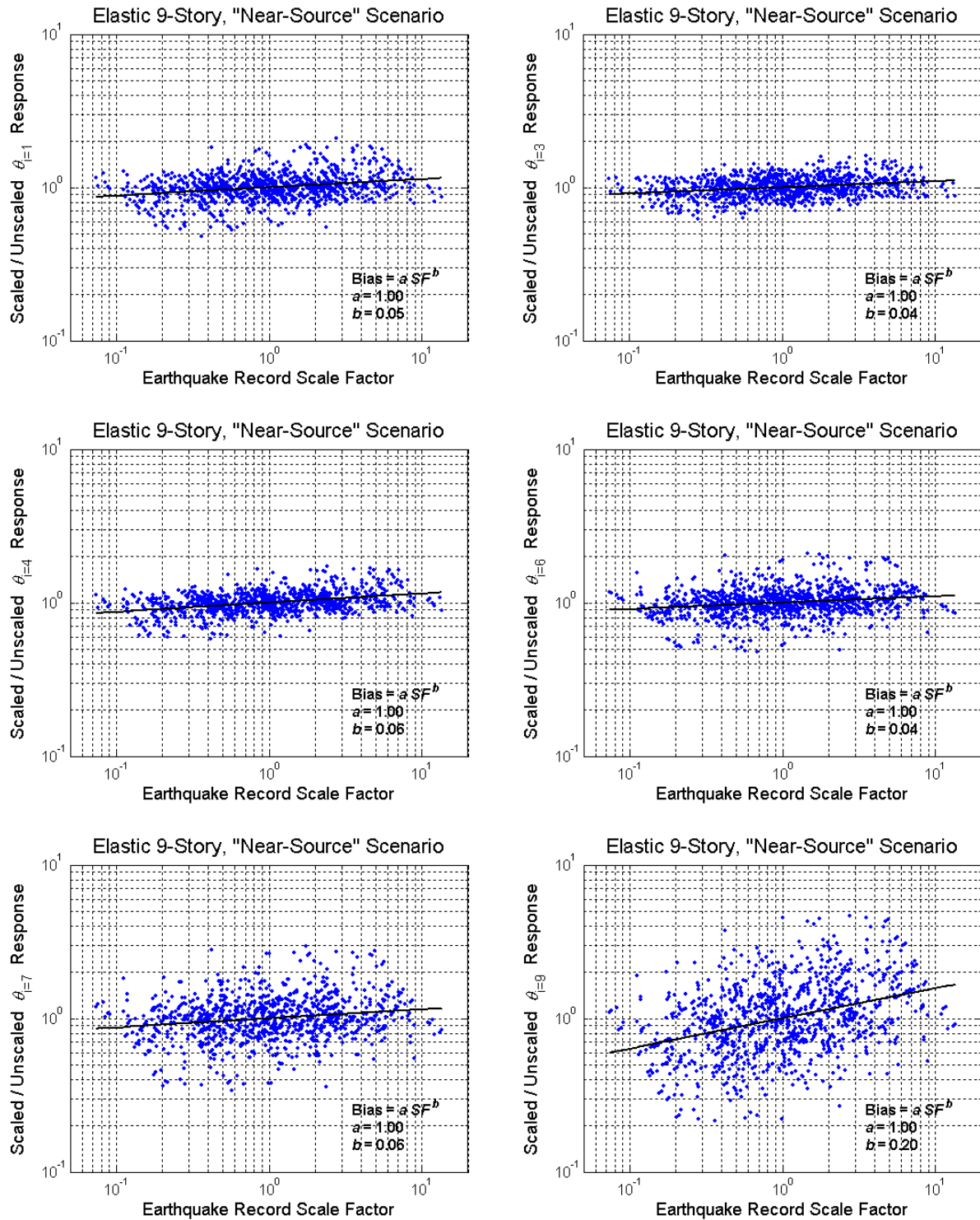


Figure A24. Intra-bin scaling results in terms of the peak inter-story drift ratios (θ_i) at the 1st, 3rd, 4th, 6th, 7th, and 9th stories of the elastic model of the 9-story building considered. The results for the other 3 of the 9 stories are given in the main text (Figure 30).

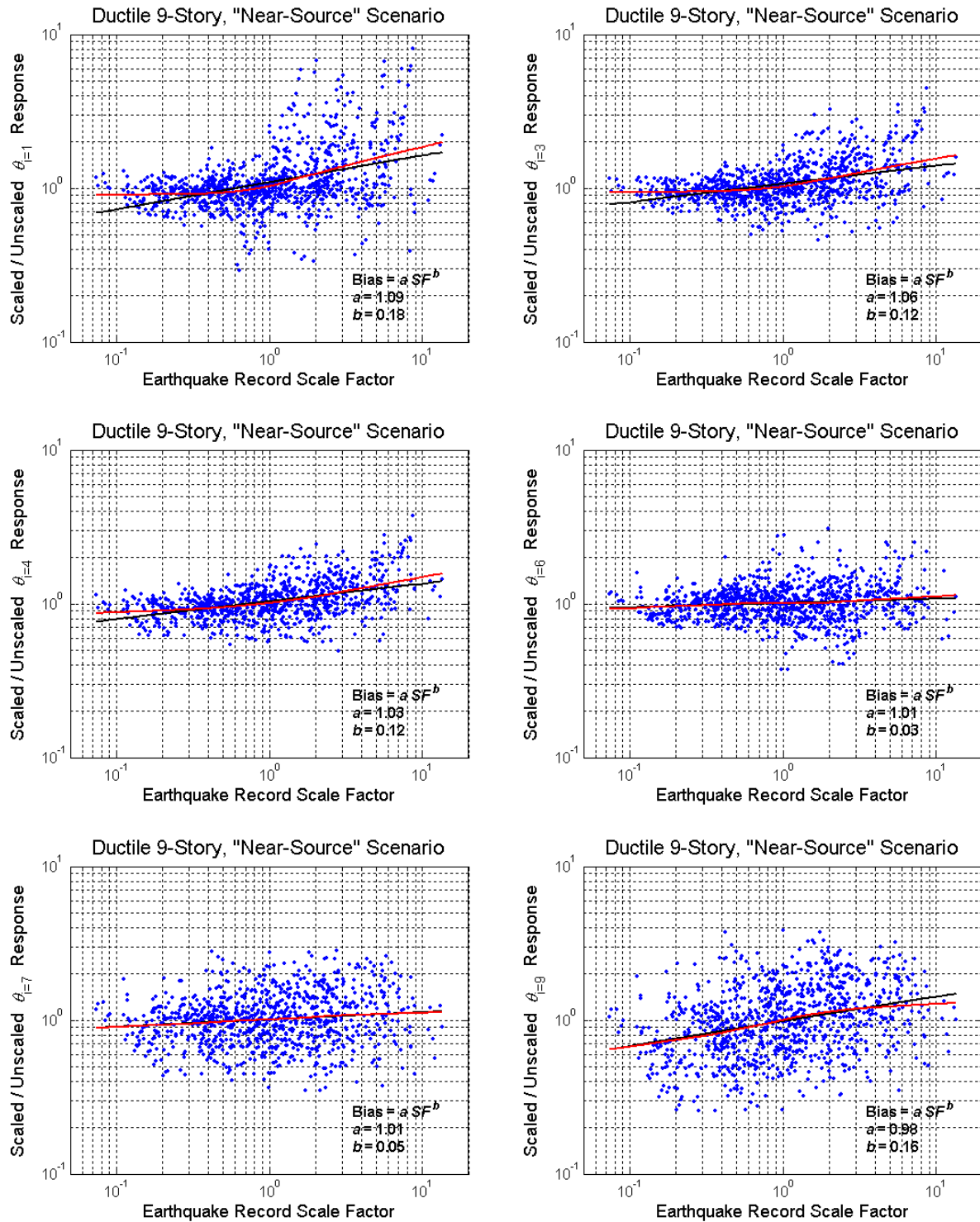


Figure A25. Intra-bin scaling results in terms of the peak inter-story drift ratios (θ_i) at the 1st, 3rd, 4th, 6th, 7th, and 9th stories of the ductile model of the 9-story building considered. The results for the other 3 of the 9 stories are given in the main text (Figure 30).